LEVEL II

12

B.S.

MSC-D674504

AD A067270

# DEVELOPMENT OF ADVANCED ALUMINUM ALLOYS FROM RAPIDLY SOLIDIFIED POWDERS FOR AEROSPACE STRUCTURAL APPLICATIONS

R. E. Lewis
Lockheed Palo Alto Research Laboratory
3251 Hanover Street
Palo Alto, California 94304



March 1979



Interim Technical Report for Period September 1978 – March 1979



Sponsored by
DEFENSE ADVANCED RESEARCH PROJECTS AGENCY
Arlington, Virginia 22209

Monitored by
AIR FORCE MATERIALS LABORATORY
AIR FORCE WRIGHT AERONAUTICAL LABORATORIES
AIR FORCE SYSTEMS COMMAND
Wright-Patterson Air Force Base, Ohio 45433

"The views and conclusions contained in this document are those of the authors and should not be interpreted as representing the official policies, either expressed or implied, of the Defense Advanced Research Projects Agency or the U.S. Government."

UNCLASSIFIED

SECURITY CLASSIFICATION OF THIS PAGE (When Data Entered)

## REPORT DOCUMENTATION PAGE

READ INSTRUCTIONS BEFORE COMPLETING FORM

| | |
|---|---|
| 1. REPORT NUMBER | 2. GOVT ACCESSION NO. |
| 3. RECIPIENT'S CATALOG NUMBER | |
| 4. TITLE (and Subtitle) DEVELOPMENT OF ADVANCED ALUMINUM ALLOYS FROM RAPIDLY SOLIDIFIED POWDERS FOR AEROSPACE STRUCTURAL APPLICATIONS. | 5. TYPE OF REPORT & PERIOD COVERED Interim Technical Report, [redacted] 5 Sep [redacted]78–4 Mar [redacted]79 |
| | 6. PERFORMING ORG. REPORT NUMBER LMSC-D674504 |
| 7. AUTHOR(s) R. E. Lewis | 8. CONTRACT OR GRANT NUMBER(s) ARPA Order No. 3575 F33615-78-C-5203 w/ ARPA Order-3575 |
| 9. PERFORMING ORGANIZATION NAME AND ADDRESS ~~Lockheed~~ Palo Alto Research Laboratory Lockheed Missiles & Space Company, Inc. 3251 Hanover Street, Palo Alto, CA 94304 | 10. PROGRAM ELEMENT, PROJECT, TASK AREA & WORK UNIT NUMBERS Project 3575 |
| 11. CONTROLLING OFFICE NAME AND ADDRESS Defense Advanced Research Projects Agency (DoD) 1400 Wilson Boulevard Arlington, VA 22209 | 12. REPORT DATE Mar [redacted]79 (12) 124 P. |
| | 13. NUMBER OF PAGES 123 |
| 14. MONITORING AGENCY NAME & ADDRESS (if different from Controlling Office) Air Force Materials Laboratory Air Force Systems Command Wright-Patterson Air Force Base, Ohio 45433 | 15. SECURITY CLASS. (of this report) UNCLASSIFIED |
| | 15a. DECLASSIFICATION/DOWNGRADING SCHEDULE |

16. DISTRIBUTION STATEMENT (of this Report)

Approved for public release; distribution unlimited.

17. DISTRIBUTION STATEMENT (of the abstract entered in Block 20, if different from Report)

18. SUPPLEMENTARY NOTES

Other principal contributors are: I. G. Palmer, LMSC, Inc.; W. Cebulak, H. Paris, and F. Billman, ALCOA; E. Starke, Jr. and E. E. Underwood, Georgia Institute of Technology; and E. Rhodes, G. Wald, and R. Simenz, Lockheed-California Company.

19. KEY WORDS (Continue on reverse side if necessary and identify by block number)

| | | |
|---|---|---|
| aerospace structures | Al-Li-Mn | alloy selection rationale |
| rapidly solidified powders | Al-Li-Zr | design trade-off studies |
| aluminum alloy | Al-Fe-Ni-Co | methodology for predicting weight savings |
| Al-Li | Al-Mn-Si | |
| Al-Cu-Li | Al-7075 | |

20. ABSTRACT (Continue on reverse side if necessary and identify by block number)

Advanced aluminum alloys are being developed that will provide major payoffs in terms of weight savings for new aerospace structures. The two property goals are: (1) a 30-percent increase in modulus of elasticity-to-density ratio, and (2) a 20-percent increase in modulus of elasticity-to-density ratio plus a 20-percent increase in strength-to-density ratio, when compared to Al 7075-T76 and without a significant loss in other properties important for structural applications.

The program is organized into three phases: 1 – a fundamental alloy and process development study; 2 – scale-up of two best alloys and evaluation of mill product forms;

DD FORM 1 JAN 73 1473 EDITION OF 1 NOV 65 IS OBSOLETE



UNCLASSIFIED 210118

SECURITY CLASSIFICATION OF THIS PAGE (When Data Entered)

3 – design evaluation involving selected redesign of aerospace components, analysis of payoffs, and recommendations for manufacturing technology development. Phase 1 activity, to be completed in the first two years, is organized into four Tasks: 1 – development of advanced aluminum alloys containing lithium; 2 – development of advanced aluminum alloys that do not contain lithium; 3 – quantitative microstructural analyses and mechanical property correlations; 4 – study of aerospace structural applications for advanced aluminum alloys including development and application of a method for predicting weight savings. Phase 1 activity is described below; Phases 2 and 3 have not been initiated.

In the development of aluminum alloys containing lithium, a detailed rationale for alloy selection was developed. The first four alloy compositions selected all contain 3 wt% Li, 2 or 4 wt% Cu, and Zr or Mn as grain refiners. The second four alloys contain 3 wt% Li and ~ 1 wt% of dispersoid-forming elements. Splat particulate is presently being prepared for these alloys.

In the development of non-lithium-containing aluminum alloys, a detailed rationale for alloy selection has been prepared. The first eight compositions include Al-Fe-Ni-Co and Al-Mn-Si alloys. Preliminary examination of splat particulate of some of these alloys reveals a relationship between solidification structure and screen fraction (plan size of the particulate), with apparently slower solidification rate incurred in the smaller particulate.

Selected analytical procedures for quantitative microstructural analyses of RSP alloys are described.

A detailed methodology for predicting weight savings in aircraft structures has been developed and an example is presented for the S-3A Viking ASW carrier-based airplane. A number of refinements to this model are identified which will further improve the accuracy of prediction.

## FOREWORD

This Interim Technical Report was prepared by Lockheed Missiles and Space Co. Inc, Palo Alto, California under USAF Contract No. F33615-78-C-5203. The work is sponsored by the Defense Advanced Research Projects Agency (DoD), Arlington, Virginia, under ARPA Order No. 3575 and is administered by the Air Force Materials Laboratory, Wright-Patterson Air Force Base, Ohio, with Dr. Lawrence R. Bidwell (AFML/LLS) as Program Manager.

This report covers the period 5 September 1978 to 5 March 1979 as part of an ongoing program to develop advanced aluminum alloys from rapidly solidified powders for aerospace structural applications.

Mr. R. E. Lewis of LMSC, Inc. is the Principal Investigator on this program. Other principal contributors to this report are listed below.

I. G. Palmer – LMSC, Inc.

Section 2.1, Development of Alloys Containing Lithium

Appendix A, Rationale for LMSC Alloy Selection

W. Cebulak, H. Paris, and F. Billman – ALCOA Research Laboratory

Section 2.2, Development of Nonlithium-containing Alloys

Appendix B, Rationale for ALCOA Alloy Selection

E. Starke, Jr. and E. E. Underwood – Georgia Institute of Technology

Section 2.3, Quantitative Microstructural Analysis and Mechanical Property Correlations

E. Rhodes, G. Wald, and R. Simenz – Lockheed-California Co.

Section 2.4, Application Studies

Appendix C, Methodology for Predicting Weight Savings

We wish to thank Dr. T. E. Tietz, Manager of the Metallurgy and Composites Laboratory, LMSC, Inc. for his helpful guidance in the conduct of this study. Drs. L. R. Bidwell (AFML), E. C. Van Reuth, and A. Bement (DARPA) provided invaluable advice and guidance in planning and supporting the subject study.

## SUMMARY

Advanced aluminum alloys are to be developed that will provide major payoffs for important new aircraft, spacecraft, and missile systems in the next decade. Payoffs will result from weight savings of structural components which, in turn, lead to increased range, payload, service life, and decreased life-cycle cost. Recently conducted feasibility and design tradeoff studies provide a basis for selecting certain property goals for improved aluminum alloys that will result in significant weight savings. These property goals are:

A. Specific Elastic Modulus $-$ $133 \times 10^6$ in.
B. Specific Elastic Modulus $-$ $122 \times 10^6$ in., and
   Specific Yield Strength $-$ $7.96 \times 10^5$ in.

## OBJECTIVE

The objective of this program is to develop advanced aluminum alloys from rapidly solidified powders that meet specific property goals. In addition, the program is to establish a metallurgical basis suitable for manufacturing scale-up and application to new weapon systems.

## SCOPE

The program is divided into three phases, each consisting of a number of tasks. Phase 1 involves fundamental alloy development studies and consolidation process development and optimization. The most promising alloys are to be selected, produced in simple mill form, and evaluated in Phase 2. Phase 3 will be a design evaluation involving selected redesign of aerospace components, analysis of payoffs, and recommendations for manufacturing technology.

The effort during the first two years will be devoted solely to Phase 1.

## TECHNICAL PROGRESS

Activity to date for this program is summarized below.

- TASK 1. Development of Aluminum Alloys Containing Lithium

  A detailed rationale for alloy selection was developed. The first four alloy compositions selected all contain 3 wt. % Li, 2 or 4 wt. % Cu, and Zr or Mn as grain refiners. The second four alloys contain 3 wt. % Li and ~ 1 wt. % of dispersoid-forming elements. Splat particulate is presently being prepared for these alloys.

- TASK 2. Development of Non-Lithium-Containing Aluminum Alloys

  A detailed rationale for alloy selection has been prepared. The first eight compositions include Al-Fe-Ni-Co and Al-Mn-Si alloys. Preliminary examination of splat particulate of some of these alloys reveals a relationship exists between solidification structure and screen fraction (plan size of the particulate), with apparently slower solidification rate incurred in the smaller particulate.

- TASK 3. Quantitative Microstructural Analysis and Mechanical Property Correlations

  A preview was performed of analytical procedures for quantitative microstructural analyses of RSP alloys from other programs. Materials prepared in the subject study were not yet available for analysis.

- TASK 4. Application Studies

  A model of predicting weight savings in selected aerospace structures was developed. This model uses assumed or known material property values of an

advanced aluminum alloy. The structural components are grouped according to seven different failure mode categories. New component weight and weight savings are calculated. The results provide guidance for alloy and process development to obtain the optimum combination of properties for maximum weight savings payoffs.

## IMPORTANT FINDINGS AND CONCLUSIONS

A number of promising compositions, with and without Li additions, have been identified which will provide a sound basis for alloy development to achieve the desired property goals.

Metallographic examination of a trial alloy splat (Al-6Mn) revealed that the smaller-size screen fraction particulate includes atomized powder which cooled at a substantially slower cooling rate than the splat particulate comprising larger-size screen fractions. Modification from cold gas to preheated gas atomization is indicated as a way to increase the cooling rate of smaller-size particulate by maintaining liquidity of atomized droplets until splatted on the cold substrate.

The methodology developed for prediction of weight savings from property data for improved aluminum alloys is simple to use and provides key guidance for alloy and process development. Refinements being developed in the analysis will further improve the accuracy of predicted weight savings.

CONTENTS

## ILLUSTRATIONS

## TABLES

# Section 1
# INTRODUCTION

## 1.1 IMPROVED STRUCTURAL MATERIAL NEEDS FOR AEROSPACE SYSTEMS IN THE NEXT DECADE

Three major new aerospace systems, to be developed in the next decade, will have significantly advanced military capabilities. They are an Advanced Tactical Fighter (Air Force), Vertical/Short Takeoff and Landing Reconnaissance Airplane (Navy), and Advanced Fleet Ballistic Missile (Navy). In each of these, structural materials exhibiting selectively improved properties are needed to realize the desired range, payload, and service-life improvements.

To achieve those property goals that will have a maximum payoff in these new systems, design tradeoff and material development studies have been and are being performed. These studies include advanced aluminum alloys, titanium alloys and composites. Two important considerations in these studies are pertinent to the subject work reported herein:

(1) Improved aluminum alloys are of major interest to aerospace manufacturers because of the extensive existing manufacturing technology and capability directly suitable for this class of alloys.
(2) The development of improved aluminum alloys that exhibit significantly higher stiffness and/or strength properties has been shown to be technically feasible.

The following subsection highlights recently completed and some ongoing design tradeoff studies that provide a basis for selecting property goals for this alloy/process development program.

## 1.2 PAYOFFS IN SELECTED AEROSPACE SYSTEMS

### 1.2.1 Advanced Tactical Fighter

As part of an ongoing study* for the U.S. Air Force for Air-to-Surface technology in 1985, one aerospace manufacturer analyzed a close-coupled canard supersonic fighter/interceptor aircraft. Analysis was made of payoffs resulting from application of advanced stiffness aluminum alloys, advanced aluminum powder metal alloys such as MA67 and MA87, textured titanium, graphite-epoxy composites, FP/aluminum composites, low-cost hybrid composites, beta titanium isothermally forged, and low-temperature formable titanium sheet. These advanced materials were included in the study on the assumption that they would be available by 1985, provided that appropriate development and scaleup attention is directed to them.

A high-stiffness aluminum alloy exhibiting a 30-percent increase in modulus-to-density ratio was identified as the best choice for a number of major structural components. Weight saved and related cost figures for these components were estimated, compared with aluminum alloys commercially available in 1975. The weight saved was projected to a life cycle cost savings of $469,000 per airplane. These savings were attributed to increased life as well as reduced maintenance and inspection.

The life-cycle cost savings results in a projected total savings of $234 million when applied to a fleet of 500 airplanes. Of the advanced materials concepts considered, the highest payoff 1985 technology identified was the high-modulus, low-density advanced aluminum alloy. Although advanced composites were found to offer competitive weight savings for many complex components such as the fuselage section, they were not recommended for development for such applications because of the high fabrication costs involved, estimated to be more than six times higher than for advanced aluminum alloys.

---

*Advance information was provided by the U.S. Air Force Materials Laboratory, Wright-Patterson AFB, Ohio.

### 1.2.2 Vertical/Short Takeoff and Landing Airplane

In the preliminary design tradeoff studies of a recently completed contract investigating the feasibility of developing advanced aluminum alloys, the following property goals were considered and weight savings calculated for each of the aluminum alloy major components in the airframe (Ref. 1). Goal A alloy assumed an increase in modulus of 20 percent and decrease in density of 10 percent compared to Al 7075-T76, without significant loss in strength, toughness, fatigue behavior, or stress corrosion resistance. Goal B alloy assumed an increase in strength of 20 percent and decrease in density of 10 percent, compared to Al 7075-T76, without significant loss in modulus, toughness, fatigue behavior, or stress corrosion resistance.

Selective application of two advanced aluminum alloys, A and B, used in the optimum combination, would increase payload 44 percent or increase range by 23 percent for a constant takeoff weight airplane. This significant payoff is achieved in a high-performance version of the V/STOL by a 17-percent weight savings in the wing, fuselage, and tail structure. The tradeoff study also indicated that the range of payload improvements are approximately proportional to the percentage improvement in stiffness and strength.

### 1.2.3 Advanced Fleet Ballistic Missile

In the same feasibility study (Ref. 1), the C-4 Trident FBM forward adaptor shell was analyzed for potential weight savings as it applies closely to the D5 Advanced Trident FBM forward adaptor. The critical design criterion for the forward adaptor shell is stiffness. Substitution of a new aluminum alloy exhibiting 33-percent higher specific stiffness (Property Goal A) resulted in an estimated 16 percent saving in weight of the

---

1 R. E. Lewis, D. Webster, and I. G. Palmer, A Feasibility Study for Development of Structural Aluminum Alloys From Rapidly Solidified Powders for Aerospace Structural Applications, Lockheed Palo Alto Research Laboratory Final Report, Contract F33615-77-C-5186, Technical Report No. AFML-TR-78-102, July 1978.

56-lb component. Relative significance of weight saved in this portion of the missile is five times the baseline first-stage motor and interstage. Consequently, the 9 lb saved in the component is equivalent to 45 lb saved in the first-stage motor. This saving contributes a significant (classified) addition to range of the missile and is equivalent to about a 15-lb increase in payload. Significant additional weight savings can be expected in other portions of the adaptor section and in the equipment section by application of a high specific stiffness alloy.

### 1.2.4 Other Prospective Payoffs

Advanced aluminum alloys exhibiting the above Goal A or B property sets will contribute significantly to other aerospace applications. For example, a design tradeoff evaluation included in the recent study by LMSC of a space payload shroud indicated that application of the improved stiffness aluminum alloy A would save about 1000 lb of the 4200-lb shroud weight (Ref. 1). This translates to a significant in-orbit payload increase of about 70 lb since the tradeoff ratio of shroud to payload weight is 14:1.

## 1.3 PLAN FOR ALLOY DEVELOPMENT

Based on the above design tradeoff studies and other considerations, a program was formulated to develop advanced aluminum alloys from rapidly quenched particulate. The objective and scope are described below.

### 1.3.1 Objective

The objective of this program is to develop advanced aluminum alloys that meet specific property goals. In addition, the program is to establish a metallurgical basis suitable for manufacturing scaleup and application to new weapon systems. Goal A is a 30-percent increase in specific modulus of elasticity, relative to Al 7075-T76, without significant loss in strength, toughness, fatigue strength, or stress-corrosion resistance.

Goal B is a 20-percent increase in specific modulus of elasticity accompanied by a 20-percent increase in specific strength, without significant loss in toughness, fatigue strength, or stress corrosion resistance. The resulting property goals are as follows:

- Goal A

  Specific elastic modulus: $133 \times 10^6$ in.

- Goal B

  Specific elastic modulus: $122 \times 10^6$ in.

  Specific yield strength: $7.96 \times 10^5$ in.

### 1.3.2 Scope

The program is divided into three phases, each consisting of a number of tasks. Phase 1 involves fundamental alloy development studies and consolidation process development and optimization. The most promising alloys are to be selected, produced in simple mill form, and evaluated in Phase 2. Phase 3 will consist of a design evaluation using the properties of the alloys evaluated in Phase 2.

This program was initiated in September 1978 and is scheduled for completion in 3-1/2 years. The effort during the first two years will be devoted to Phase 1 only. This report describes activity to date in each of the four tasks comprising Phase 1.

Section 2

# EXPERIMENTAL PROCEDURES AND RESULTS

This section describes activities to date only on Phase 1, Alloy Development. Activity on Phases 2 and 3 will not be initiated until Phase 1 is completed.

## 2.1 TASK 1 – DEVELOPMENT OF ALLOYS CONTAINING LITHIUM

This task is being conducted by the Lockheed Palo Alto Research Laboratories.

### 2.1.1 Alloy Compositions

Alloy compositions of the first iteration of eight alloys have been selected and contain 3 wt.% Li to meet program goal A of 30% increase in specific modulus. A full description of the rationale for selection of the alloy compositions is given in Appendix A.

The first four alloys are based on the Al-Cu-Li system. One alloy will contain commercial purity lithium; the other three will contain high purity lithium. Two different Cu levels and two different grain refining elements have been selected. The second four alloys contain approximately 1 wt.% of the following elements, or combinations of two elements: Zr, Mn, Fe + Ni, Fe + Co, along with 3 wt.% Li. These elements have been selected to produce a fine dispersion of non-deformable particles which will serve two primary functions.

1. To inhibit the localization of slip which occurs in Al-Li alloys, and which leads to low toughness.
2. To stabilize the fine grain size produced by the rapid solidification.

The alloy compositions are given in Table 1.

TABLE 1. LMSC FIRST ITERATION ALLOYS

| Alloy No. | Composition[a] (Weight Percent) | | | | | | |
|---|---|---|---|---|---|---|---|
| | Li[b] | Cu | Zr | Mn | Fe | Ni | Co |
| 1.1 | 3.0 | 4.0 | 0.2 | – | – | – | – |
| 1.2 | 3.0 | 2.0 | 0.2 | – | – | – | – |
| 1.3 | 3.0[c] | 4.0 | 0.2 | – | – | – | – |
| 1.4 | 3.0 | 4.0 | – | 0.4 | – | – | – |
| 1.5 | 3.0 | – | 1.0 | – | – | – | – |
| 1.6 | 3.0 | – | – | 1.5 | – | – | – |
| 1.7 | 3.0 | – | – | – | 0.5 | 0.5 | – |
| 1.8 | 3.0 | – | – | – | 0.5 | – | 0.5 |

(a) Balance Aluminum.
(b) High purity except as noted.
(c) Commercial purity.

The subcontract for the manufacture of the first iteration of eight alloys was initiated with the Alcoa Research Laboratories, who will use a proprietary splat process that produces cooling rates $\gtrsim 10^6$ K/s.

### 2.1.2 Prediction of Modulus and Strength Requirements

From the chemical composition for a developmental alloy the density can be predicted within 2 to 3 percent accuracy using the rule of mixtures. Then, for each alloy and predicted density, the modulus and strength values required to meet the program property goals can be calculated. These calculations have been made for the first eight alloys to be evaluated by LMSC and are presented in Table 2. Such data can be used for calculating anticipated weight savings in specific aerospace structures, thereby contributing useful direction in revising primary property goals, if appropriate, and in setting secondary property priorities. The primary class aerospace structure to be analyzed this way will be a high performance fighter. Space, missile, and other aircraft will also be examined as time allows.

TABLE 2. MODULUS AND STRENGTH VALUES REQUIRED TO MEET PROGRAM GOALS
LMSC First Iteration Alloys

| Alloy No. | Rule of Mixtures Density[a] | | Modulus of Elasticity Required to Meet Property Goal A[b] | | Modulus of Elasticity Required to Meet Property Goal B[c] | | Yield Strength Required to Meet Property Goal B | |
|---|---|---|---|---|---|---|---|---|
| | ($kg/m^3$) | ($lb/in^3$) | (GPa) | (ksi × $10^3$) | (GPa) | (ksi × $10^3$) | (MPa) | (ksi) |
| 1.1 | 2470 | 0.089 | 81.8 | 11.9 | 75.1 | 10.9 | 490 | 71.0 |
| 1.2 | 2440 | 0.088 | 80.8 | 11.7 | 74.1 | 10.8 | 484 | 70.1 |
| 1.3 | 2470 | 0.089 | 81.8 | 11.9 | 75.1 | 10.9 | 490 | 71.0 |
| 1.4 | 2470 | 0.089 | 81.9 | 11.9 | 75.2 | 10.9 | 490 | 71.1 |
| 1.5 | 2420 | 0.087 | 80.1 | 11.6 | 73.5 | 10.7 | 480 | 69.6 |
| 1.6 | 2430 | 0.088 | 80.4 | 11.7 | 73.8 | 10.7 | 481 | 69.8 |
| 1.7 | 2420 | 0.087 | 80.2 | 11.6 | 73.6 | 10.7 | 480 | 69.6 |
| 1.8 | 2420 | 0.087 | 80.2 | 11.6 | 73.6 | 10.7 | 480 | 69.6 |

(a) Rule of Mixtures Density may differ from experimental density, especially for Li-containing alloys.
(b) Property Goal A: specific modulus = $133 \times 10^6$ in.
(c) Property Goal B: specific modulus = $122 \times 10^6$ in. and specific strength = $7.96 \times 10^5$ in.

### 2.1.3 Lithium

Sufficient lithium to make 35 lb each of the first iteration of eight alloys was ordered from Research Inorganic Chemical Corporation, Sun Valley, CA. Four pounds of commercial purity lithium (0.04 – 0.05 wt.% Na) and 26 lb of high purity lithium (0.007 wt.% Na max.) were ordered. The high-purity lithium is made by Research Inorganic using an electrolytic purification process.

The 4 lb shipment of commercial purity lithium was delivered to ALCOA on December 5, 1978, together with an analysis, shown in Table 3.

TABLE 3. COMPOSITION OF LITHIUM INGOT, ORDINARY PURITY
(Lot. No. 450-95 dr. 16, under argon)

| Element | Wt. %[(a)] |
|---|---|
| Li | 99.9 |
| Na | 0.05 |
| Fe | 0.002 |
| Ca | 0.01 |
| Si | 0.002 |
| N | 0.005 |
| Cl | 0.002 |
| K | <0.01 |

(a) Analysis reported by Research Organic/Inorganic Chemical Corporation.

The 26-lb shipment of high-purity lithium was delivered to ALCOA on January 26, 1979, together with an analysis, shown in Table 4. At LMSC's request, one of the sealed 1 lb canisters was sent to LMSC for confirmation of the supplier's analysis. The LMSC analysis, also presented in Table 4, showed a sodium content of 0.0054%, which is well within the specification level of 0.0075%. ALCOA has been given approval to initiate manufacture of Al-Li developmental alloys and the first particulates are expected to be made in March 1979.

### 2.1.4 Melting and Splat-Making

The ALCOA splat-making facility was revised with ALCOA funds to provide a reduced oxygen (< 6 wt. %) environment for the collection of flakes in batches ≤ 45 kg. The system was tested after a 0.3-min purge with argon and was found to maintain ≤ 3 wt. % oxygen. After collection, the particulate will be exposed for a short time to a normal air atmosphere.

TABLE 4. COMPOSITION OF HIGH PURITY LITHIUM INGOT
(under Argon)

| Element | Wt. % Supplier[a] | Check[b] |
|---|---|---|
| Na | 0.0075 | 0.0054 |
| Ca | <0.06 | 0.0069 |
| K | <0.01 | 0.0005 |
| Fe | <0.01 | 0.0095 |
| Si | 0.01 | (c) |
| N | <0.03 | 0.14 |
| Cl | <0.006 | 0.002 |
| Mg | (c) | 0.0008 |
| Pb | (c) | 0.048 |
| Ni | (c) | 0.007 |
| Cu | (c) | 0.002 |
| Ag | (c) | 0.001 |

(a) Analysis reported by Research Organic/Inorganic Chem. Corp.
(b) Average of two samples, performed by LMSC.
(c) Not reported.

Melting of the Al-Li alloys will be performed in oxynitride-bonded, SiC crucibles and with a melt cover flux of high-purity boric acid. Atomization for the splat-making will be performed in an argon atmosphere. The special high flow rate argon delivery system required is presently being constructed and should be operational by March 25, 1979. High-purity aluminum will be used as a base for the developmental alloys, and in the case of the high purity Li alloys (those containing low Na), the aluminum charge will be purged with chlorine gas to reduce Na to <0.005 wt. % before Li is added.

### 2.1.5 Consolidation and Processing

Samples of 7050 alloy splat were provided by ALCOA so that the handling qualities of typical splat could be assessed in advance of receiving the Al-Li splat materials. The

packing density versus pressure plot was determined (Figure 1) and used for the design of cold and hot pressing dies. In the cold compaction step, the splat will be compressed from its initial low packing density of 10% to approximately 40%, using a pressure of about 3 ksi. The compact will then be transferred to a graphite-lined steel die for the vacuum degassing and hot pressing steps. After hot pressing to a density close to the theoretical value, the compact will be canned and hot extruded, using initially an extrusion ratio of 8:1.

## 2.2 TASK 2 – DEVELOPMENT OF NONLITHIUM-CONTAINING ALLOYS

This task is being conducted by the ALCOA Research Laboratories.

### 2.2.1 Selection of Initial Alloy Compositions

Selection of the first eight compositions was based on the rationale presented in Appendix B. Composition No. 6A (Al – 9.68 Mn – 2.47 Si) was chosen for later use in fundamental studies of deformation processing. Hereafter, all compositions refer to Al-x weight percentage solute elements.

ALCOA personnel retain some element of concern over the availability and cost of cobalt. Al-Fe-Ni-Co compositions, however, continue to show strong promise for the intended applications of this contract.

### 2.2.2 Generation of Splat Particulate

Splat-making activities with ALCOA's proprietary drum-quench technique were initiated on January 5, 1979 after the self-contained batch flake collection system was completed. The continuous cyclone collection system was still under construction at this time. A series of preliminary trials with pure aluminum and dilute alloy compositions was conducted through January 19 under independent ALCOA funding.

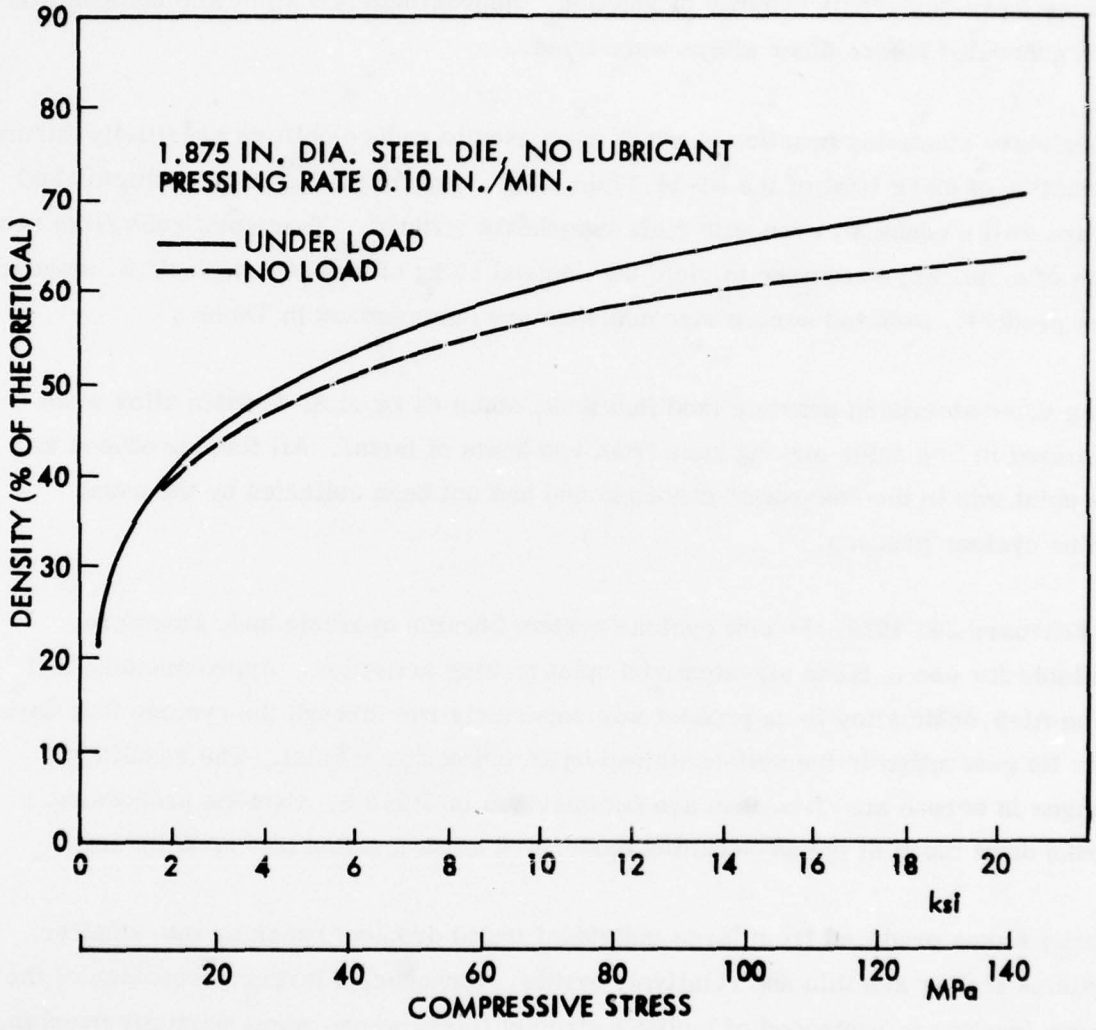


Figure 1. Room temperature compression of ALCOA 7050 splat.

Contract Materials Produced. Several attempts were then made to generate Al-3.27Fe-3.44Ni-3.45Co alloy splat using usual procedures and the available cold atomizing air supply. Despite use of 982°C melt temperatures, nozzle chilling problems precluded bulk quantity production. Approximately 4 kg of this composition were generated before other alloys were tried.

Proprietary atomizing practice changes were used to reduce chilling sensitivity during production of 62 kg total of the Al-14.17Mn alloy. Nozzle problems were diminished but are still a concern, even with melt superheats ≥200°C. Four splat runs from two heats of metal were required to yield the desired 45 kg of 8 to 200 mesh (U.S. standard) flake product. Detailed screen size analyses are summarized in Table 5.

Using these atomizing practice modifications, some 64 kg of Al-9.68Mn alloy were generated in five splat-making runs from two heats of metal. All flake produced to this point was in the "as-splat" condition and had not been collected by the usual in-line cyclone process.

On February 24, 1979, the new cyclone system became operable and, therefore, available for use in these air-atomized splat making activities. Approximately half of the Al-9.68Mn alloy flake product was separately run through the cyclone four days after its generation in the self-contained batch collection system. The resulting changes in screen size fractions are summarized in Table 5. Cyclone processing breaks down much of the as-solidified coarse +8 mesh fraction into smaller sizes.

Coarse flakes produced from large individual liquid droplets break up into smaller particles if they are thin and relatively brittle. However, a larger percentage of the coarse fraction is composed of multiple-droplet flakes whose edges partially overlap. This effect is produced by an overly dense droplet distribution within certain areas of the atomized spray pattern. Such multiple-droplet flakes separate readily during the cyclone operation.

TABLE 5. SCREEN SIZE ANALYSES OF ALCOA'S SPLAT FLAKE MATERIALS

| ALCOA Alloy | Target Melt Composition (Wt. % Solute) | Weight Produced (~kg) | Screen Size – U.S. Standard | | | | | | | |
|---|---|---|---|---|---|---|---|---|---|---|
| | | | +8 | -8 +16 | -16 +30 | -30 +50 | -50 +100 | -100 +200 | -200 +325 | -325 |
| 1A | Al-3.27Fe-3.44Ni-3.45Co | 4[a] | 2 | 11 | 16 | 25 | 23 | 14 | 5 | 4 |
| 8A | Al-14.17Mn | 62[b] | 27 | 35 | 18 | 14 | 4 | 1 | 0.5 | 0.5 |
| 5A | Al-9.68Mn | 64[b] | 30 | 38 | 15 | 9 | 5 | 2 | 0.5 | t |
| Same as above plus separate processing through cyclone | | 38 of above | 3 | 32 | 25 | 24 | 12 | 3 | 0.5 | 0.5 |
| 6A | Al-9.68Mn-2.47Si Generated with continuous in-line cyclone process | 170 | 3 | 39 | 25 | 20 | 8 | 3 | 1 | 1 |

(a) Nozzle freezing problems with cold air atomizing at usual metal/air ratios yielding smaller +8 fraction.
(b) Increased metal/air ratios reduce nozzle problems but increase +8 fraction.

During late February, 1979 the Al-9.68Mn-2.47Si alloy was produced with continuous in-line cyclone processing. Approximately 170 kg total were generated in eight runs from three metal heats. All were atomized with cold air from a minimum melt temperature of approximately 954°C. Screen size fractions of this material are also shown in Table 5. Some alloy influence is expected, but there is a reasonable size similarity between the flake products generated with either "separate-step" or with "in-line" cyclone collection.

Disposition of Initial Splat Materials. A small quantity of the Al-3.27Fe-3.44Ni-3.45Co flakes was used for preliminary metallographic observations as were typical samples of the other three alloys produced to date. The Al-14.17Mn alloy product is currently being broken down into its constituent screen fractions for use in a flake size versus cold compaction characteristics study.

Sample quantities of Al-9.68Mn alloy flakes produced both with and without cyclone processing will be subjected to various time/temperature exposures in phase stability evaluations, to determine the effect of the resultant strain energy input on decomposition kinetics of the supersaturated solid solution.

The Al-9.68Mn-2.45Si alloy is the principal composition designated for subsequent hot compaction studies, and the entire amount (~161.5 kg) of 8 to 200 mesh product made in these first splat making runs will be directed to that effort.

New Production of Splat Materials. Provisions for supply of preheated atomizing air to the ALCOA splat facility are underway, at no cost to this contract, and should be completed in March 1979. Generation of new 45-kg quantities of 8 to 200 mesh splat flakes in each of the eight alloy compositions will begin upon completion of this preheated air installation. This short additional delay in materials generation will resolve the nozzle chilling complications and thereby eliminate the current need for multiple heats and/or runs of a given composition. New splat materials generated with hot atomizing air should have improved recovery of the desired particle size range and will be comparatively smaller in size while exhibiting equal or superior microstructural features compared to the cold air-produced splat.

### 2.2.3 Characterization of Loose Particulate

Characterization of loose particulate of the compositions in Table 5 has begun. Guinier phase analysis of the alloy used for the trial run, Al-5.98Mn, and alloy No. 8A, Al-14.7Mn, is completed. Optical metallography of all four compositions of Table 5 has begun but is complete only for the trial run alloy and contract alloys 1A, 5A, and 8A. Analysis of the trial composition was done with independent ALCOA funds. Detailed chemical analysis is not completed; therefore, compositions are identified by their nominal values.

Guinier Analysis of Al-5.98Mn Trial Alloy. The particulate of this composition has been screened into size fractions based on area, from +8 mesh to -325 mesh. Visual examination indicates that particulate in screen fractions of +200 and larger is

essentially all splat, while particulate smaller than 200 mesh is primarily atomized powder. Three screen fractions to span from atomized powder to the coarser splat were selected for Guinier analysis to evaluate any effects of changes in cooling rate with flake size on retained solid solubility of Mn. The results of the test run are presented in Table 6. The amount of phases present is rated qualitatively by an experienced observer on the basis of relative diffraction line intensities on the Guinier film. As expected, the only phases present are $MnAl_6$ and silicon stabilized $MnAl_4$ noted as $Mn_3SiAl_{12}$ or (Mn, Si)$Al_4$ (Ref. 2). The fact that these two phases are present in extremely small amounts, indicates that the rapid solidification effectively maintained a large solid state supersaturation of Mn.

TABLE 6. GUINIER PHASE ANALYSIS OF Al-5.98Mn

| Screen Fraction[a] | Percent of Sample | Qualitative Amount of Phases Present | | |
|---|---|---|---|---|
| | | Al | $MnAl_6$ | $Mn_3SiAl_{12}$ |
| -16 +30 | 29.6 | Large$^+$ | – | Very small$^+$ |
| -50 +100 | 8.8 | Large$^+$ | Possible Trace | Small$^-$ |
| -325 | 0.6 | Large$^+$ | Possible Very small$^-$ | Small |

(a) Screened by plan area, not thickness of splat.

Guinier Analysis of Alloy No. 8A, Al-14.7Mn. Using the previous observation on splat versus atomized powder content in various screen fractions, three screen fractions of the splat particulate shown in Table 7 were selected for Guinier analysis. This analysis disclosed the higher solute alloy did not retain the degree of supersaturation that the Al-5.98Mn alloy did (compare Tables 6 and 7). The results for Al-14.7Mn are surprising since there is no evidence of equilibrium compounds of the

2 W. B. Pearson, Handbook of Lattice Spacings and Structures of Metals, New York, Pergamon Press, 1958, p. 338.

Al-Mn system or of those compounds commonly associated with ancillary elements in the Al-Mn system. Significant amounts of an unidentified phase were detected. The Joint Committee of Powder Standards (Ref. 3) and other sources do not contain a compound which can account for the observed diffraction lines. Further effort may be directed towards identification using diffractometer lattice parameter measurements and STEM analysis of thin foils.

TABLE 7. GUINIER PHASE ANALYSIS OF ALLOY 8A (Al-14.7Mn)

| Screen Fraction[a] | Percent of Sample | Qualitative Amount of Phases Present | | |
|---|---|---|---|---|
| | | Al | $MnAl_6$ | Unidentified |
| +8 | 27 | Large+ | – | Medium |
| -16 +30 | 18 | Large+ | – | Small+ |
| -50 +100 | 4 | Large+ | – | Small+ |

(a) Screened by plan area, not thickness of splat.

ALCOA Alloys 1A, 5A, and 6A. Guinier analysis is not completed at this time.

Optical Metallography of Al-5.98Mn-Trial Alloy Uncycloned). This alloy was used to assess cooling rates as measured by dendrite arm spacing and to assess flake geometry in three screen fractions. Figures 2 and 3 are as-polished and etched transverse structures of flakes in the +30 and +100 mesh fractions. Guinier analysis shows this fraction to have the least amount of precipitated phases. As can be seen, many flakes are predominately free of a dendritic structure. The typical thickness of most flakes is 16 to 24 $\mu$m in this run. Figures 2b and 3a show that flakes usually exhibit a transition from nondendritic to dendritic solidification morphology in this

3 Joint Committee of Powder Standards (1978), Swarthmore, PA.

(a)

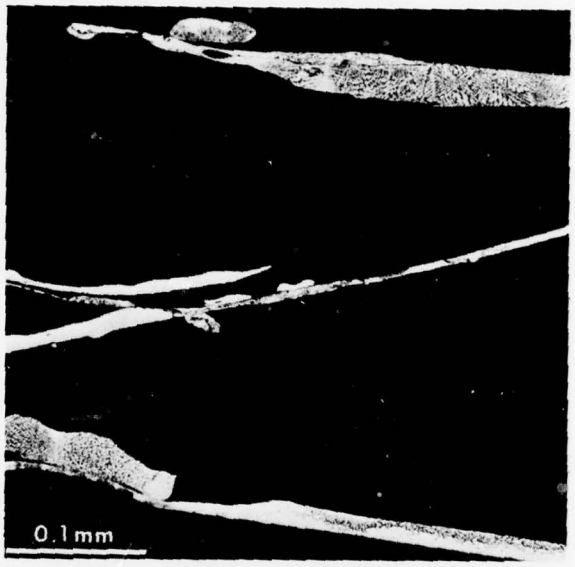


(b)

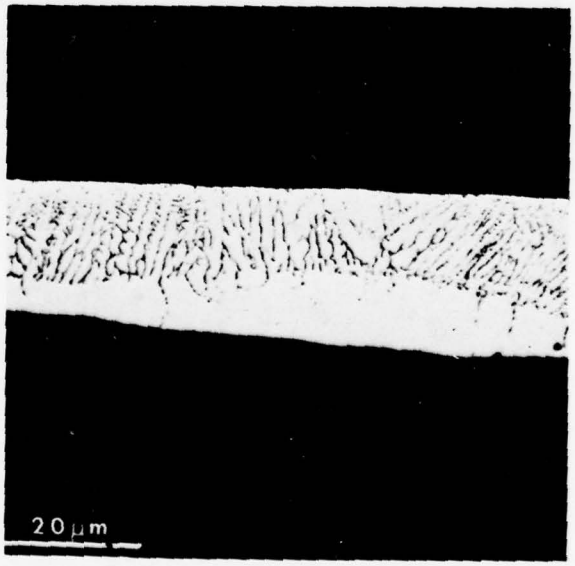


Figure 2. Optical microstructures of the trial alloy, Al-5.98 wt % Mn, showing (a) the typical particulate morphology of the +30 screen fraction, (b) the nondendritic to dendritic transition in particulate solidification morphology in the +30 screen fraction. (Keller's Etch)

(a)

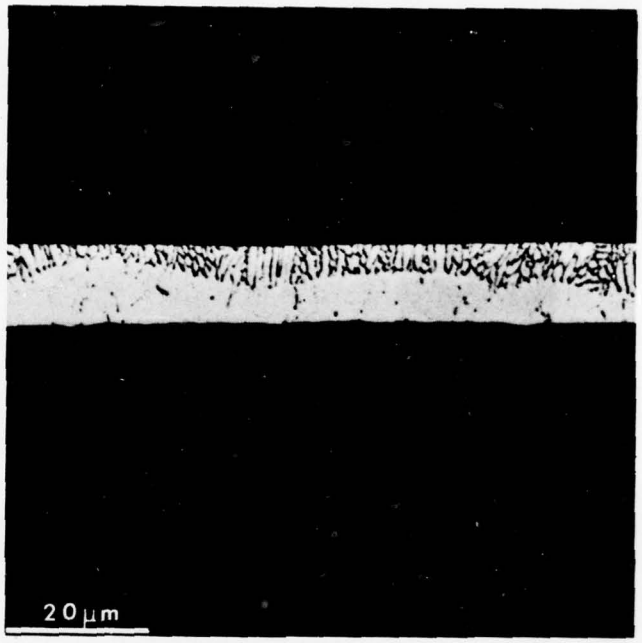


(b)

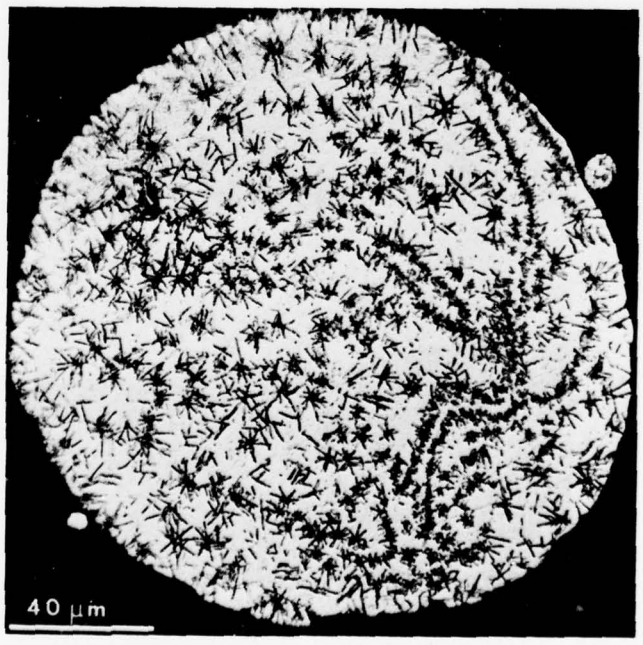


Figure 3. Optical microstructures of the trial alloy, Al-5.98 wt % Mn, showing (a) the nondendritic to dendritic transition in solidification morphology in the +100 screen fraction, (b) typical atomized powder with evidence of precipitation in the +100 screen fraction.

thickness range. The dendrite arm spacing was measured in this transition zone. The average of 24 measurements yields an average spacing of 0.9 $\mu$m, which coincides with a cooling rate of $\sim 5 \times 10^5$ °K $s^{-1}$, using the correlations of dendrite arm spacing and cooling rate (Ref. 4). Similar measurements in Figure 3a of 28 dendrites yield an average spacing of 0.7 $\mu$m corresponding to a cooling rate of $6 \times 10^5$ °K $s^{-1}$. Since the basis of dendrite arm spacing to cooling rate at high solidification rates is uncertain, changes in dendrite arm spacing will be used only to infer relative improvement in cooling rates. Figure 3b shows an example of atomized powder in the +100 mesh fraction product. This is an atomized powder with a substantially lower cooling rate as indicated by the degree of precipitation. Observations of significant precipitation in the atomized powder and negligible precipitation in the flake particulate suggests that the phases detected by Guinier analysis of this alloy are primarily in the atomized powder.

Optical Metallography of Alloy No. 8A, Al-14.7Mn. Figures 4 and 5 are a series of micrographs of three splat screen fractions of this alloy. It can be seen that significant precipitation has occurred, likely the result of cool air atomizing. Several observations are to be noted. The +8 fraction in Figure 4a contains many multiple layered splats while the smaller screen fractions do not (Figure 5). The smaller flakes are also featureless, indicating minimal precipitation. This suggests the multiple-layer flakes experienced a significantly lower cooling rate. The typical flake thickness of the +8 fraction is $\sim 40$ $\mu$m, a factor which also contribute to a slower cooling rate compared to the Al-5.9Mn alloy, which has a typical flake thickness of $20 - 30$ $\mu$m in the +30 size fraction.

Optical Metallography of Alloy, 1A, Al-3.27Fe-3.44Ni-3.45Co. Very limited characterization of this alloy has begun. Figures 6 and 7 show the microstructures of particulate from three screen fractions. These flakes exhibit a variety of different shapes, probably reflecting melt viscosity differences. For example, long continuous flakes are rare except in the +16 screen fraction. In screen fractions of -16 mesh,

---

4 H. Matyja, B. C. Giessen, N. J. Grant, "The Effect of Cooling Rate on the Dendrite Spacing in Splat-Cooled Aluminum Alloys," J. of the Institute of Metals, Vol. 96, 1968, p. 30.

(a)

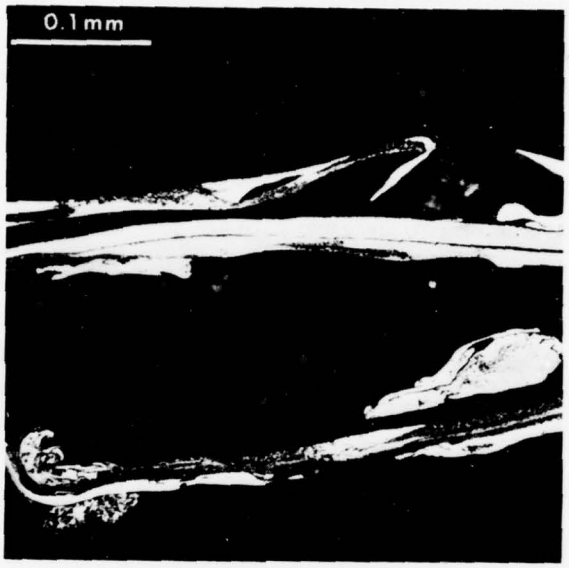


(b)

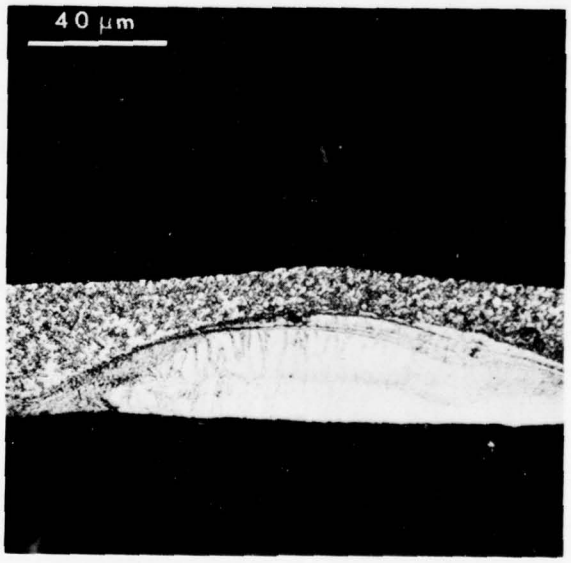


Figure 4. Optical microstructures of alloy 8A, Al-14.7 wt % Mn, showing (a) multiple layered splat flakes in the +8 screen fraction, (b) complex solidification front in the +8 screen fraction. (Keller's Etch)

(a)

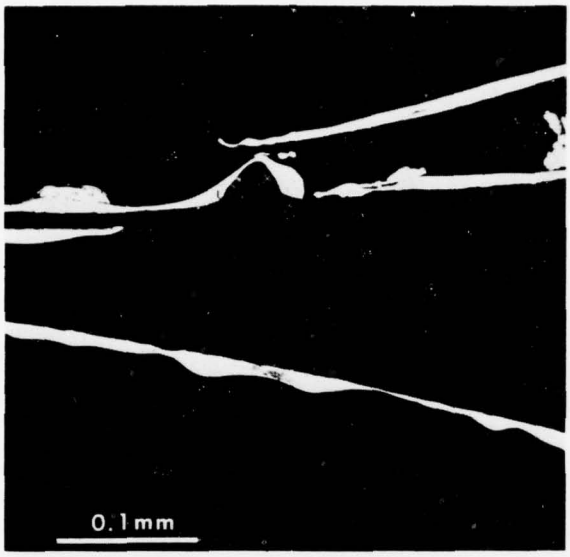


(b)

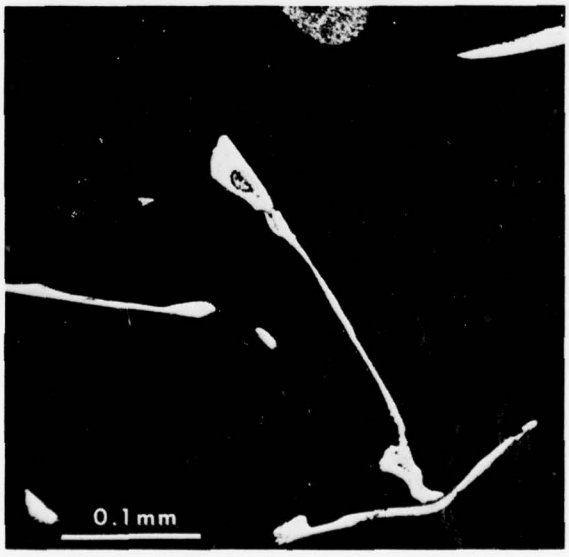


Figure 5. Optical microstructures of alloy 8A, Al-14.7 wt % Mn, showing the typical particulate morphology in the (a) +30 screen fraction and (b) +100 screen fraction. (Keller's Etch)

(a)

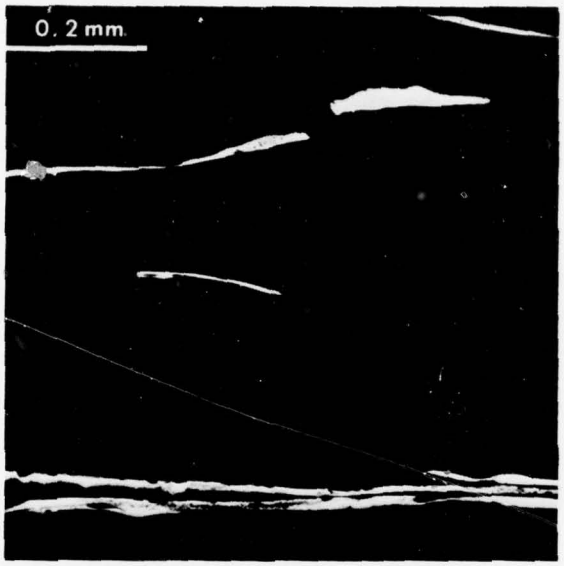


(b)

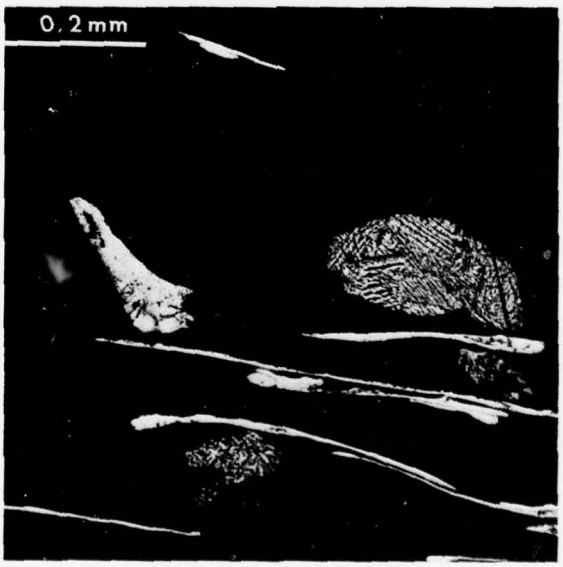


Figure 6. Optical microstructures of the alloy 1A, Al-3.27 wt % Fe-3.44 wt % Ni-3.45 wt % Co, showing typical particulate morphology in the (a) +16 screen fraction and (b) +100 screen fraction. (Keller's Etch)

(a)

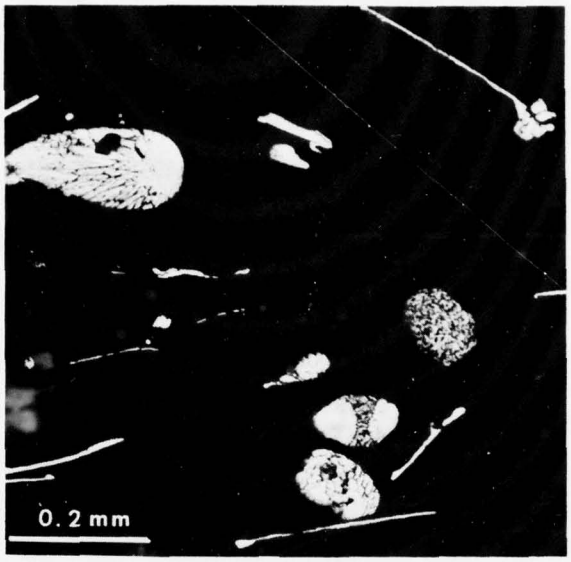


(b)

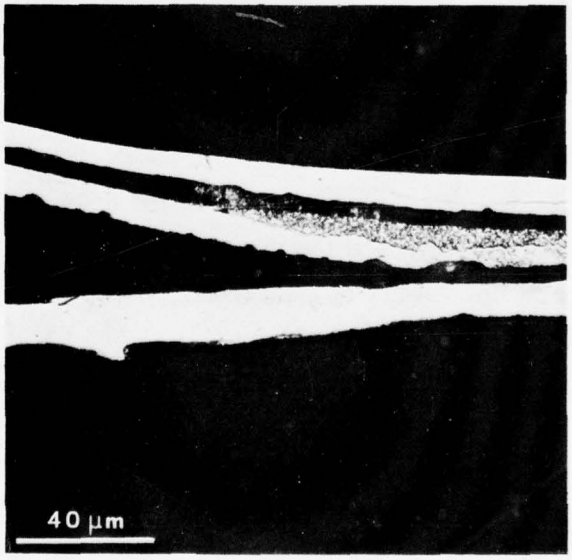


Figure 7. Optical microstructures of alloy 1A, Al-3.27 wt % Fe-3.44 wt % Ni-3.45 wt % Co, showing (a) typical particulate morphology of the +200 screen fraction, (b) the nondendritic to dendritic transition in solidification morphology in the +16 screen fraction (Keller's Etch)

there is a higher proportion of atomized powder than in the Mn alloys. Figure 7b shows the relatively featureless, nondendritic flakes interspersed with flakes containing coarse precipitation. It is believed that heated air atomization of this alloy will promote both uniform flake morphology and increased solid solubility.

Optical Metallography of Alloys 5A and 6A, Al-9.68Mn and Al-9.68Mn-2.47Si. Optical metallography of these alloys is not available at this time.

## 2.3 TASK 3 – QUANTITATIVE MICROSTRUCTURAL ANALYSIS AND MECHANICAL PROPERTY CORRELATIONS

This task is being performed by the Georgia Institute of Technology.

Since official start of activity at Georgia Tech was mid-February 1979, there is no specific work to report at this time. However, a discussion of some of the techniques and problems involved in quantitative microstructural analyses of similar powder metallurgy products is considered of value. To this end, we discuss and analyze some MA87 microstructures being investigated currently at Georgia Tech; two microstructures of an Al 7075 alloy from rapidly solidified powders (from work performed at LMSC); two microstructures of MA87 with A-upset and draw or ABC-upset and draw (from work performed at ALCOA); and the microstructure of a special alloy selected to illustrate some analysis problems in TEM (from work being done at Georgia Tech).

### 2.3.1 Quantitative Microstructural Analysis of Anisotropic Grain Structure

Figure 8 shows a composite view of the three orthogonal planes of extruded MA87 aluminum alloy (Al-6.5 Zn-2.5 Mg-1.6 Cu-0.4 Co). In view of its marked anisotropy, or layering, several quantities are calculated to express this lack of randomness quantitatively (Ref. 5). These are the mean intercept length between layers, $\bar{L}_{\perp}$; the mean aspect ratio, Q; and the degree of orientation, $\Omega_{12}$, of lines in a plane.

---

5 E. E. Underwood, Quantitative Stereology, New York, Addison-Wesley, 1970, p. 48.

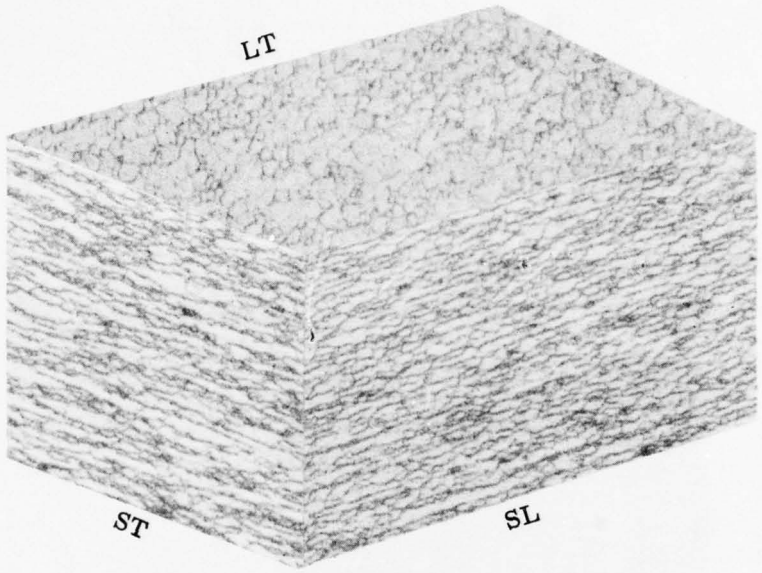


Figure 8. Composite view of three orthogonal planes of extruded MA87 aluminum alloy. 800×. (L = longitudinal, T = transverse, S = short transverse)

The value of $\Omega_{12}$ varies from 0 to 1, depending on the percentage of linear segments of the grain-boundary traces that are aligned in the extrusion (or orientation) direction. Appropriate equations for these three quantities are

$$\bar{L}_{\perp} = 1/\left(P_L\right)_{\perp} \tag{1}$$

for the spacing parameter,

$$Q = \bar{L}_{\parallel} \sqrt{\bar{L}_{\perp}} = \left(P_L\right)_{\perp} / \left(P_L\right)_{\parallel} \tag{2}$$

for the elongation parameter, and

$$\Omega_{12} = \frac{\left(P_L\right)_{\perp} - \left(P_L\right)_{\parallel}}{\left(P_L\right)_{\perp} + 0.571\left(P_L\right)_{\parallel}} \tag{3}$$

for the degree of orientation of lines in a plane.

The actual analysis was performed on three SEM photomicrographs taken at 7000×. Figure 9 shows the appearance of the three orthogonal planes SL, ST, and LT.

(a) LT Plane

(b) ST Plane

(c) SL Plane

Figure 9. SEM pictures of three orthogonal planes of extruded MA87 aluminum alloy. 7000×.

The results of the calculations are summarized in Table 8.

TABLE 8. ANALYSIS OF EXTRUDED MA87 MICROSTRUCTURE

| Plane | $\bar{L}_{\perp}$ ($\mu$m) | Q | $\Omega_{12}$ |
|---|---|---|---|
| SL | 1.52 | 2.2 | 43.7 |
| ST | 1.64 | 2.4 | 47.0 |
| LT | 0.98 | 1.7 | 32.0 |

It is apparent that the two values of $\bar{L}_{\perp}$ for the SL and ST planes are approximately equal – as would be expected. Moreover, $\bar{L}_{\parallel}$ for the ST plane should equal $\bar{L}_{\perp}$ for the LT plane. The values of Q for the SL and ST planes do not necessarily have to be equal, since the elongated, flattened grains are generally longer in the extrusion direction. The degree of orientation of grain-boundary traces in the extrusion direction reaches almost 50 percent for the ST plane; a considerably lower value of orientation is found for the LT plane.

Other quantities could be calculated for this microstructure, as desired. Normally, we would want to assess the basic microstructural quantities (Ref. 5) (such as grain size, volume fraction, spacings, particle size, etc.), and these methods are independent of anisotropy or other microstructural configurations. Special parameters are calculated as required by the microstructure and the type of property being measured (Ref. 6, p. 23).

---

6 E. E. Underwood and E. A. Starke, Jr., "Quantitative Stereological Methods for Analyzing Important Microstructural Features in Fatigue of Metals and Alloys," ASTM STP on Fatigue Mechanisms, to be published 1979.

### 2.3.2 Quantitative Microstructural Analysis of Particle Distribution

An important type of microstructure that requires special analysis is an alloy containing particles or precipitates aligned preferentially in the extrusion or rolling direction. One frequently wishes to express the extent of "stringering" or alignment of the particles quantitatively, if at all possible.

Two such microstructures with definite stringering of particles are shown in Figures 17 and 18 of a technical report by Lockheed Palo Alto Research Laboratory to AFML (Ref. 1). The microstructures were analyzed according to a method developed recently (Ref. 6) for a fatigue study. Since the procedure is new, it will be described briefly in this report. To express quantitatively the degree of particle randomness or nonrandomness, a parameter is proposed which is the ratio of the $\chi^2$ measured experimentally to that obtained from $\chi^2$ tables. This ratio, or parameter, merely expresses the degree of divergency of the experimental data from a theoretical uniform particle distribution. Since the particles exhibit a preferential alignment, a modified cell shape is employed in the form of parallel strips running in the same direction as the particle alignment. The density of particles in each strip (or cell) is counted, then analyzed according to a conventional $\chi^2$ test for goodness of fit. For perfectly uniform particle distributions, the particle density from strip to strip remains uniform; however, with pronounced stringering, the densities vary widely from strip to strip. Accordingly, the ratio

$$r = \chi_m^2 / \chi_{th}^2 \tag{4}$$

is close to unity for uniform locational distributions and can increase to 4 or 5 for nonuniform particle distributions. Here, $\chi_m^2$ stands for the measured value, and $\chi_{th}^2$ represents the tabular (or theoretical) value of $\chi^2$.

A central portion of 5 cm × 10 cm was analyzed as described above for the degree of particle positional alignment. Ten parallel, horizontal strips were laid down on each microstructure and the particle density counted in each strip. The pertinent data are given in Table 9. Surprisingly enough, the r-values are 2.75 and 2.76 for Figures 10a and 10b, respectively, confirming the qualitative observation that the microstructures appeared similar except for the number and size of particles. To quantify the particle density, we calculated the quantity $N_A$, which is defined as the number of particles per unit area of the test plant. For Figure 10a, $N_A = 81,000\ mm^{-2}$, while for Figure 10b, $N_A = 47,600\ mm^{-2}$. Thus, there appears to be a substantial coarsening of large particles and diminution of finer particles associated with the STA treatment. The particle positional distribution, however, does not appear to change substantially.

TABLE 9. ANALYSIS OF LOCATIONAL DISTRIBUTION OF PARTICLES IN Al 7075 ALLOYS FROM PWA (Ref. 1)(a)

| Specimen | Total No. of Particles | E | $\chi^2_m$ | $\chi^2_{th}$ | r |
|---|---|---|---|---|---|
| Hot pressed and Extruded (Figure 17, D3279) | 1621 | 162.1 | 42.8 | 15.5 | 2.75 |
| Hot pressed Extruded and STA (Figure 18, D3546) | 952 | 95.2 | 42.7 | 15.5 | 2.76 |

(a) E is the expected value; $\chi^2_m$ and $\chi^2_{th}$ are the measured and tabular values of $\chi^2$, respectively; the degrees of freedom, $\nu = 8$; the probability, $p = 0.05$; and $r = \chi^2_m/\chi^2_{th}$.

2.3.3 Microstructural Analyses Related to Processing Variables

The effects of various process variables on the structure-property relationships were recently investigated by ALCOA Research Laboratories in several MA87-type powder

Figures 17 and 18 from the reference AFML Report (Ref. 1) are reproduced here as Figure 10.

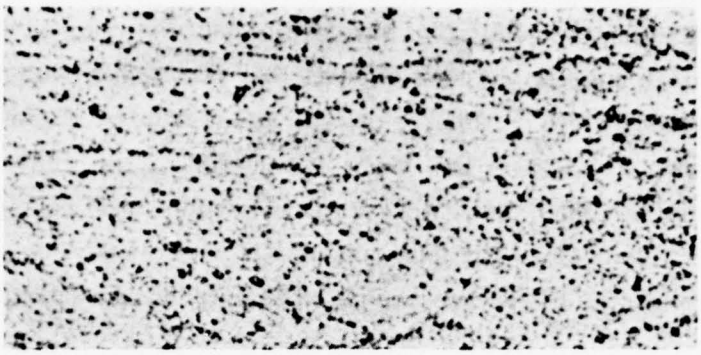

(a) As-extruded condition. 500×
(Figure 17 in AFML Report, Ref. 1)

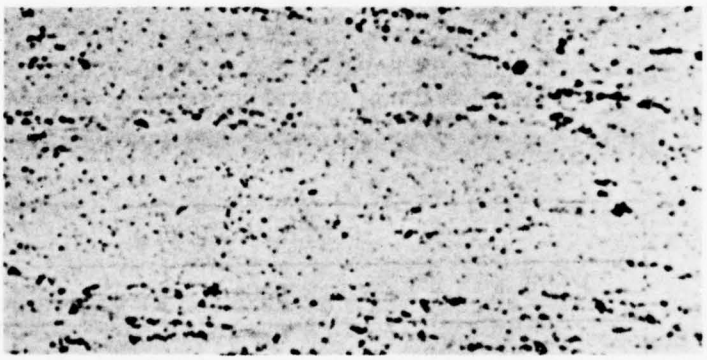

(b) Solution-treated and aged. 500×
(Figure 18 in AFML Report, Ref. 1)

Figure 10. Al 7075 alloys from helium atomized rapidly solidifed particulate, hot-pressed and extruded at 700 K. (After Ref. 1)

metallurgy alloys (Ref. 7). Two microstructures are particularly significant, primarily because "no obvious structural differences" could be seen between the two; and yet, the ABC-triple upset and draw forgings had "greatly improved fatigue behavior" over the A-single upset and draw forgings.

Two photomicrographs from W. L. Otto's report to AFML (Ref. 7), Figures 27 and 30, are reproduced here as Figure 11, Parts a and b, respectively. Several points of difference in these microstructures are noted and discussed below for consideration.

1. In Figure 11a, the grain boundaries are quite irregular, are loaded with particles, and show "depleted" zones (light regions along the boundaries and at particles), whereas, in Figure 11b there appear to be fewer irregularities at grain boundaries (smoother, planar), much fewer coarse particles at grain boundaries, and little of the depletion at grain boundaries.
2. In Figure 11b, dark halos are seen around larger Co-rich particles, there appear to be more of the intermediate-size Co-particles, and there are almost no particles at grain boundaries acting as pinning points. In Figure 11a, there appear to be relatively more of the darker Co particles. Size distributions should be different, and a rough idea can be gained by visual inspection of Figures 11a and 11b (provided that foil thicknesses in the two cases are approximately equal).
3. In Figure 11b, dislocation pinning is almost absent compared with Figure 11a, where loops, dislocation line breakaways, and some interactions are visible. Some evidence for planar dislocation arrays are seen in Figure 11b, but none in Figure 11a. Moreover, localized strain fields seems more common in Figure 11a than in Figure 11b. Note that the localized darkening in otherwise homogeneous grains occurs mostly on the concave side of the boundary.
4. It is also noteworthy that the grain size in Co-free alloys is much larger than in Figures 11a or 11b. Apparently grain growth in these alloys is controlled somewhat by Co in solid solution, since particles are in grain boundaries only in Figure 11a.

---

7 W. L. Otto, Jr., Metallurgical Factors Controlling Structure in High Strength P/M Products, AFML-TR-76-60, May 1976.

Figure 11a. MA87, A-upset and draw hand forging. T6 temper. (Figure 27 in Ref. 7).

Figure 11b. MA87, ABC-upset and draw hand forging. T6 temper. (Figure 30 in Ref. 7).

Any conclusions drawn from the microstructural differences in Figures 11a and 11b must be based on the assumption that the photomicrographs are representative and typical. On this basis, the most obvious implication of the serrated, rough, particle-loaded boundaries in Figure 11a is that the ledges and particles act as excellent sources for dislocation activity. By contrast, in Figure 11b, the smooth (ledge-free) boundaries without appreciable particles are not as potent dislocation sources. Moreover, the depleted boundary zones in Figure 11a would correspond to a softer boundary layer, permitting easier dislocation generation. The lack of dislocation pinning in Figure 11b can be taken as indirect evidence of a lower level of dislocation generation from boundaries and particles than in Figure 11a.

Several results can be attributed to the triple upset operation (Figure 11b). The severe plastic deformation during hot working should promote a more homogeneous microstructure through recrystallization, particle dissolution, and grain-boundary migration to equilibrium positions. Enhanced diffusion rates, particularly along grain boundaries, would help to dissolve particles at grain boundaries. Thus, the matrix Co-content should be greater in the ABC-upset MA87. The factors emerging from this microstructural analysis appear to support the finding of enhanced mechanical properties in the triple-upset MA87 alloys in the following ways: (1) fewer dislocation sources at grain-boundary ledges and grain-boundary particles, (2) higher Co-concentration in solid solution, thus a higher strength matrix, and (3) fewer sites with localized strain gradients (lower internal stress).

An important additional consideration in this study of the effects of 0.4-percent Co is that of grain-boundary segregation of solute element(s). Equilibrium segregation to boundaries, which may be either positive or negative, tends to occur whenever the total free energy of the system is lowered thereby. Previous studies of third-element (trace) effects on solute diffusivity and segregation are striking. In one investigation, trace amounts of Cr caused Zn in an Al-base alloy to segregate strongly to grain boundaries. With a nominal 19-percent Zn concentration, the addition of a fraction of a percent of Cr was accompanied by Zn segregation to boundaries in the amount of 50 percent or more. The opposite effect (depletion) at grain boundaries has also been studied

experimentally in other systems. Thus, microprobe studies of Co-concentrations and Co-gradients at selected locations, although important in their own right, may also relate to significant segregational effects of other solutes (Zn, for example). Crack growth rates may well be influenced by these segregational effects at grain boundaries.

Co particle-size distribution studies, although laborious and inexact in thin foils, may prove useful in assessing the degree of (thermal) homogenization which has occurred in the alloy. Also, the size and location of particles have influence on crack growth rates as well as dislocation activity. Accordingly, microscopical studies of crack growth paths should be correlated with quantitative particle information (grain-boundary density, spacing in matrix, volume fractions, area fractions occupied on grain-boundary surfaces, etc.) and solute segregational behavior (equilibrium segregation, uniformity in matrix, grain-boundary depletion, partitioning of Co between boundaries and matrix, and effects on other solutes).

The above comments document a significant body of microstructural differences between the two alloys shown in Figures 11a and 11b. It is possible that a detailed, quantitative metallographic analysis will provide further insight into the reasons for the improved fatigue behavior of the triple-upset and draw alloy.

### 2.3.4 Microstructural Analyses of Features Revealed by Transmission Electron Microscopy

The final topic discussed on this task concerns some general problems in the analysis of particulate microstructures as seen by TEM. Figure 12 represents some fairly spherical particles clustered together in a thin foil. Some overlapping can be seen, and truncation of particles near the upper or lower foil surface is probable, but not detectable.

We wish to analyze this structure as accurately as possible; this is basically a problem involving projected images (Ref. 8). A procedure is indicated whereby the volume fraction, $V_V$, and number of particles per unit volume, $N_V$, can be calculated for

---

8 E. E. Underwood, "The Stereology of Projected Images," Jnl. of Microscopy, Vol. 95, Pt. 1, 1972, p. 25.

Figure 12. Clustered particles in thin foil. 20,000×.

various conditions. We start by counting the number of particles, $N' = 31$, which yields $N'_A = 2.06\ \mu m^{-2}$. (Note that the prime signifies a quantity appearing on the projection plane.) A point count gives $P'_P = 0.11$, so that the mean projected area $\bar{A}' = A'_A/N'_A = 0.11/2.06 = 0.053\ \mu m^2$. Now, to calculate $V_V$ and $N_V$, some assumptions are required. We assume that the particles have a spherical shape and that the foil thickness $t = 2000$ A. Thus, the mean projected diameter $\bar{H}' = 0.26\ \mu m$ for spheres of mean diameter D.

The volume fraction can now be calculated for three cases: (1) no correction for truncation or overlap; (2) a truncation correction only, and (3) both a truncation and overlap correction. The applicable equations and results for spherical particles are, respectively:

$$\text{Case 1:} \quad V_V = (2/3) A'_A D/t = \frac{2}{3}(0.11)(0.26)/0.2 = 0.0953 \tag{5}$$

$$\text{Case 2:} \quad V_V = A'_A [2D/(2D + 3t)] = (0.11)[0.52/(0.52 + 0.5)] = 0.0511 \tag{6}$$

$$\text{Case 3:} \quad V_V = -\ell n(1 - A'_A)[2D/(2D + 3t)] = -\ell n\, 0.89\,[0.52/(0.52 + 0.6)] = 0.0541 \tag{7}$$

Note that the uncorrected volume fraction decreases when the truncation correction is applied, and that the latter increases slightly when the overlap correction is included.

The values of $N_V$ can also be calculated for the same three cases:

$$\text{Case 1:} \quad N_V = N'_A/t = 2.06/0.2 = 10.30\ \mu m^{-3} \tag{8}$$

$$\text{Case 2:} \quad N_V = N'_A/(D + t) = 2.06/(0.26 + 0.2) = 4.48\ \mu m^{-3} \tag{9}$$

$$\text{Case 3:} \quad N_V = (N'_A + M'_A)/D + t) = (2.06 + M'_A)/0.46 \tag{10}$$

Here $M'_A$ is the number of particle images per unit area lost by overlap. $M'_A$ is a function of the degree of particle overlap and the ability to resolve overlaps into the constituent particle images. It may be approximated by $M'_A = (3/2)\, V_V\, (t/D)$ $N'_A = 0.014\ \mu m^{-2}$, which, when introduced into Equation (10) gives

$$\text{Case 3:} \quad N_V = (2.06 + 0.014)/0.46 = 4.51\ \mu m^{-3} \tag{11}$$

This value amounts to above a 1% increase in $N_V$ due to overlap effects. As a rule of thumb, a correction for overlap should not be necessary if $V_V\, (t/D) < 0.04$. Here we find that this quantity equals 0.039. It is obvious that the truncation correction can be appreciable, although sometimes its magnitude cannot be estimated. In any event, the value of $A'_A$ should never be used for $V_V$, although this is seen occasionally in the literature.

The above examples should help to illustrate some available approaches for quantitative microstructural analysis of various alloys to be studied. After processing procedures are established, adequate statistical sampling and measurements will be necessary to obtain correlations of selected alloys with mechanical properties.

## 2.4 TASK 4 – APPLICATION STUDIES

Task 4 is being performed by the Lockheed-California Company of Lockheed Corporation.

### 2.4.1 Model for Prediction of Weight Savings

A model has been developed for predicting weight savings in certain aircraft structures resulting from substitution of advanced aluminum alloys for currently used aluminum and other structural materials. The present form of this model is described in detail in Appendix C. The model is relatively simple and is suitable for computerized calculation of weight savings for a selected aircraft when many sets of mechanical and physical properties of either hypothetical alloys or actual experimental alloys are considered.

The purpose of such model development is to provide useful guidance for alloy and process development where priorities in selected properties would significantly increase payoffs in terms of weight savings and related benefits. The model described in Appendix C was first developed for analysis of the S-3A Viking carrier-based naval patrol plane because the structural configuration, critical structural design criteria, and weight breakdowns were readily available. However, the model is applicable to weight savings analyses for any aerospace structure for which the detailed design criteria are known. Some illustrations of the usefulness of the model are presented in the following.

The method described in Appendix C was used to calculate the weight savings of primary aluminum structure for the S-3A Viking assuming substitution of alloys exhibiting a wide range of properties. The properties and ranges assumed were: modulus of elasticity from 10 to $14 \times 10^6$ psi (68.9 to 103.4 GPa), density from 0.09 to 0.11 lb $in.^{-3}$ (2.49 to 3.04 g $cm^{-3}$), and strength (yield strength, ultimate strength in tension and compression) from 100 to 140 percent. Weight savings calculated in terms of percent of primary aluminum structure are presented in Figures 13, 14, and 15 for assumed strengths of 100, 120, and 140 percent, respectively. The dotted lines

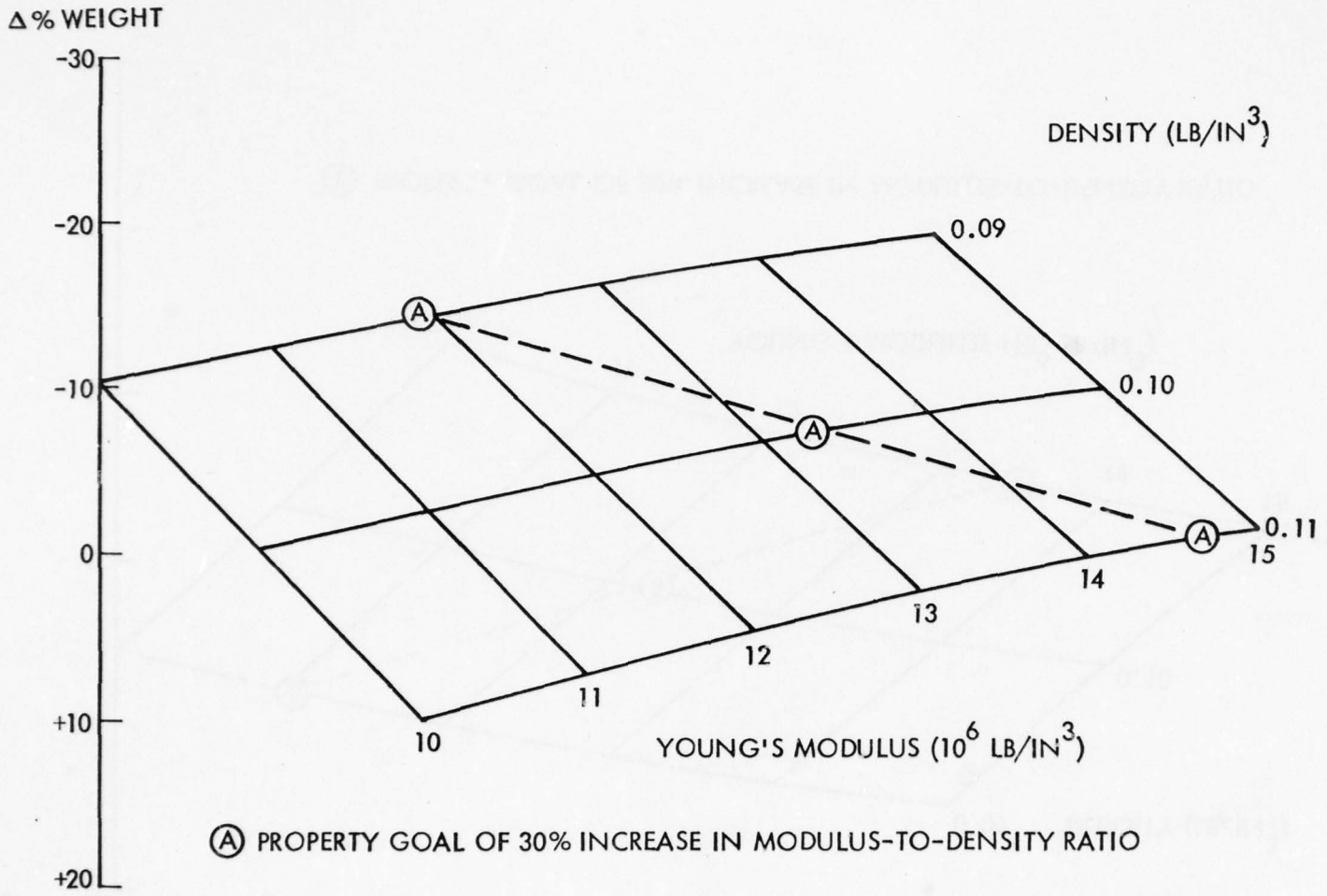


Figure 13. Effect of elastic modulus and density on calculated weight change of primary aluminum structure in S-3A Viking airplane. Assumed no change in strength.

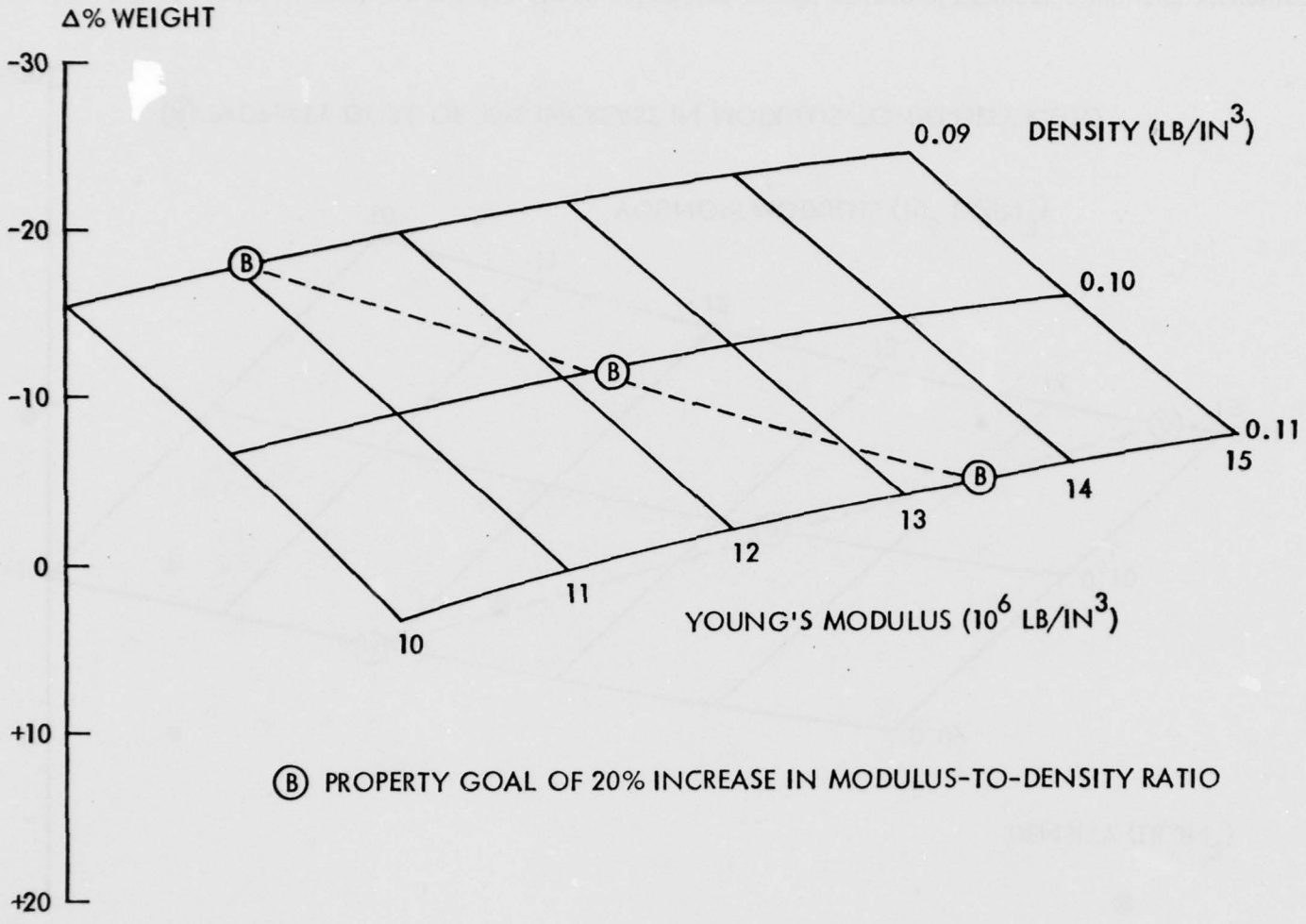


Figure 14. Effect of elastic modulus and density on calculated weight change of primary aluminum structure in S-3A Viking airplane. 20% increase in strength assumed.

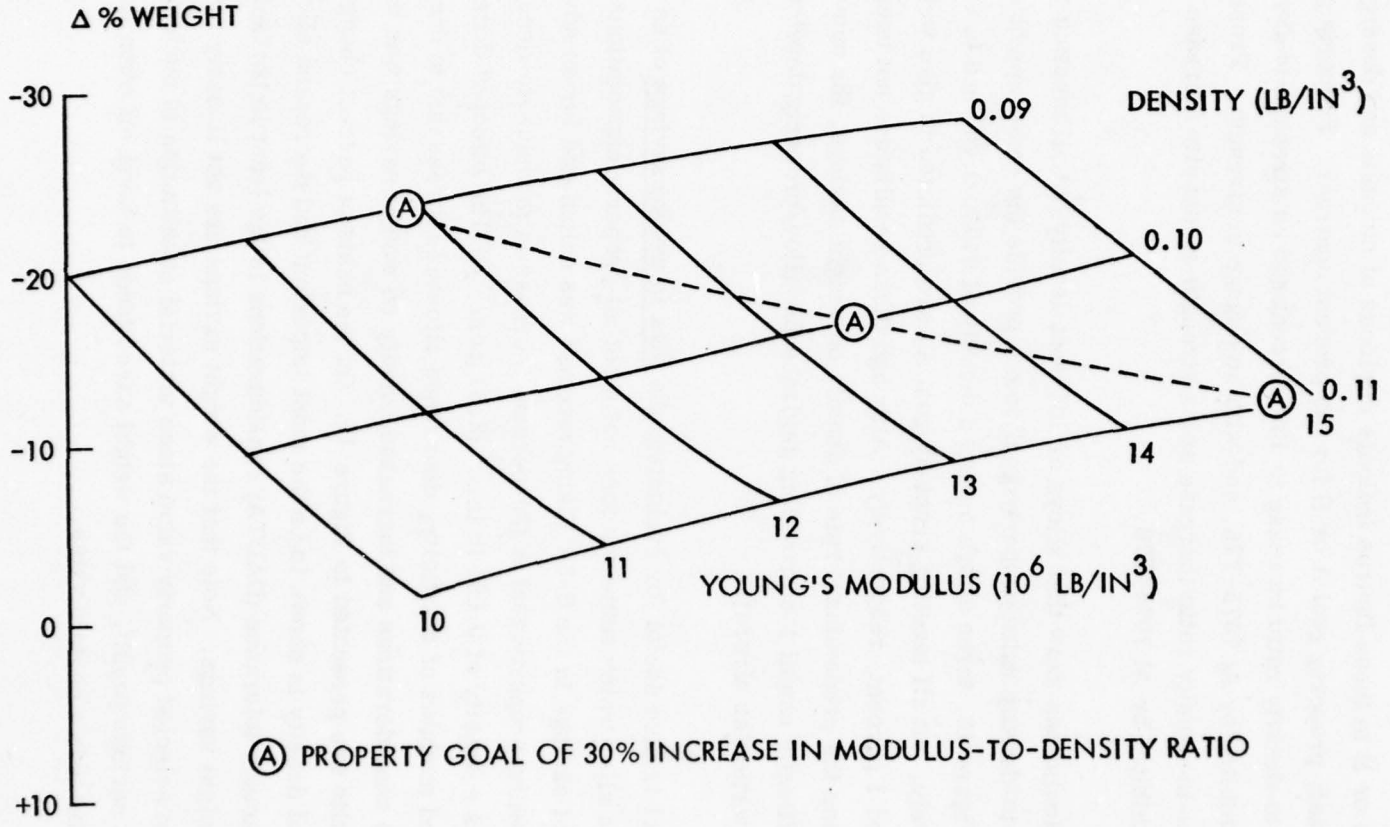


Figure 15. Effect of elastic modulus and density on calculated weight change of primary aluminum structure in S-3A Viking airplane. 40% increase in strength assumed.

marked A or B in these figures indicate the locus of modulus and density combinations which satisfy property goal A or B for the present contract. Property goal A is a modulus-to-density ratio increase to 130 percent and no strength-to-density increase of that exhibited by Al 7075-T76, and with no change in strength. Property goal B is a modulus-to-density ratio increase and a strength-to-density increase to 120 percent of that exhibited by Al 7075-T76.

These calculations show that alloys of different density but all meeting the same modulus-to-density ratio property goal do not provide the same weight savings. As seen in Figure 13, three alloys having a density of 0.09, 0.10, and 0.11 lb $in.^{-3}$, respectively, but all meeting property goal A, are predicted to give weight savings of 14, 7, and 1 percent, respectively. Although these results are not unexpected, recognizing the predominant role of density on weight savings, the numerical values are specifically useful for providing guidance for alloy/property development goals for this particular aircraft.

The model is also useful for evaluating the loss in weight savings of an advanced aluminum alloy which somehow does not meet all property expectations. For example, the weight savings in the S-3A Viking aircraft was calculated for an advanced aluminum alloy meeting property goal A (30-percent increase in modulus-to-density ratio) but which has a density of 0.091 lb $in.^{-3}$ (2.51 g $cm^{-3}$). The effect of decreased strength, decreased modulus of elasticity, decreased allowable stress due to damage tolerance (DADTA) considerations and increased density on weight savings was then calculated. The results are presented in Figure 16. On the basis of percent change in property, increased density is shown to be the most important and decreased allowable stress due to damage tolerance (DADTA) considerations is the least important for retaining initial weight savings. Note that the weight savings are not linearly proportional to change in selected property value since material substitution is made where there is a weight savings payoff, and the weight saved tends to level off when the property change exceeds a certain value.

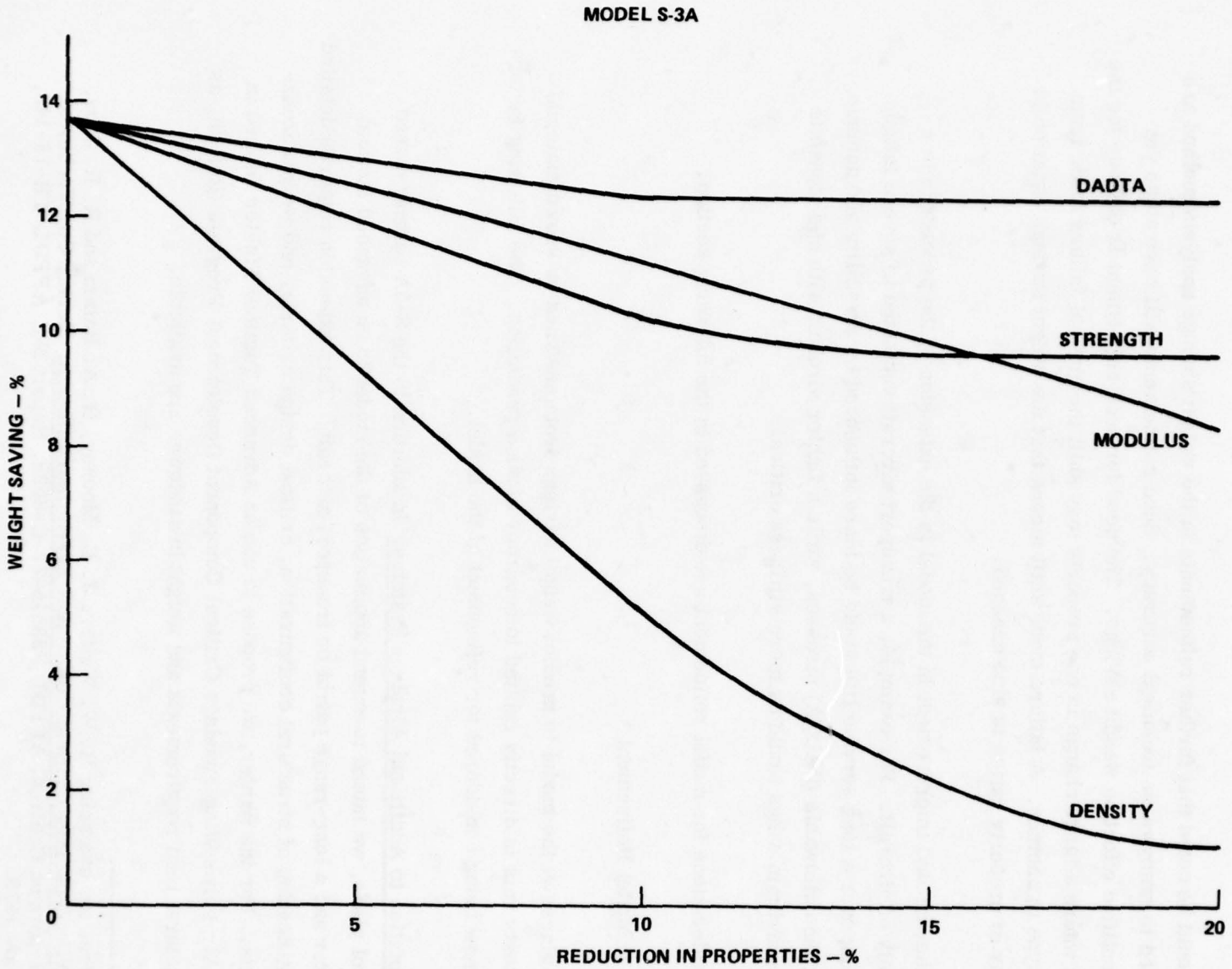


Figure 16. Effect of reduction in properties on weight saving.

It should be noted that further refinements in the weight savings analysis method are needed to improve its technical accuracy. Such refinements will have some yet unidentified effect on weight savings. The need for such refinement is obvious for the case where a large change in one property may shift the critical failure mode from one type to another. A failure mode shift means that the weight savings equation in terms of property ratios is also changed.

Another needed improvement in the model is the extension of the procedure to a variety of aircraft. For example, a transport aircraft subjected to severe fatigue loading over a long service life would be more influenced by durability and damage tolerance allowable (DADTA) stresses, while a fighter aircraft with high dynamic loads and thin wings would be more stiffness critical.

Considerations for model refinement are discussed in the following section.

### 2.4.2 Model Refinement

Usefulness of the model to predict weight savings from assumed or known material property sets is directly related to accuracy of such prediction. The following factors are now being considered for refinement of the model.

Adaptation to Additional Airplane Systems. In addition to the S-3A carrier-based patrol plane, we intend to extend application of the model to an advanced tactical fighter and a long-range patrol or transport aircraft. This extension requires detailed identification of structural configuration, critical design criteria, and weight breakdowns. For the fighter, we propose to use an Advanced Tactical Fighter defined in the Air Force Wing Fuselage Critical Component Development Program (Ref. 9), as structural load requirements and weight breakdowns are available.

---

9 See, for example, R. W. Walter, J. E. Mooney, R. A. Hamm and R. R. June, Wing/Fuselage Critical Component Preliminary Design, Boeing Co. Technical Report on Contract AFFDL F33615-77-C-5228, Report No. AFFDL-TR-78-146, Nov 1978.

The results obtained from weight savings analysis of the S-3A are translatable to various versions of the V/STOL aircraft, as demonstrated previously (Ref. 1).

For the long-range patrol or transport aircraft, the P-3 ASW patrol plane is proposed for analysis. The structural service load requirements for this plane are similar to cargo jets or wide body transports, and a suitable design base and service history are both available.

Extension of Advanced Aluminum Alloy Usage. In the preliminary model described in Appendix C, the primary structures considered for advanced aluminum alloy substitutions include only about 75 percent of the total airframe weight. A refinement in the model will obtain by considering aluminum usage in additional parts of the airframe. This includes portions of the landing gear, and engine nacelles. Additionally, substitution of advanced aluminum alloys in nonprimary structure of fixed equipment will also be considered. These components include equipment racks, access doors and fillets, fairing, and controls. As shown in Table 10, the weight of fixed equipment for a variety of airplane types equals or exceeds the weight of the wing structure. This table presents the structural weight groups in terms of percent of gross weight for a carrier ASW patrol, fighter, transport, and long-range patrol planes. Inspection of this table reveals significant weight savings are to be expected by substituting low density aluminum alloys in fixed equipment applications.

Increase in Critical Failure Categories. The weight savings analysis model presently incorporates seven critical failure categories, described in Appendix C. Refinement of the model may result from the inclusion of additional critical failure categories as follows.

TABLE 10. PERCENTAGE GROSS WEIGHT BREAKDOWN

| | Carrier ASW Patrol | Transport | Fighter | Long Range Patrol |
|---|---|---|---|---|
| Empty Weight | 55.2 | 51.8 | 62.5 | 48.8 |
| Structure | (27.9) | (31.3) | (35.7) | (21.5) |
| Wing | 10.1 | 10.9 | 13.4 | 6.5 |
| Tail | 2.5 | 2.0 | 2.0 | 1.4 |
| Body | 10.3 | 11.6 | 13.1 | 7.3 |
| Landing Gear | 3.4 | 4.7 | 4.3 | 2.7 |
| Air Induction, Nacelles and Pylons | 1.6 | 2.1 | 2.9 | 3.6 |
| Propulsion | 7.1 | 9.1 | 16.8 | 11.0 |
| Fixed Equipment | 20.2 | 11.5 | 10.0 | 16.3 |
| Fuel | 23.0 | 24.4 | 24.3 | 42.8 |
| Payload, Crew and Operating Equipment | 21.8 | 23.7 | 13.2 | 3.0 |

| Number of Additional Categories | Description |
|---|---|
| 2 | Nonoptimum Factors: Add categories for minimum gage for handling and attachment and for parasitic weight. |
| 2 | Compression Surface: Extend single category to three based on loading intensity (N) of 1500 lb/in., 5000 lb/in. and 10,000 lb/in. Include substructure spacing changes. |
| 3 | Shear: Include shear categories based on loading index (q) of 200 lb/in., 500 lb/in., and 500 lb/in. Include substructure spacing changes. |
| 3 | Aeroelastic Stiffness: Consider load/in. and type of structure. Include substructure spacing and ratio of skin to skin-and-stiffener area. |
| 2 | DADTA – Cutoff: Consider different cutoff values for fuselage, wing and tail, and type of structure. |

Extension of the compression surface failure category has been started. The basic equations for weight ratio calculation have been modified to include the effect of load intensity level (N) and structural shape. A higher load level requires a higher allowable stress, which results in more importance of the plastic stress-strain behavior of the structural material.

To meet this requirement, the tangent modulus in the column equation and the secant modulus in the crippling equation, based on Ramberg-Osgood stress-strain representation, must be included. The allowable stress versus load intensity/rib spacing, N/L, for a typical structural shape is shown in Figure 17. The allowable stress curve flattens out at high load intensity due to inclusion of plasticity effects.

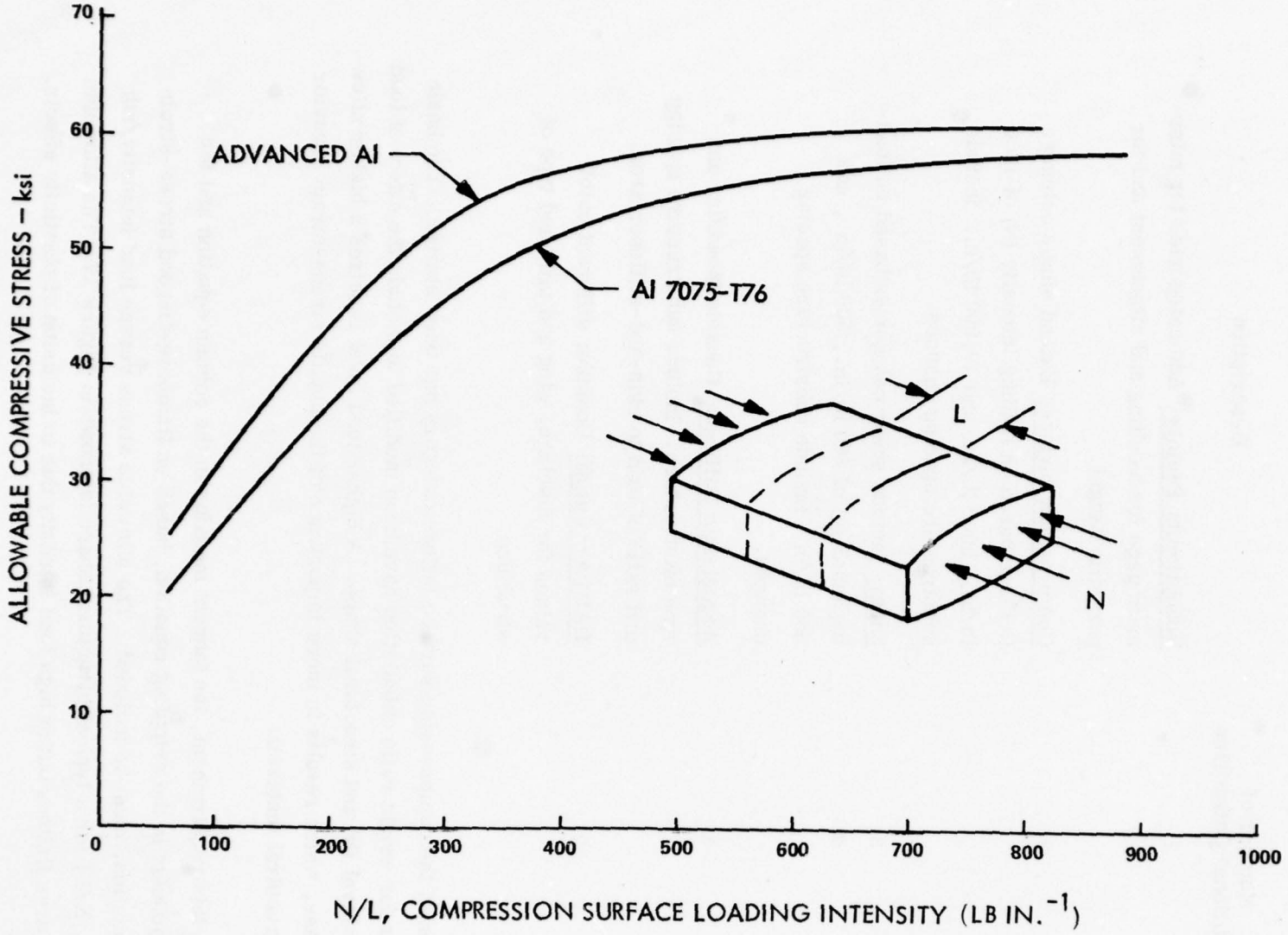


Figure 17. Effect of compression surface loading intensity on allowable compressive stress for Al 7075-T76 alloy and an advanced aluminum alloy having 30 percent higher modulus of elasticity. Compressive yield strength, $F_{0.7}$, of 64.7 ksi and Ramberg-Osgood parameter, n, of 25 are assumed.

Two curves are shown on this figure, one based on 7075-T76 properties and the other based on an advanced alloy with a modulus (E) increase of 30%.

Figure 17 also shows the effect of rib spacing on allowable stress. At a high load intensity, the rib spacing can be increased with little effect on allowable stress. At lower load intensity, the rib spacing is more critical. This finding demonstrates the importance of including rib weight and rib spacing in the analysis.

The rib weight versus distance from wing root for the S-3A Viking is shown in Figure 18.

This rib weight function will be combined with allowable stress based on loading intensity represented by Figure 16 to derive the weight ratio equation for each of three levels of load intensity. This derivation will provide the additional compression surface category extension. An approach similar to this will be derived for additional load categories.

Consideration of Shift in Governing Properties. For each particular structural component, one or more properties dominate in controlling weight savings. If a large change in one of these properties is invoked, then the weight savings may no longer be controlled by the same properties and another design criterion may become critical. This criterion requires refinement of the weight savings method to accommodate such changes. Consequently, a second tier screening procedure is to be developed, as follows.

| 1st Tier | 2nd Tier |
|---|---|
| DADTA | Stiffness |
| Strength | Stiffness |
| Stiffness | Strength |
| Stiffness | DADTA |

A limitation of allowable thickness will be assigned to all items.

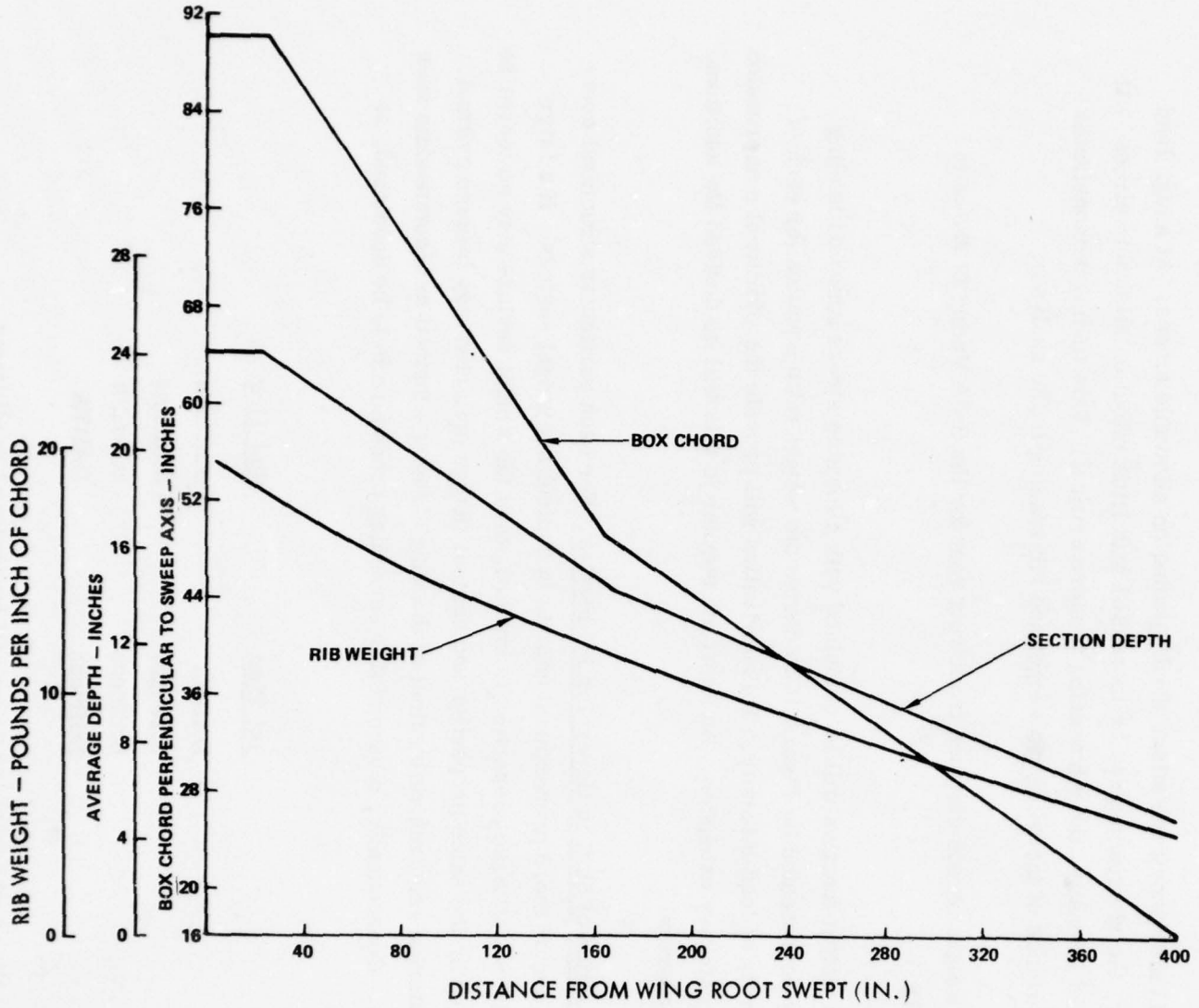


Figure 18. Effect of distance from wing root on rib weight, section depth and box chord length for S-3A Viking airplane wing.

Review of Allowable Stress for Durability and Damage Tolerance Assessment (DADTA). Various factors involved in the DADTA analysis for allowable stress are to be reviewed, and improvements in accuracy are to be developed which affect prediction of weight savings. The factors which affect ultimate stress cutoff (upper limit for ultimate stress) are fatigue, residual strength, crack growth behavior, and stress corrosion resistance. Approaches being pursued in each of these categories for improving the accuracy of weight savings analysis are described below.

- Fatigue. A preliminary equation relating design stress and fatigue life has been established. The service life data of operational aircraft have been reviewed in terms of design stress cutoff and service life achieved. Data for the Electra, F-104, and T-33 were used to determine the relation between design or reference stress and service of full-scale fatigue test life. These data are plotted in Figure 19. The data for 2024-T3 aluminum tested under spectrum loading indicates a typical log-linear relationship for fatigue. Each aircraft type will have a stress/life relationship which is nearly parallel to the experimental data for 2024-T3 aluminum alloy. Note the distinctly different curves for the fighter/trainer aircraft and for transport aircraft.
- Residual Strength. The residual strength cutoff is related to the material fracture toughness properties and the critical crack size applicable to a particular type of aircraft. This information is to be evaluated to determine minimum fracture toughness properties applicable to a high-performance fighter and long-range patrol aircraft. The relation between design stress and fracture toughness will also be reviewed. This review will include data from the F-104, Electra, and P-3 aircraft.
- Crack Growth. The crack growth properties of a material are important for defining frequency of inspections necessary to find detectable cracks. The rate of crack growth for service aircraft will be reviewed to improve the equation used for establishing the DADTA cutoff. An inspectable crack size will be selected, and the stresses and da/dN properties applicable to specific aircraft will be evaluated. These crack growth rates will be compared with necessary inspection intervals obtained from service experience. Data for the Electra, P-3 and a fighter aircraft will be reviewed to define applicable criteria.

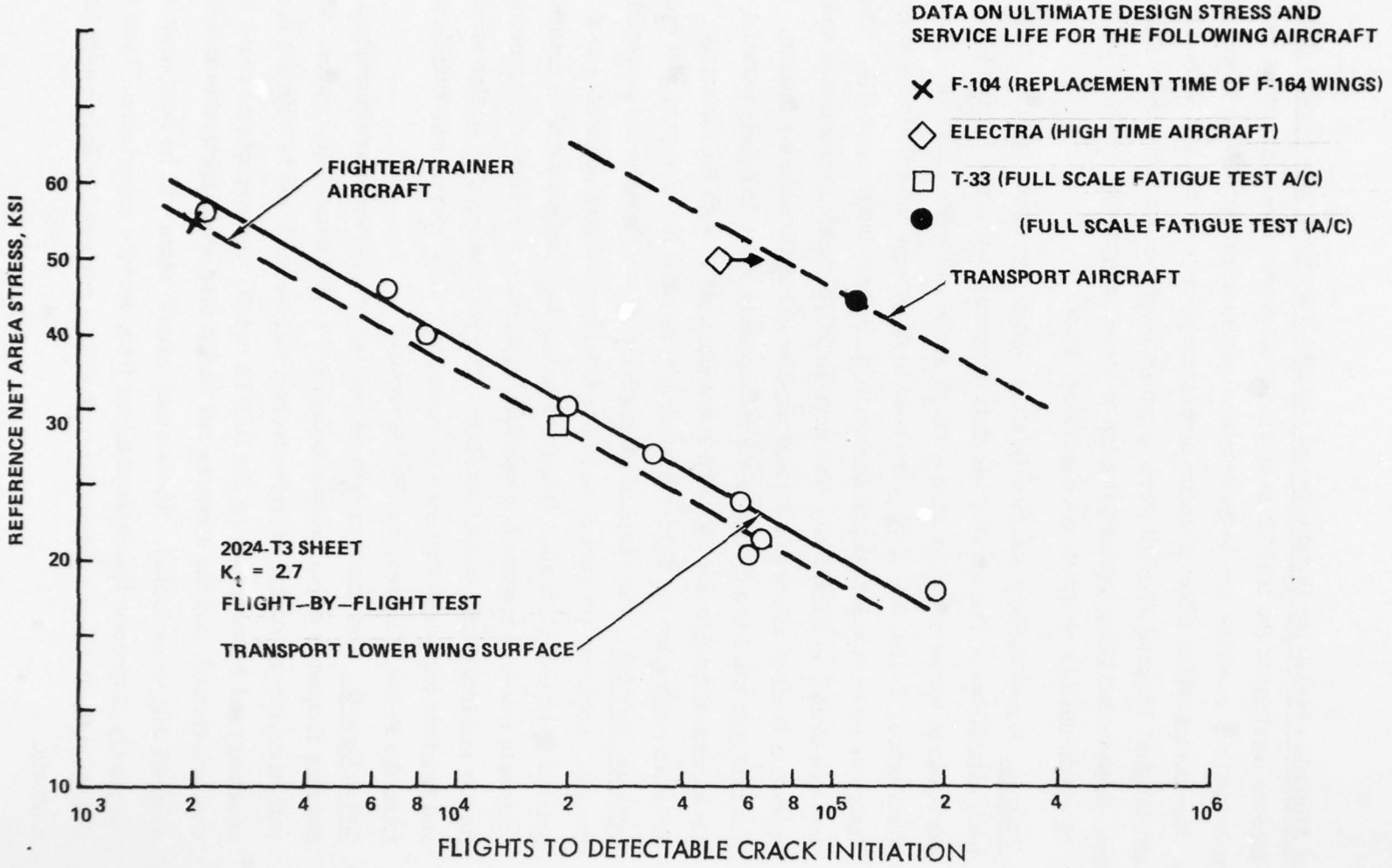


Figure 19. Relation of net area stress to flights required to obtain detectable crack initiation for fighter/trainer and transport aircraft.

- Stress Corrosion. The cutoff values for stress corrosion will be reviewed with an increased emphasis on residual stresses. Material processing and fabrication procedures influence the residual stress magnitude, and this affects the allowable stress and cutoff values. The objective of this study will be to establish minimum acceptable stress-corrosion values for screening of developmental alloys. Levels above the minimum acceptable stress will be considered in appropriate weight savings equations.

## Section 3
## CONCLUSIONS

1. A number of promising compositions, with and without Li additions, have been identified which will provide a sound basis for development of advanced aluminum alloys to achieve the desired property goals.

2. Metallographic examination of a trial alloy splat (Al-6Mn) revealed that the smaller-size screen fraction particulate includes atomized powder which cooled at a substantially slower cooling rate than the splat particulate comprising larger-size screen fractions. Modification from cold gas to preheated gas atomization is indicated as a way to increase the cooling rate of smaller-size particulate by maintaining liquidity of atomized droplets until splatted on the cold substrate.

3. The methodology developed for prediction of weight savings from property data for improved aluminum alloys is simple to use and provides key guidance for alloy and process development. Refinements being developed in the analysis will further improve the accuracy of predicted weight savings.

## Section 4
## REFERENCES


1 R. E. Lewis, D. Webster, and I. G. Palmer, A Feasibility Study for Development of Structural Aluminum Alloys From Rapidly Solidified Powders for Aerospace Structural Applications, Lockheed Palo Alto Research Laboratory Final Report, Contract F33615-77-C-5186, Technical Report No. AFML-TR-78-102, July 1978

2 W. B. Pearson, Handbook of Lattice Spacings and Structures of Metals, New York, Pergamon Press, 1958, p. 338

3 Joint Committee of Powder Standards (1978), Swarthmore, PA

4 H. Matyja, B. C. Giessen, N. J. Grant, "The Effect of Cooling Rate on the Dendrite Spacing in Splat-Cooled Aluminum Alloys," J. of the Institute of Metals, Vol. 96, 1968, p. 30

5 E. E. Underwood, Quantitative Stereology, New York, Addison-Wesley, 1970, p. 48

6 E. E. Underwood and E. A. Starke, Jr., "Quantitative Stereological Methods for Analyzing Important Microstructural Features in Fatigue of Metals and Alloys," ASTM STP on Fatigue Mechanisms, to be published in 1979

7 W. L. Otto, Jr., Metallurgical Factors Controlling Structure in High Strength P/M Products, AFML-TR-76-80, May 1976

8 E. E. Underwood, "The Stereology of Projected Images," Jnl. of Microscopy, Vol. 95, Pt. 1, 1972, p. 25

9 See, for example, R. W. Walter, J. E. Mooney, R. A. Hamm and R. R. June, Wing/Fuselage Critical Component Preliminary Design, Boeing Co. Technical Report on Contract AFFDL F33615-77-C-5228, Report No. AFFDL-TR-78-146, Nov 1978

A-1 T. H. Sanders, and E. S. Balmuth, "Aluminum-Lithium Alloys: Low Density and High Stiffness," Metal Progress, Vol. 113, No. 3, 1978, p. 32

A-2 D. Webster, Unpublished LMSC Independent Research Work, 1977

A-3 K. K. Sankaran, "Structure and Properties of Splat Quenched 2024-Type Aluminum Alloys Containing Lithium," Ph. D. Thesis, MIT, Cambridge, MA. 1978

A-4 T. H. Sanders and R. R. Sawtell, "Structure and Fracture Behavior of Al-Li Sheet," 107th AIME Annual Meeting, Denver, CO, Feb 26 – Mar 2, 1978

A-5 T. H. Sanders, J. W. Evancho, and J. T. Staley, "Microstructure and Mechanical Behavior of Al-Mg-Li Alloys," 107th AIME Annual Meeting, Denver, CO, Feb 26 – Mar 2, 1978

A-6 T. H. Sanders and R. R. Sawtell, "Fatigue, Fracture, and Microstructure of Al-Cu-Li Alloys," 107th AIME Annual Meeting, Denver, CO, Feb 26 – Mar 2, 1978

A-7 A. Kelly and R. B. Nicholson, "Precipitation Hardening," Progress in Material Science," Vol. 10, No. 3, 1963, p. 372

A-8 E. A. Starke and G. Lutjering, "Cyclic Plastic Deformation and Microstructure," ASM Materials Science Seminar, Fatigue and Microstructure, St. Louis, MO, 14 – 15 Oct 1978

A-9 G. T. Hahn and A. R. Rosenfield, "Metallurgical Factors Affecting Fracture Toughness of Al Alloys," Met. Trans. A., Vol. 6A, 1975, p. 653

A-10 G. G. Garrett and J. F. Knott, "The Influence of Compositional and Microstructural Variations on the Mechanism of Static Fracture in Aluminum Alloys," Met. Trans. A., Vol. 9A, 1978, p. 1187

A-11 Fulmer Research Institute advertising flyer, undated

A-12 F. R. Billman, private communication, 1978

A-13 J. M. Silcock, "The Structural Aging Characteristics of Al-Cu-Li Alloys," J. Inst. Metals, Vol. 88, 1959 – 1960, p. 357

A-14 E. Sahin and H. Jones, "Extended Solid Solubility, Grain Refinement and Age-Hardening in Al – 1 to 13 wt% Zr Rapidly Quenched From the Melt," Third International Conference on Rapidly Solidified Metals, University of Sussex, Brighton, England, 3 – 7 July 1978

A-15 G. Thursfield and M. J. Stowell, "Mechanical Properties of Al-8 wt% Fe-Based Alloys Prepared by Rapid Quenching From the Liquid State," J. Mater. Sci., Vol. 9, 1974, p. 1644

A-16 J. P. H. A. Durand, R. M. Pelloux, and N. J. Grant, "Properties of Splat Quenched 7075 Al Type Alloys," Proc. Second Int. Conf. on Rapidly Quenched Metals, Vol. II, 1978, p. 247

A-17 J. P. Lyle and W. S. Cebulak, "Powder Metallurgy Approach for Control of Microstructure and Properties in High Strength Al Alloys," Met. Trans., Vol. 6A, 1975, p. 685

A-18 W. L. Otto, Metallurgical Factors Controlling Structure in High Strength Al P/M Products, Final Report, Contract No. F33615-74-C-5077, AFML-TR-76-60, May 1978

A-19 E. A. Starke, Jr., "Aluminum Alloys of the 70's: Scientific Solutions to Engineering Problems," An invited review, Material Sci. Eng., Vol. 29, 1977, p. 99

B-1 W. Koster, W. Rauscher, "The Relationship Between the Modulus of Elasticity of Two-Phase Alloys and Their Structure," Z. Metallkunde, Vol. 39, 1948, p. 111

B-2 G. Bradfield, "Influence of Electron Concentration on the Elasticity of Al Alloys," Phil Mag., Vol. 13, 1966, p. 211

B-3 K. R. VanHorn, "Aluminum," Vol. 1, Properties, Physical Metallurgy and Phase Diagrams, ed. K. R. VanHorn, American Society for Metals, 1967, p. 181

B-4 E. Kovacs-Csetenyk, "The Effect of a Small Amount of Additional Elements on the Young's Modulus of High Purity Aluminum," Aluminum, Vol. 11, 1976, p. 669

B-5 P. Ganesan, G. A. Sargetn, R. J. DeAngells, "A Method to Estimate the Volume Fraction of Precipitates With Ellipsoidal Morphology From Elastic Modulus Data," Metallography, Vol. 10, 1977, p. 399

B-6 H. Gleiter, E. Hornbogen, "Precipitation Hardening by Coherent Particles," Mat. Sci. Engr., Vol. 2, 1968, p. 285

B-7 L. M. Brown, R. K, Ham, "Dislocation-Particle Interactions," Strengthening Mechanisms in Crystals, Eds. A. Kelly and R. B. Nicholson, New York, John Wiley and Sons, 1971, p. 12

B-8 A. W. Thompson, "Substructure Strengthening Mechanisms," Met. Trans., 1977, Vol. 8A, p. 833

B-9 R. J. McElroy, Z. C. Szkopiak, "Dislocation-Substructure-Strengthening in Mechanical-Thermal-Treatment of Metals," Intn'l Met. Rev., Vol. 17, 1972, p. 178

B-10 G. Waldman, G. Sulinski, and H. Marcus, "The Effect of Ingot Processing Treatments on the Grain Size and Properties of Al Alloy 7075," Met. Trans., Vol. 5, 1974, p. 573

B-11 M. F. Ashby, "The Deformation of Plastically Non-Homogeneous Alloys," Strengthening Methods in Crystals, Eds. A. Kelly, R. B. Nicholson, New York, John Wiley and Sons, 1971, p. 137

B-12 W. S. Cebulak, Program to Develop High-Strength Aluminum Powder Metallurgy Products, Phase IVa, Vacuum Process Verification, Second Quarterly Report, Contract DAA25-72-C-0593, 1973 January 31

Appendix A

# LMSC FIRST ITERATION ALLOYS: RATIONALE FOR ALLOY SELECTION (Phase I, Task I)

## A.1 INTRODUCTION

All alloys will be based on the Al-Li system in order to achieve the high elastic modulus and low density which are characteristic of this alloy system (Ref. A-1). The high elastic modulus is achieved by the precipitation of a high volume fraction of the coherent ordered $\delta'$ phase ($Al_3Li$). The low density is a direct result of the low density of Li. Rapid solidification is not required to extend solid solubility of Li, but will be used in an effort to overcome the problems which have been experienced with conventional ingot cast Al-Li alloys, namely segregation effects, and low fracture toughness. Specifically, the rapid solidification approach will be used to achieve the following objectives:

(1) To reduce, or eliminate, segregation effects

(2) To reduce the grain size, and hence increase both strength and toughness

(3) To extend solid solubility of additional elements, added to control secondary properties.

Previous work on Al-Li alloys made from rapidly solidified powders (Refs. A-2 and A-3) has shown that the powders can be made and consolidated successfully. The expected modulus and density values of the final product were obtained. Segregation effects were minimized, and a fine grain size maintained throughout the consolidation process. However, in the alloys so far investigated, the fracture toughness, at the

---

A-1 T. H. Sanders, and E. S. Balmuth, "Aluminum-Lithium Alloys: Low Density and High Stiffness," Metal Progress, Vol. 113, No. 3, 1978, p. 32.

A-2 D. Webster, Unpublished LMSC Independent Research Work, 1977.

A-3 K. K. Sankaran, "Structure and Properties of Splat Quenched 2024-Type Aluminum Alloys Containing Lithium," Ph.D. Thesis, MIT, Cambridge, MA. 1978.

strength levels of interest, has been found to be lower than desired. Hence the approach in the present work will be to design alloys for improved toughness and strength, while maintaining the primary properties of modulus and density, and other secondary properties of fatigue and stress corrosion resistance.

## A.2 GENERAL CONSIDERATIONS

### A.2.1 Alloying Additions

All first iteration alloys will contain 3 wt.% Li in order to meet goal A of the program, i.e., a 30% increase in specific modulus over 7075-T76. Previous work on binary Al-3 wt.% Li alloys has shown that the yield strength and toughness are too low. For example, Sanders (Ref. A-4), using ingot Al-3 wt.% Li found a maximum yield strength of 53 ksi, and Webster (Ref. A-2), using P/M Al-3 wt.% Li found a maximum yield strength of 55 ksi; the program goal A is the same yield strength (67 ksi) as 7075-T76. Additional elements will therefore be added to increase strength and toughness. The influence of the purity level of the lithium on toughness will be determined using a ternary alloy rather than a binary so that the comparison will be made at a higher strength level where any embrittling effects should be greater.

### A.2.2 Heat Treatment after Consolidation

The optimum aging temperature for precipitation of $Al_3Li$ in Al-Li alloys is <200°C. This temperature will be greatly exceeded during consolidation; therefore, it will be necessary to solution treat, quench, and age after consolidation. (Note that this will not be done with the non-Li-containing alloy systems being investigated by Alcoa.)

---

A-4 T. H. Sanders and R. R. Sawtell, "Structure and Fracture Behavior of Al-Li Sheet," 107th AIME Annual Meeting, Denver, CO, Feb. 26 – Mar 2, 1978.

A.2.3 Previous Work on Ternary Alloys

Most of the work so far performed on ternary Al-Li-X alloys has been on two systems, Al-Li-Mg and Al-Li-Cu, using alloys made by conventional ingot casting (Ref. A-1). (See Figure A-1.)

Al-Li-Mg Alloys. Mg only gives solid solution hardening, no precipitation hardening, and the strength-toughness line lies below that for binary Al-Li (Sanders, Ref. A-5); no increase in toughness was therefore achieved. The fracture mode was intergranular even in unrecrystallized material. Although rapid solidification would give a very fine grain size and some increase in both strength and toughness, this is probably not the best system to use, unless an alloy showing decreased density is of prime interest.

Al-Li-Cu Alloys. Cu gives precipitation strengthening, and the strength-toughness line lies above that for Al-Li-Mg alloys (Ref. A-1). This is therefore considered a more probable system to meet the program goals than Al-Li-Mg. A considerable amount of work has been performed on these alloys (Refs. A-1 and A-6). The first four alloys in the present study will therefore be based on the Al-Li-Cu system.

In previous work on rapidly solidified Al-Cu-Li alloys, Sankaran (Ref. A-3) studied two alloys, 2024 + 1% Li and 2024 + 3% Li. Despite achieving a fine grain size (1 – 2 $\mu$m) the toughness was too low, especially in the 3% Li alloy. Sankaran suggested that this was due to the low solubility of Cu at the solution treatment temperature (500$^{o}$C) resulting in a significant amount of incoherent second phase particles based on Cu. For further work, he recommended:

(1) Higher purity alloys – less Fe and Si.

---

A-5 T. H. Sanders, J. W. Evancho, and J. T. Staley, "Microstructure and Mechanical Behavior of Al-Mg-Li Alloys," 107th AIME Annual Meeting, Denver, CO, Feb 26 – Mar 2, 1978.

A-6 T. H. Sanders and R. R. Sawtell, "Fatigue, Fracture, and Microstructure of Al-Cu-Li Alloys," 107th AIME Annual Meeting, Denver, CO, Feb 26 – Mar 2, 1978.

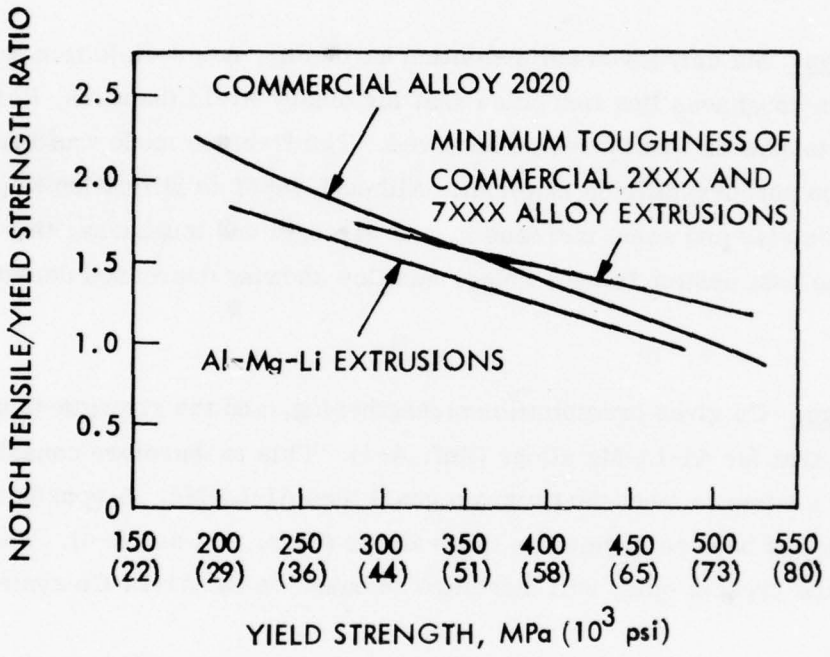


Figure A-1. Notch tensile/yield strength ratio as a function of yield strength for Alloy 2020 and Al-Mg-Li (after Ref. A-1)

(2) Lower Cu content.

(3) Removal of Mg – to allow higher solution treatment temperatures.

(4) Addition of Cd to control nucleation and growth of Al-Cu precipitates upon aging.

### A.2.4 Factors Affecting Fracture Toughness

The second four alloys will be specifically designed to improve fracture toughness. The low toughness of Al-Li alloys, in the peak aged condition, is generally attributed to the localization of slip which occurs in these alloys (Ref. A-1). This slip localization results in severe stress concentration at grain boundaries, followed by grain boundary failure, especially when the boundary contains brittle particles (such as $Al_2MgLi$), or impurity elements, such as Na and K. Alternatively the localization of slip can result in low ductility shear failure. The slip localization is a direct result of the presence of a large volume fraction of a coherent ordered phase ($Al_3Li$). Slip dislocations tend to move in pairs through the ordered phase in order to minimize the area of anti-phase boundary which exists between them, and this means that cross slip is very difficult. Also, as the coherent particles are sheared on one particular slip plane, the area of precipitate particles on that slip plane decreases, and the movement of subsequent dislocations is easier. Hence the slip occurs in a highly localized, inhomogeneous, planar manner. This inhomogeneous planar slip is in fact a general feature of high-strength Al alloys aged to peak strength and containing coherent shearable particles.

### A.2.5 Effect of Nonshearable Particles

It has been shown that the presence of a dispersion of particles which are not sheared causes slip to be dispersed and hence deformation to be more homogeneous (Refs. A-7 and A-8). These nonshearable particles can be obtained in two ways:

A-7 A. Kelly and R. B. Nicholson, "Precipitation Hardening," Progress in Material Science," Vol. 10, No. 3, 1963, p. 372.

A-8 E. A. Starke and G. Lutjering, "Cyclic Plastic Deformation and Microstructure," ASM Materials Science Seminar, Fatigue and Microstructure, St. Louis, MO, 14 – 15 Oct 1978.

(1) By overaging to produce partially coherent or incoherent precipitate particles
(2) By use of a dispersion of insoluble incoherent dispersoid particles

The presence of nonshearable particles results in a higher strain hardening exponent as a result of the dislocation looping around particles, and the operation of multiple slip systems (Refs A-7 and A-8). The effect of increased strain-hardening capacity has been shown to increase fracture toughness (Refs A-9 and A-10). The beneficial effects of slip dispersal by the use of nonshearable particles, in improving the low cycle fatigue behavior of Al alloys has also been demonstrated (Ref. A-8).

A.2.6 Effect of Grain Size

A second general method for increasing the homogeneity of slip is by reducing the grain size, and one of the benefits of rapid solidification is the very fine grain size which is produced. It is considered essential to maintain this fine grain size since this will increase both strength and toughness, and to a greater extent in the Al-Li system than in other alloys such as 7075 or 2024, as a result of the planar slip in the Al-Li alloys. The elements added for grain refinement by dispersoid formation will be selected to give very stable dispersoids that will resist coarsening during consolidation and subsequent heat treatments. Rapid solidification will allow the use of greater amounts of relatively insoluble elements than is normally possible, and will ensure the formation of a much finer dispersion of particles. The presence of oxide particles from the surface of the splat particles will also assist in maintaining a fine grain size.

---

A-9 G. T. Hahn and A. R. Rosenfield, "Metallurgical Factors Affecting Fracture Toughness of Al Alloys," Met. Trans. A., Vol. 6A, 1975, p. 653.
A-10 G. G. Garrett and J. F. Knott, "The Influence of Compositional and Microstructural Variations on the Mechanism of Static Fracture in Aluminum Alloys," Met. Trans. A, Vol. 9A, 1978, p. 1187.

### A.2.7 Effect of Other Microstructural Features

Other microstructural features, such as degree of recrystallization, grain boundary morphology, and precipitate free zone width also affect the localization of slip (Ref. A-8) and hence the toughness and other secondary properties. The effects of these other parameters will also be investigated.

## A.3 SELECTION OF FIRST ITERATION ALLOYS

### A.3.1 First Four Alloys

A.3.1.1 Compositions – The first four alloys are based on the Al-Cu-Li system and will contain 3 wt.% Li. One alloy will contain commercial purity lithium; the other three will contain high-purity lithium. Two different Cu levels and two different grain refining elements have been selected. The major factors involved in selection of the first four alloys are summarized in Table A-1, and the compositions are given in Table A-2.

A.3.1.2 Factors Affecting Composition Levels – The following paragraphs discuss the factors affecting composition levels:

(1) Lithium Content. Three wt.% is considered necessary to meet program goal A. Sankaran (Ref. A-3), using 2024 + 3 wt.% Li found an increase in specific modulus of about 30%. Webster (Ref. A-2) also using 2024 + 3 wt.% Li found an increase of 28%. Lower Li levels can be examined if necessary in the second iteration of alloys. Two wt.% Li would probably meet the lower specific modulus requirement of goal B and at the same time allow increased strengthening contribution from other elements such as Cu as a result of the increased solid solubility of these elements at the solution treatment temperature. A lower Li level would also be expected to increase fracture toughness.

TABLE A-1. SELECTION OF ALLOYS CONTAINING LITHIUM
SUMMARY OF MAJOR FACTORS INVOLVED

All Alloys

Contain 3 wt % Li to meet goal A

Contain other elements to control secondary properties

First Four Alloys

Based on Al-Cu-Li system

Compare high purity and commercial purity lithium

Evaluate two different Cu levels

Compare two different grain refining elements

Second Four Alloys

Contain approximately 1 wt % of dispersoid forming elements

Evaluate effect of dispersoid on toughness

Evaluate effect of dispersoid on grain stabilization

TABLE A-2. LMSC FIRST ITERATION ALLOYS

| Alloy No. | Composition[a] (Weight Percent) | | | | | | |
|---|---|---|---|---|---|---|---|
| | Li[b] | Cu | Zr | Mn | Fe | Ni | Co |
| 1.1 | 3.0 | 4.0 | 0.2 | – | – | – | – |
| 1.2 | 3.0 | 2.0 | 0.2 | – | – | – | – |
| 1.3 | 3.0[c] | 4.0 | 0.2 | – | – | – | – |
| 1.4 | 3.0 | 4.0 | – | 0.4 | – | – | – |
| 1.5 | 3.0 | – | 1.0 | – | – | – | – |
| 1.6 | 3.0 | – | – | 1.5 | – | – | – |
| 1.7 | 3.0 | – | – | – | 0.5 | 0.5 | – |
| 1.8 | 3.0 | – | – | – | 0.5 | – | 0.5 |

(a) Balance aluminum
(b) High purity except as noted
(c) Commercial purity

(2) Lithium Purity. (a) High purity: Highest purity available at reasonable cost ($70/lb for 20 – 30 lb lots) contains 0.007% Na, maximum, and is purified by vapor distillation or electrolysis. This Na level will give about 2 ppm in the final alloy, probably comparable with the Na content of the Al which will be used. (b) Commercial purity: Typical commercial purity Li containing 0.05% Na will be used for comparison purposes.

(3) Cu Content. A lower Cu content has been selected than in 2020 (4.5% Cu) and 2024 (4.5% Cu) in order to produce less undissolved second phase at the solution treatment temperature. (Note that 2048 contains 3.3% Cu and less Fe and Si than 2024 and shows 50% higher toughness at the same strength level.) Two levels have been selected for first iteration alloys – 4% and 2%. Four-percent Cu will have some insoluble second phase particles at solution treatment temperatures in the range 500° to 525°C, but they should be present as a very fine incoherent dispersion as a result of the rapid solidification. They should therefore assist in the dispersal of slip. Two-percent Cu will show only a small amount of insoluble second phase. These two Cu levels have been selected to define the probable range within which second iteration compositions will be examined.

(4) Mg Content. No Mg will be used in the first iteration alloys. Small amounts can be added in second iteration alloys if desirable. Advantages of Mg are that it intensifies strengthening (in Al-Cu-Mg alloys) and gives a small density improvement. Disadvantages are that in alloys containing Cu and Mg a eutectic occurs at a temperature ~508°C, limiting solution treatment temperatures to less than 500°C. Also, the presence of Mg may allow heterogeneous grain boundary precipitation of $Al_2MgLi$ to occur and decrease the fracture toughness.

(5) Grain Stabilizing Elements. Elements which have been used in high-strength Al alloys are Mn, Zr, Cr, and Co. Mn and Zr are usually used

in 2000 series alloys. Cr is usually used in 7000 series alloys. Co is used in MA87. For Cu-containing alloys, solution treatment temperatures as high as 500° to 525°C may be required to dissolve as much as possible of the Cu-containing phases. This procedure will probably require use of Zr rather than Mn for grain stabilization. Sanders (Ref. A-4) found that in binary Al-Li alloys Zr (0.14%) suppressed recrystallization far better than Mn (0.32%), and far better in the Al-Li alloy than in other Al alloys. After solution treatment temperatures of 552°C, the microstructure was basically unrecrystallized. The grains were highly elongated, and the grain width appeared to be ~ 2 μm. Thus, 0.14% was sufficient to stabilize this grain size. Fulmer Research Institute (Ref. A-11) used 0.2% Zr in its Al-Mg-Li-Zr alloys. For the present study, 0.2 wt.% Zr has been selected for the first three alloys and 0.4 wt% Mn for the fourth alloy.

Increased amounts of Zr will be examined in the second iteration of alloys if 0.2% is found insufficient. It should be noted that other grain-stabilizing particles are also present, such as oxide particles from the surface of the splats. For example, MA87 made from atomized powder contains approximately 0.5% by volume of oxide. The amount of oxide in splat is reportedly less than in atomized powder by a factor of two (Ref. A-12). Also, the composition of the oxide is different. These factors will be investigated in the present work.

(6) Impurity Elements (Fe and Si). Rapid solidification will give a very fine dispersion of Fe- and Si-containing particles and probably eliminate the normal deleterious effect of these elements on toughness, which occurs in ingot cast alloys. Nevertheless, it was decided to keep both Fe and Si levels less than 0.1% with target values of Fe 0.06%, Si 0.04%, since no significant cost increase is incurred by using Al of this purity level.

---

A-11 Fulmer Research Institute advertising flyer, undated.
A-12 F. R. Billman, private communication, 1978.

(7) Addition of Cd. Small amounts of Cd (and other elements such as Sn) are known to improve the properties of Al-Cu-Li alloys. However, in Al-Cu-Li alloys containing 0−2.5% Li, Silcock (Ref. A-13) found that significant increases in hardness and yield stress resulting from Cd additions were only observed for low Li contents in the range of 1 to 2%, and at 2 to 2.5% Li there was very little effect of Cd. This suggests that there may be little effect at the 3% Li level. Also, OSHA requirements dictate against the inclusion of toxic elements such as Cd and Be. Therefore, no Cd additions will be made in first-iteration alloys. Additions can be considered for second-iteration alloys, if desired.

A.3.2 Second Four Alloys

Compositions. The alloys will contain 3 wt% Li to meet the property goal A. In addition, each alloy will contain approximately 1 wt% of the following elements, or combinations of two elements − Zr, Mn, Fe + Ni, Fe + Co. These elements have been selected to produce a fine dispersion of nondeformable particles which will serve two primary functions:

(1) To inhibit the localization of slip which occurs in Al-Li alloys, and which leads to low toughness
(2) To stabilize the fine grain size produced by the rapid solidification

The major factors involved in selection of the second four alloys are summarized in Table A-1, and the alloy compositions are given in Table A-2.

Factors Affecting Composition Levels. The optimum volume fraction of nondeforming dispersoid for dispersing slip and improving toughness is not known, but is likely to be in the range of 1 to 5%. More than this amount will probably decrease

---

A-13 J. M. Silcock, "The Structural Aging Characteristics of Al-Cu-Li Alloys," J. Inst. Metals, Vol. 88, 1959−1960, p. 357.

toughness as a result of the particles acting as sites for void initiation. The optimum amount will be a function of the composition, structure, size, and degree of coherency of the dispersoid particles, and also the volume fraction of the coherent, ordered $Al_3Li$ phase. Factors used in selecting dispersoid-forming elements for the second four alloys were: (1) the ability to disperse slip, (2) the thermal stability, and (3) the grain refining ability. These estimated properties together with other expected contributions to strength and modulus are shown in Table A-3 for the various dispersoids. The concentration levels were selected to give the anticipated optimum volume fraction for each individual alloy system. The concentrations were not selected to give the same volume fraction of dispersoid for each alloy, since it was believed that this would have required more Zr than desirable, and less Mn than desirable, based on previous results in the literature. The optimum concentrations will be determined in subsequent alloy iterations, after promising systems have been identified.

Advantages and disadvantages of each alloy system are summarized below:

Al-Li-Zr:

(1) Ability to disperse slip. $Al_3Zr$ when first precipitated is coherent and would not disperse slip, which could be a disadvantage. However, it would stabilize a very fine grain size and provide a useful test of the ability of a fine grain size without nonshearable particles to disperse slip. By prolonged aging it might be possible to overage the $Al_3Zr$ and obtain an incoherent dispersoid which would disperse slip.

(2) Extended solid solubility of Zr is achieved by rapid solidification (Sahin and Jones , Ref. A-14).

(3) $Al_3Zr$ is isostructural with $Al_3Li$; hence Zr may substitute for Li, and thereby modify the strength and stability of the $Al_3Li$ phase.

---

A-14 E. Sahin and H. Jones, "Extended Solid Solubility, Grain Refinement and Age-Hardening in Al – 1 to 13 wt % Zr Rapidly Quenched from the Melt," Third International Conference on Rapidly Solidified Metals, University of Sussex, Brighton, England, 3–7 July 1978.

TABLE A-3. PROPERTIES OF DISPERSOID-FORMING ELEMENTS SELECTED FOR SECOND FOUR ALLOY COMPOSITIONS

| Element | Zr | Mn | Fe + Ni | Fe + Co |
|---|---|---|---|---|
| Dispersoid | $Al_3Zr$ | $Al_6Mn$ | $Al_9(Fe,Ni)_2$ | $Al_9(Fe,Co)_2$ |
| Degree of Coherency | Coherent/ Incoherent | Incoherent | Incoherent | Incoherent |
| Ability to Disperse Slip | Poor/Good | Good | Good | Good |
| Thermal Stability | Excellent | Reasonable | Excellent | Excellent |
| Grain Refining Ability | Excellent | Good | Excellent | Excellent |
| Wt % Selected | 1.0 | 1.5 | 1.0 | 1.0 |
| Calculated Vol % of Dispersoid | 1.2 | 5.2 | 2.5 | 2.5 |
| Contribution to Strength | Significant | Reasonable | Significant | Significant |
| Contribution to Modulus | Small | Small | Small | Small |

(4) Dispersion of $Al_3Zr$ is very stable because of (a) low diffusivity of Zr, and (b) high stability of $Al_3Zr$ (melting point 1580°C).

(5) Dispersion of $Al_3Zr$ is very effective in preventing recrystallization and grain growth.

(6) Zr shows a substantial age hardening response in rapidly solidified material (Ref. A-14).

(7) Zr can be expected to show a small contribution to an increase in modulus as a result of (a) precipitation of $Al_3Zr$, and (b) decreasing the solid solubility of Li.

(8) Previous work on rapidly solidified Al-8 wt % Fe alloys showed significant increases in strength as a result of the addition of 1 wt % Zr, although the ductility was lower (Ref. A-15).

---

A-15 G. Thursfield and M. J. Stowell, "Mechanical Properties of Al-8 wt % Fe-Based Alloys Prepared by Rapid Quenching From the Liquid State," J. Mater. Sci., Vol. 9, 1974, p. 1644.

Al-Li-Mn:

(1) Mn forms an incoherent, nonshearable dispersoid of $Al_6Mn$ which should be very effective in dispersing slip.

(2) Extended solid solubility of Mn is achieved by rapid solidification. Also for relatively high Mn contents in the range 1 to 2 wt %, rapid solidification will allow finer dispersion of $Al_6Mn$ to be precipitated than is possible by heat treatment of ingot alloys.

(3) Dispersion of $Al_6Mn$ is reasonably stable, although not as stable as $Al_3Zr$.

(4) Dispersion of $Al_6Mn$ is reasonably effective in preventing recrystallization and grain growth.

(5) Dispersion of $Al_6Mn$ will provide a small strength contribution.

(6) Mn will provide a small modulus contribution as a result of (a) precipitation of $Al_6Mn$, and (b) decreasing the solid solubility of Li.

(7) Previous work on rapidly solidified Al-8 wt % Fe alloys showed significant strength increases as a result of the addition of 1–3 wt % Mn, although the ductility was lower (Ref. A-15).

Al-Li-Fe-Ni and Al-Li-Fe-Co:

(1) Fe + Ni and Fe + Co form incoherent, nonshearable dispersoids based on $Al_9(Fe,Ni)_2$ and $Al_9(Fe,Co)_2$ that should be very effective in dispersing slip.

(2) Extended solid solubility of Fe + Ni and Fe + Co is achieved by rapid solidification.

(3) Dispersions of $Al_9(Fe,Ni)_2$ and $Al_9(Fe,Co)_2$ are very stable.

(4) Dispersions of $Al_9(Fe,Ni)_2$ and $Al_9(Fe,Co)_2$ are very effective in preventing recrystallization and grain growth.

(5) Dispersion of $Al_9(Fe,Ni)_2$ and $Al_9(Fe,Co)_2$ should provide significant contributions to strength.

(6) Dispersions of $Al_9(Fe,Ni)_2$ and $Al_9(Fe,Co)_2$ should provide a small contribution to modulus.

(7) Previous work on rapidly solidified 7075 type alloys has shown significant increases in strength, with reasonable ductility, as a result of the addition of 1 wt % Fe + 1 wt % Ni (Ref. A-16). MA87 alloy contains approximately 0.5 wt % Co for grain refinement and secondary property improvement (Refs. A-17 and A-18). Al conductor alloys have been developed, containing small amounts (approximately 0.5 wt %) of Fe + Co and Ni + Co, to form fine stable dispersoids (Ref. A-19).

---


A-16 J. P. H. A. Durand, R. M. Pelloux, and N. J. Grant, "Properties of Splat Quenched 7075 Al Type Alloys," Proc. Second Int. Conf. on Rapidly Quenched Metals, Vol. II, 1975, p. 247

A-17 J. P. Lyle and W. S. Cebulak, "Powder Metallurgy Approach for Control of Microstructure and Properties in High Strength Al Alloys," Met. Trans., Vol. 6A, 1975, p. 685

A-18 W. L. Otto, Metallurgical Factors Controlling Structure in High Strength Al P/M Products, Final Report, Contract No. F33615-74-C-5077, AFML-TR-76-60, May 1976

A-19 E. A. Starke, Jr., "Aluminum Alloys of the 70's: Scientific Solutions to Engineering Problems," An invited review, Material Sci. Eng., Vol. 29, 1977, p. 99

Appendix B

ALCOA FIRST ITERATION ALLOYS: RATIONALE FOR ALLOY SELECTION

(Phase I, Task II)

## B.1 INTRODUCTION

The attainment of a high specific modulus of elasticity, $E/\rho$, in conventional aluminum alloys produced by ingot metallurgy techniques is complicated by several fundamental problems. It is well known that one may obtain modulus increases in alloys by the precipitation of a second phase of high modulus, by texture manipulation and solid solution alloying (Refs. B-1 through B-5). Concomitantly, one may add a solute species of sufficiently low density relative to aluminum to reduce the overall density of the alloy, and at equivalent modulus values, increase the specific modulus.

These approaches are generally confounded in aluminum metallurgy by the low solidification rates of ingot metallurgy. Low solidification rates do not allow a sufficiently large saturation of the melt to be retained as large solid-state supersaturation; therefore, neither a uniform distribution of small, high modulus precipitates nor the necessary volume fraction of them can be obtained. The phase nucleates in the melt or during the solidification process as large inhomogeneously distributed constituent particles and dispersoids, in which case their influence on modulus is minimal (Ref. B-5). It is also known that increase in modulus by solid solution alloying can be

---


B-1 W. Koster, W. Rauscher, "The Relationship Between the Modulus of Elasticity of Two-Phase Alloys and Their Structure," Z. Metallkunde, Vol. 39, 1948, p. 111

B-2 G. Bradfield, "Influence of Electron Concentration on the Elasticity of Al Alloys," Phil Mag, Vol. 13, 1966, p. 211

B-3 K. R. VanHorn, "Aluminum," Vol. 1, Properties, Physical Metallurgy and Phase Diagrams, ed. K. R. VanHorn, American Society for Metals, 1967, p. 181

B-4 E. Kovacs-Csetenyk, "The Effect of a Small Amount of Additional Elements on the Young's Modulus of High Purity Aluminum," Aluminum, Vol. 11, 1976, p. 669

B-5 P. Ganesan, G. A. Sargent, R. J. DeAngells, "A Method to Estimate the Volume Fraction of Precipitates with Ellipsoidal Morphology from Elastic Modulus Data," Metallography, Vol. 10, 1977, p. 399

obtained, but the increase is relatively low unless significant supersaturation is obtained. If such a situation is obtained, the loss of solid solution in subsequent thermal treatments does not make this approach worthwhile unless the precipitate itself leads to modulus increase. Furthermore, many available solute species for this method (Ref. B-4) are of greater density than aluminum, so that the variation of density counters the increase in modulus. As a result, there is little specific modulus increase by solid solution alloying.

The purpose of this work is to explore the use of excess solute additions and subsequent controlled precipitation in the consolidation, forming and aging processes of aluminum alloys made from rapidly solidified particulates (RSP), and to apply sound principles of alloy design and development in the selection of composition, production, and consolidation in order to obtain alloys of high specific modulus meeting program goals.

## B.2 OBJECTIVE

The objective of this work is to produce RSP aluminum alloys of 30 percent higher specific modulus than 7075-T76 with minimal loss of strength, toughness, fatigue, and stress-corrosion cracking properties. To achieve this end, it will be necessary to characterize the interaction of alloy composition and deformation with consolidation and forming processes.

### B.2.1 Scientific Rationale

It is believed that a direct method to obtain a high specific modulus can be achieved by using the rapid solidification rates of RSP alloys. Rapid solidification will allow retention of high supersaturation of solute in the solid state. During the subsequent consolidation and forming processes, and possibly during later thermal treatments, the decomposition of the supersaturated solid solution will be manipulated to produce a uniform dispersion of intermetallic precipitate phases of high modulus in sufficient volume fraction that the resultant alloy's specific modulus attains program goals.

Further improvements in specific modulus will be sought by additions of solutes of lower density than aluminum to lower alloy density.

Because of the high supersaturation of the alloy and the need for exposure to deformation and at least moderately high temperatures during consolidation and forming, it is believed that the finished product form will contain a high volume fraction of the modulus hardening phase in an "overaged," or incoherent, condition. Although solute species with low atomic diffusivities are intended to be used, unless unique combinations of solute and solidification rates are found that severely depress the normal kinetics of precipitation, the alloy microstructures will be characterized by the dispersion-hardened state of incoherent precipitates. To obtain the optimum distribution of precipitate sizes and shapes in such a situation, the decomposition of the alloy will have to be manipulated by composition choice and thermal treatment during consolidation.

B.2.2 Considerations of Strengthening Mechanisms

In consideration of the foregoing comments, the discussion of strengthening mechanisms in these alloys needs only to distinguish between coherent and incoherent precipitates, the strengthening due to grain size, and the influence of size and volume fraction of second phases. Precipitation hardening can be usefully divided into two classes depending on the precipitate coherency. In the case of coherent precipitates, as the volume fraction of the precipitated phase increases relative to its size, the incremental change in flow stress increases due to dislocation interaction with precipitate structure and strain fields until the precipitates lose coherency. At this point, a transition to Orowan hardening and lower flow stress occurs (Refs. B-6 and B-7). This is

---

B-6 H. Gleiter, E. Hornbogen, "Precipitation Hardening by Coherent Particles," Mat. Sci. Engr., Vol. 2, 1968, p. 285

B-7 L. M. Brown, R. K. Ham, "Dislocation-Particle Interactions," Strengthening Mechanisms in Crystals, Eds. A. Kelly and R. B. Nicholson, New York, John Wiley and Sons, 1971, p. 12

illustrated schematically in Figure B-1. It is expected that the realm of hardening in the proposed alloy systems will be confined to the right of the maximum flow stress peak. By suitable manipulation of deformation and time at temperature exposure of the of the RSP during consolidation and fabrication, it is intended to produce dispersions of precipitates which lead to high specific modulus and also lead to higher flow stresses on the right side of the flow stress peak on the curve in Figure B-1.

A further strengthening mechanism which is accessible in RSP alloys is grain size strengthening. In the range of grain sizes of ingot metallurgy, significant strengthening cannot be obtained by this method (Refs. B-8 and B-9) unless unusual thermal mechanical treatments are employed (Ref. B-10). However, at sufficiently small grain sizes, $\lesssim 5\ \mu m$, the contribution of grain size to alloy flow stress may become significant.

B.2.3 Considerations of Alloy Ductility

The intent of this work is to use relatively large volume fractions of high modulus intermetallic precipitates. When one is dealing with large volume fractions of small coherent or incoherent precipitates, there will be a loss of macroscopic ductility. The absolute loss will depend on the strength of the precipitates, their size and spatial distribution, and the strength of the particle-matrix interface. Although high modulus intermetallic phases are generally phases of limited ductility, it is possible to manipulate the ductility of the phase by alloy additions that alter either the long range order parameter or the ordering energy. It may be possible with this approach to increase particle plasticity (and alloy ductility) without detriment to the high modulus of the phase. A more ductile precipitate will allow more plastic accommodation of slip

---


B-8 A. W. Thompson, "Substructure Strengthening Mechanisms," Met Trans., 1977, Vol. 8A, p. 833

B-9 R. J. McElroy, Z. C. Szkopiak, "Dislocation-Substructure-Strengthening in Mechanical-Thermal-Treatment of Metals," Intn'l Met. Rev., Vol. 17, 1972, p. 175

B-10 G. Waldman, G. Sulinski, and H. Marcus, "The Effect of Ingot Processing Treatments on the Grain Size and Properties of Al Alloy 7075," Met. Trans., Vol. 5, 1974, p. 573

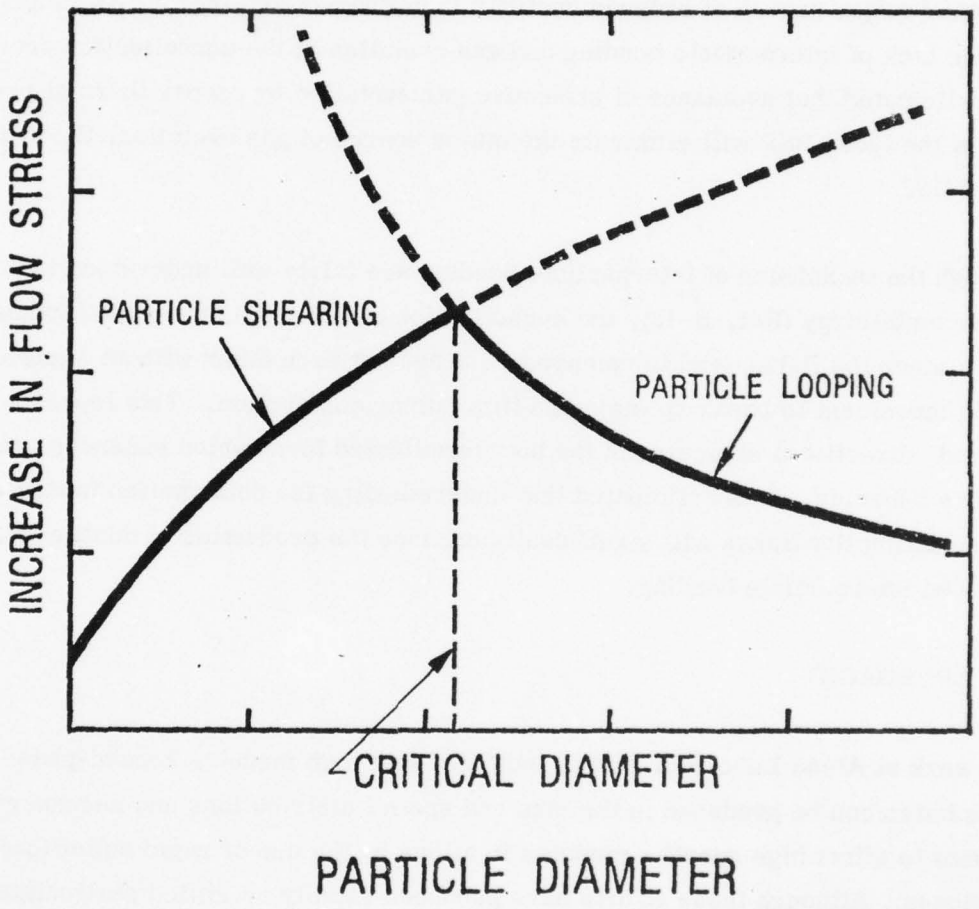


Figure B-1. Effects of particle diameter on flow stress.

dislocations at the particle-matrix interface and will reduce the tendency for brittle fracture of the precipitate (Ref. B-11). The uniform distribution of small precipitates will increase fracture ductility by avoiding localized plasticity associated with large particles in a heterogeneous distribution.

The other major source of reduced ductility in powder-metallurgy alloys is associated with the lack of interparticle bonding and gas evolution in the consolidation process. It is anticipated that avoidance of excessive gas evolution by proper thermal pretreatment of the loose RSP will eliminate the major source of gas evolution, the hydrated oxide film.

Although the techniques of interparticle bonding are fairly well understood in atomized powder metallurgy (Ref. B-12), the consolidation of flat flakes presents further difficulties since the flakes tend to compress flat against each other without significant plastic movement to break up the oxide film during compaction. This leaves a highly oriented, directional structure in the hot consolidated form which enhances premature fracture behavior. It is anticipated that understanding the deformation fundamentals of compacting flat flakes will significantly enhance the production of ductile alloys by improved interparticle bonding.

## B.3 APPROACH

Past work at Alcoa Laboratories has indicated that high modulus second-phase precipitates can be produced in the size and spatial distributions and necessary amounts to effect high specific modulus in alloys by the use of rapid solidification techniques. Although these efforts have produced rapidly solidified particulate alloys of specific modulus ranging from 10 to 38 percent higher than 7075-T76, their ductility-related properties and/or strength properties have suffered. Analysis of the early

---

B-11 M. F. Ashby, "The Deformation of Plastically Non-Homogeneous Alloys," Strengthening Methods in Crystals, Eds. A. Kelly, R. B. Nicholson, New York John Wiley and Sons, 1971, p. 137

B-12 W. S. Cebulak, Program to Develop High-Strength Aluminum Powder Metallurgy Products, Phase IVa, Vacuum Process Verification, Second Quarterly Report, Contract DAA25-72-C-0593, 1973 January 31

work suggests that this has occurred because of an incomplete understanding of the importance of control of microstructural decomposition in the consolidation and forming processes, the mechanics of particle bonding and gas evolution in consolidation and the interaction of alloy composition with these processes. More recent results at this laboratory indicate that the cooling rate during solidification of atomized powders is not sufficient to obtain optimum supersaturation for high specific modulus in some alloys, but that the newly developed Alcoa splat process has significantly higher solidification rates and subsequently higher solid-state supersaturations.

On the basis of the preceding discussion, we believe the optimum high specific modulus alloy with acceptable secondary properties will be obtained in material with a large volume fraction of uniformly dispersed, small precipitates of an intermetallic compound. It is believed that the necessary solute supersaturation required for this approach can be best obtained with the use of rapidly solidified particulate materials. It is further maintained that the consolidation of loose RSP for the successful conclusion of the program will require an understanding of the interplay between alloy composition, deformation in consolidation processing, and strength and ductility-related properties. The following guidelines will be used in the program of research. It is desired to obtain precipitation reactions of slow kinetics. Solute additions will be sought which have low solid-state diffusivities and which form either equilibrium or metastable equilibrium ordered compounds of high modulus. The use of oxides for precipitation hardening is not anticipated. Use of splat solidification techniques and comparison with atomized powder (P/M) techniques is desired to obtain large solid-state supersaturation of desired solute species. It is necessary to develop understanding of optimum combinations of alloy composition, consolidation parameters, and thermal and deformation processing to maximize the resultant precipitate distribution. No specific attempt will be made to suppress nucleation and growth of solid-state precipitates except in cases where unusual solid solution metastability indicates such an approach to be worthwhile. For the alloys of interest, decomposition is inevitable and re-solutionizing is impossible because of limited solid-state solubility. Consequently,

it will be necessary to manipulate the decomposition process to obtain useful precipitate distributions. Deformation processing in the consolidation process may aid this manipulation of the precipitation reaction. Successful development of new alloys may also require understanding of the details of gas evolution from loose RSP.

## B.4 FIRST ITERATION ALLOYS

The first eight alloy compositions are listed in Table B-1. The chosen alloys are based on the Al-Fe-Co and Al-Mn(Si) systems. Development of Al-Fe-Co and Al-Mn alloys, among many others, in the AFML Contract F33615-77-C-5086 has shown that these systems exhibit particularly high modulus of elasticity. Similarly, ALCOA internal research and development has shown that very high specific modulus values are potentially obtainable with the use of rapid solidification technology.

TABLE B-1. ALCOA FIRST ITERATION ALLOYS

| Alloy No. | Al-Fe-Ni-Co Compositions | | | | | | Total Solute, At. % |
|---|---|---|---|---|---|---|---|
| | At. % | | | Weight % | | | |
| | Fe | Ni | Co | Fe | Ni | Co | |
| 2.1 | 1.67 | 1.67 | 1.67 | 3.27 | 3.44 | 3.45 | 5 |
| 2.2 | 1.67 | 1.11 | 2.22 | 3.27 | 2.28 | 4.59 | 5 |
| 2.3 | 1.67 | 2.22 | 1.11 | 3.27 | 4.57 | 2.29 | 5 |
| 2.4 | 2.5 | 2.5 | 2.5 | 4.77 | 5.00 | 5.03 | 7.5 |

| Alloy No. | Al-Mn-Si Compositions | | | | Total Solute, At. % |
|---|---|---|---|---|---|
| | At. % | | Weight % | | |
| | Mn | Si | Mn | Si | |
| 2.5 | 5.0 | 0 | 9.68 | 0 | 5 |
| 2.6 | 5.0 | 2.5 | 9.68 | 2.47 | 5 |
| 2.7 | 2.5 | 5.0 | 4.95 | 5.06 | 5 |
| 2.8 | 7.5 | 0 | 14.17 | 0 | 7.5 |

The following data are limited to tensile properties. In several cases, different product forms, i.e., extrusions and forgings, and variations in thermal processing during consolidation were used. Therefore, caution must be exercised in using these data for absolute quantitative comparisons. The data do suggest alloy families and alloy design approaches that may improve mechanical properties to the level of program goals.

Figures B-2, B-3 and Table B-2 illustrate the relationship of specific modulus to specific strength and ductility in four alloy systems. It is clear that Al-Fe-Co and Al-Fe-Ni produce combinations of specific strength and modulus near those of the contract goals. The Al-Mn data show that improvement in specific strength with the same modulus values can result in higher values of both specific strength and modulus, if the alloy density is reduced.

TABLE B-2. PROPERTY VALUES USED IN FIGURE B-2

| Alloy | Density (lb/in.$^3$) | $E/\rho$ ($\times 10^6$ in.) | $\sigma_y/\rho$ ($\times 10^3$ in.) | |
|---|---|---|---|---|
| 4.8 Fe-5.0 Co | 0.105 | 120.9 | 509.1 | Forging |
| 4.8 Fe-5.0 Co | 0.105 | 118.0 | 744.5 | Forging |
| 2.2 Fe-5.1 Co | 0.104 | 113.5 | 347.5 | Extrusion |
| 4.7 Fe-6.9 Ni | 0.107 | 123.3 | 452.3 | Extrusion |
| 4.5 Fe-7.0 Ni | 0.107 | 121.0 | 565.4 | Extrusion |
| 4.6 Fe-5.0 Ni | 0.104 | 114.9 | 475.0 | Forging |
| 4.6 Fe-5.0 Ni | 0.104 | 117.8 | 757.2 | Forging |
| 15.6 Mn | 0.108 | 147.2 | 590.0[a] | Extrusion |
| 10.6 Mn | 0.104 | 125.0 | 390.4 | Extrusion |
| 9.5 Mn | 0.104 | 125.5 | 432.9 | Forging |
| 29.6 Si | 0.093 | 136.6 | 200.0 | Extrusion |
| 18.5 Si | 0.095 | 124.6 | 149.5 | Extrusion |
| 17.8 Si | 0.095 | 117.9 | 252.6 | Extrusion |

(a) Invalid yield strength due to premature failure.

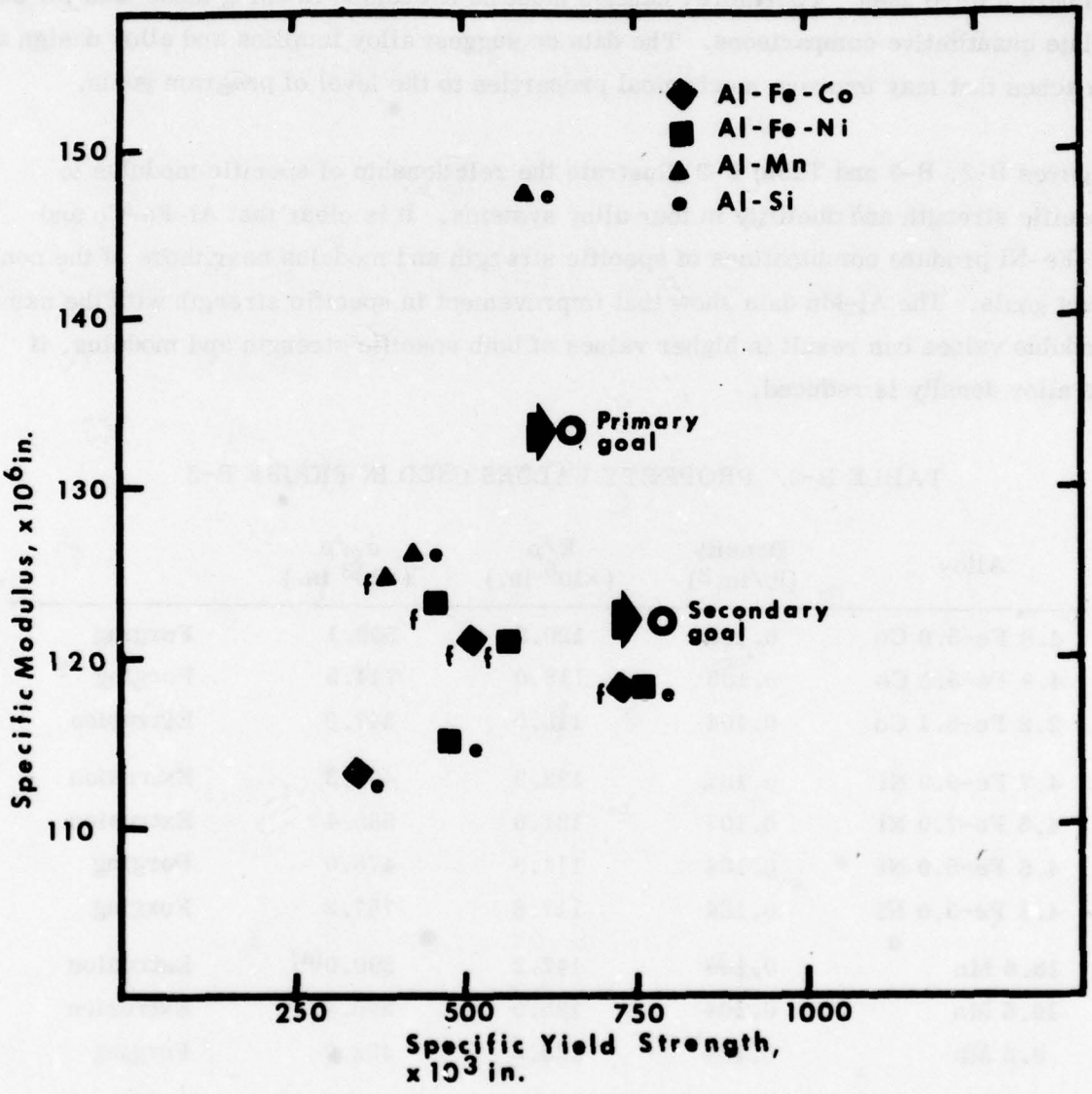


Figure B-2. The variation in specific modulus and specific strength in ALCOA, IRAD, and AFML Contract F33615-77-C-5086 Alloys. (e denotes extrusion, f denotes forging. Compositions are identified in Table B-2.).

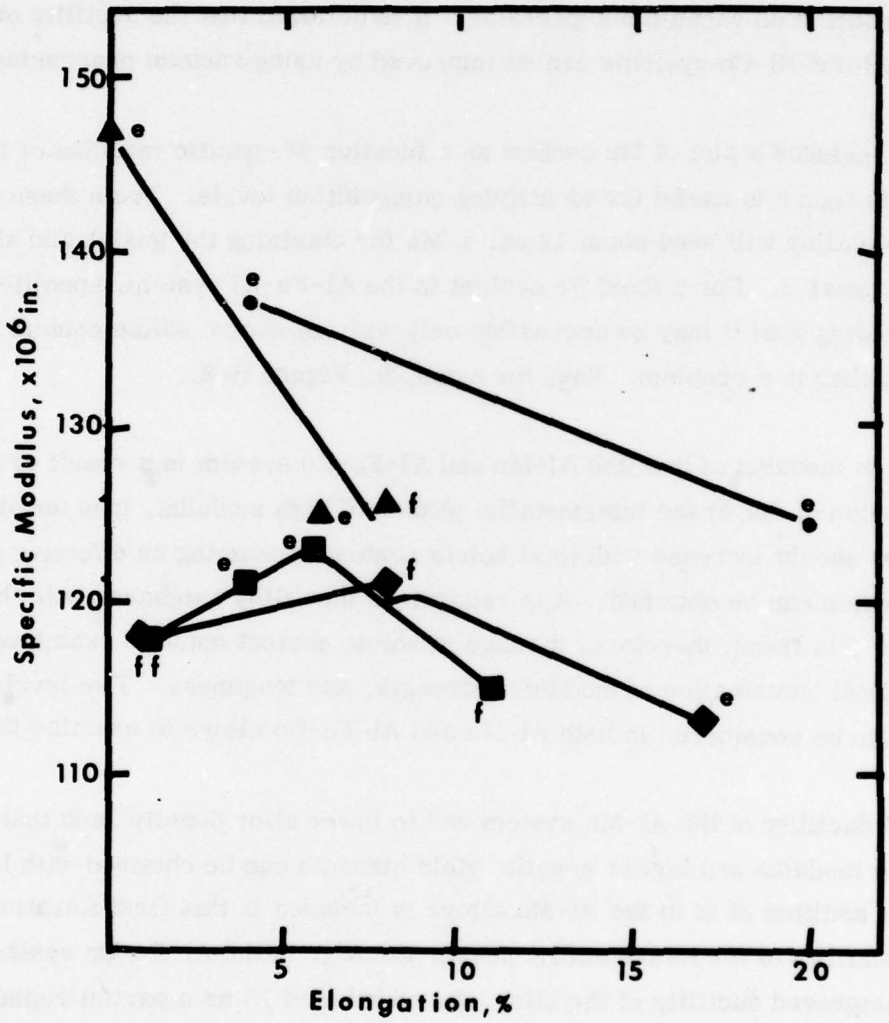


Figure B-3. The variation in specific modulus and tensile elongation in the same alloys as in Figure B-2.

The variations in alloy ductility, shown in Figure B-3, indicate the importance of billet processing. In general, the trend that is observed is one of decreasing ductility with increasing specific modulus. The low values of ductility in Al-Fe-Co and Al-Fe-Ni are likely the result of no vacuum hot-pressing. It is believed that the ductility of both the Al-Mn and Al-Fe-Ni-Co systems can be improved by using vacuum processing.

Figure B-4 includes a plot of Mn content as a function of specific modulus of F-temper alloys. This figure is useful for identifying composition levels. From these data, a binary Al-Mn alloy will need about 12 wt. % Mn for obtaining the goal A and about 10 wt. % for goal B. For a fixed Fe content in the Al-Fe-Ni system, specific modulus values exceeding goal B may be accessible only with excessive solute content where reduced ductility is a problem. See, for example, Figure B-3.

Since the high modulus of both the Al-Mn and Al-Fe-Co system is a result of a large volume fraction of dispersed intermetallic phases of high modulus, it is understandable that modulus should increase with total solute content presuming an effective precipitate distribution can be obtained. It is recognized that alloy toughness will change inversely with this trend; therefore, a range of solute content must be examined to identify the optimal combination of modulus, strength, and toughness. Two levels of solute need to be considered in both Al-Mn and Al-Fe-Co alloys to examine the effect.

To improve ductility of the Al-Mn system and to lower alloy density such that equivalent specific modulus and higher specific yield strength can be obtained with lower Mn content, the addition of Si to the Al-Mn alloys is included in this first iteration. To improve the ductility of the intermetallic phase, $Co_2Al_9$, in the Al-Fe-Co system, which may offer improved ductility of the alloy, the addition of Ni as a partial replacement for Co is included. As Table B-3 shows, the limited data suggest that higher specific modulus can be obtained for weight ratios of Ni:Fe greater than 1. It also will be useful to vary the relative proportions of Fe, Co, and Ni to examine this effect on modulus since the modulus increase is due to the presence of the intermetallic, ordered compounds. With the proper experimental design, these trends will be examined at one total solute level and extrapolated to the other solute level.

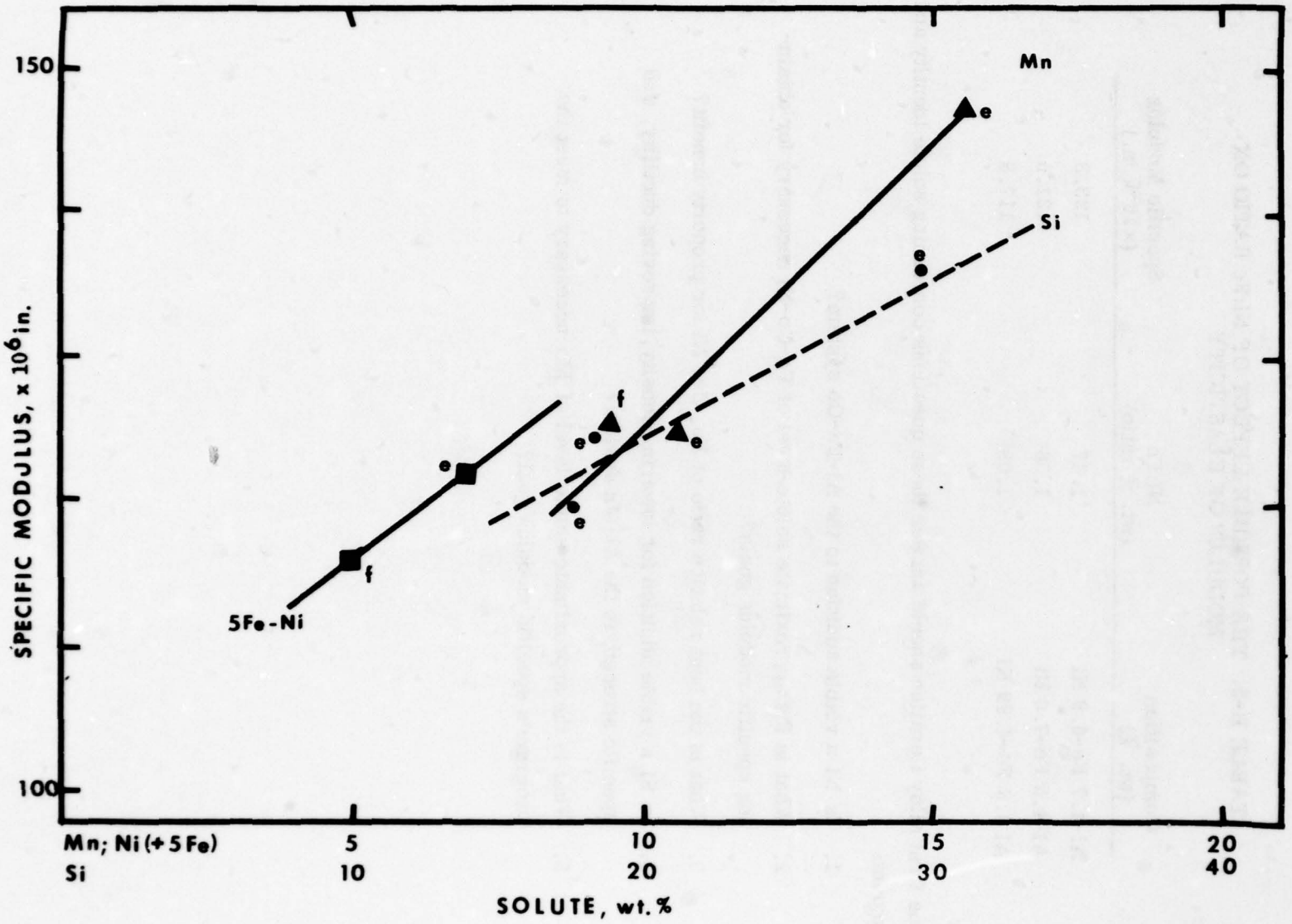


Figure B-4. The variation of specific modulus and solute content in the F-temper alloys of Figure B-2. Symbols identify the same alloys as in Figure B-2.

TABLE B-3. THE POSSIBLE EFFECT OF Ni:Fe RATIO ON MODULUS OF ELASTICITY

| Composition (wt. %) | Ni:Fe (wt. % ratio) | Specific Modulus ($\times 10^{-6}$ in.) |
|---|---|---|
| Al-4.7 Fe-6.9 Ni | 1.47 | 123.3 |
| Al-4.5 Fe-7.0 Ni | 1.56 | 121.0 |
| Al 4.6 Fe-4.99 Ni | 1.08 | 117.8 |

The first alloy iteration should answer these questions concerning solute identity and amount:

1. Is Ni a viable addition to the Al-Fe-Co system?
2. What is the approximate solute level of Fe-Co-Ni necessary for obtaining specific modulus goals?
3. What is the best relative ratio of Fe, Co, Ni for property benefit?
4. Is Si a viable addition for lowering density, improving ductility, and specific strength in the Al-Mn system?
5. What is the approximate solute level of Mn necessary to meet the program's specific modulus goal?

Appendix C

# METHODOLOGY FOR PREDICTION OF WEIGHT SAVINGS FROM STRUCTURAL MATERIAL PROPERTY DATA

Major payoffs for new aerospace structures in terms of weight savings, performance, and life-cycle cost are anticipated from the successful development of advanced aluminum alloys. To optimize weight savings for a particular aerospace structure, an accurate prediction is desired of weight savings resulting from specific values of primary and secondary structural design properties. The primary properties include density, modulus of elasticity, and strength. The secondary properties include fatigue, fracture toughness, and stress corrosion resistance. A method of predicting weight savings resulting from material (property set) substitution for specific aircraft structures has been developed. This analytical tool is intended to be simple and suitable for computerized calculations so that direction can be provided for both alloy development and process development. As a result, optimum weight savings payoffs can be made by identifying optimum primary and secondary properties for specified aircraft structures. In the following, the analytical procedure is described with an example included for the S-3A Viking carrier-based ASW patrol plane. It should be noted that refinements to this model are being developed as described in the body of this report.

## C.1 DEFINITION OF TERMS

| | | |
|---|---|---|
| $a$ | = | length or crack length |
| $b$ | = | width |
| $t$ | = | thickness |
| $t_e$ | = | equivalent thickness, $\frac{\text{stringer area + skin area}}{\text{stringer spacing}}$ |
| $L$ | = | rib or frame spacing |
| $L_o$ | = | effective rib spacing for column |

| | | |
|---|---|---|
| $F_{tu}$ | = | ultimate tensile strength |
| $F_{ty}$ | = | tensile yield strength |
| $F_{cy}$ | = | compressive yield strength |
| $F_c$ | = | compression stress |
| $F_{cc}$ | = | allowable column stress |
| $F_{c_{cr}}$ | = | initial buckling stress |
| $F_{cr}$ | = | allowable crippling stress |
| $F$ | = | DADTA ultimate stress cutoff |
| $\sigma$ | = | applied stress |
| $\sigma_{max}$ | = | maximum applied stress |
| $\bar{\sigma}$ | = | $\sigma_{max} (1 - R)^{1/2}$ |
| $R$ | = | ratio of minimum to maximum applied stress |
| $E_t$ | = | Modulus of elasticity – tension |
| $E_c$ | = | modulus of elasticity – compression |
| $E_S$ | = | secant modulus |
| $E_T$ | = | tangent modulus |
| $G$ | = | shear modulus $\frac{E}{2(1 + \mu)}$ |
| $\mu$ | = | Poisson ratio |
| $n$ | = | Ramberg Osgood parameter for fatigue |
| $K$ | = | stress intensity or stability constant |
| $K_{max}$ | = | maximum stress intensity |
| $\Delta K$ | = | $K_{max} (1 - R)$ |
| $\overline{\Delta K}$ | = | $K_{max} (1 - R)^m$ ; m = 0.5 for aluminum alloys |
| $K_t$ | = | stress concentration factor |
| $K_s$ | = | structural shape factor |
| $C$ | = | geometric shape factor |
| $I$ | = | moment of inertia |
| $A$ | = | cross sectional area |
| $\rho$ | = | radius of gyration $\frac{I}{A}$ |
| $\delta$ | = | material density |
| $N$ | = | unit compression loading or number of cycles |

| | | |
|---|---|---|
| $q$ | = | unit shear loading |
| $W$ | = | weight |
| $W_1$ | = | component weight using basic original structural material |
| $W_2$ | = | component weight using new structural material |

## C.2 ANALYTICAL PROCEDURE

Four steps are taken in the analytical procedure:

1. Define the primary and secondary structural properties which size an airframe
2. Compute equivalent weight ratios for each failure mode criterion
3. Determine fraction of aircraft structural weight sized by each failure mode criterion
4. Determine weight reduction payoff
   [1 - (weight ratio) (fraction of structural weight)] (basic weight)

The steps are discussed below.

### C.2.1 STEP 1 – Define Structural Parameters That Size the Vehicle

- Static Strength

  Ultimate tensile strength = $F_{tu}$

  Tensile yield strength at 0.2% offset strain = $F_{ty_{0.2}}$ (if less than 2/3 $F_{tu}$)

  Compressive yield strength at 0.7% offset strain = $F_{cy_{0.7}}$

- Stiffness

  Tensile modulus of elasticity = $E_t$

  Compression modulus of elasticity = $E_c$

Compression secant modulus = $E_S$

Compression tangent modulus = $E_T$

Poisson ratio = $\mu$

Shear modulus = $\frac{E}{2(1+\mu)}$

(The required values for static strength and stiffness requirement are obtained from the stress-strain curve as shown below in Figure C-1.)

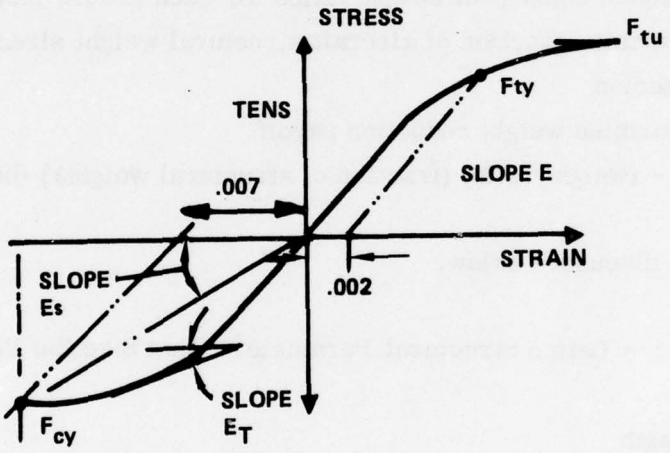


Figure C-1. Illustration of selected properties related to stress-strain curve.

- Durability and Damage Tolerance Assessment (DADTA)

DADTA criteria for a new material are based upon fatigue life, crack propagation, residual strength (fracture toughness), and stress-corrosion behavior. A cutoff of maximum allowable stress is derived for the new material based upon considerations described in the following paragraphs. The lowest cutoff stress is used for weight computation where durability and damage tolerance assessment is a critical factor in the structural design.

A fatigue-allowable stress cutoff at ultimate design load for a new material is obtained from S-N fatigue data as shown in Figure C-2.

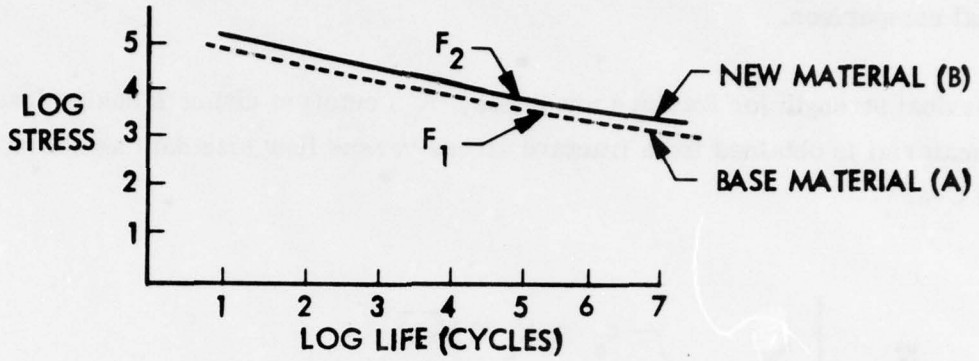


$K_t = 4.5$, $R = 0.3$

Figure C-2. Illustration of fatigue cutoff stress from S-N data for new material.

From Figure C-2, the cutoff stress for fatigue of the new material (B) is the ratio of $F_2/F_1$ times the cutoff stress of the original material (A). A 100,000-cycle fatigue design requirement is illustrated here.

The crack propagation cutoff stress at ultimate design load for a new material is obtained from da/dN crack growth data as shown in Figure C-3.

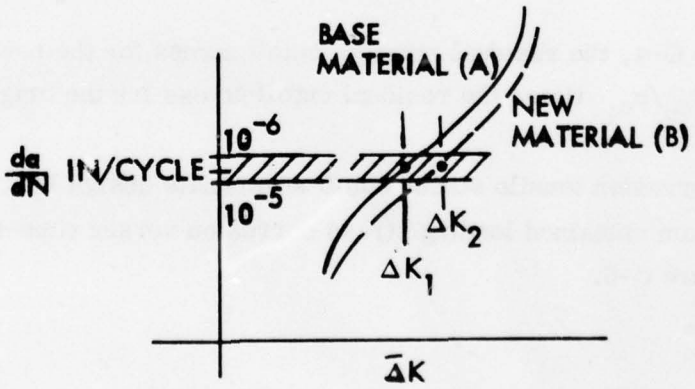


Figure C-3. Illustration of crack propagation cutoff stress terms for new material substitution. $\sigma_1 = C\Delta K_1$ ; $\sigma_2 = C\Delta K_2$.

From Figure C-3, the crack propagation cutoff stress for the new material (B) is the ratio of $\sigma_2/\sigma_1$ times the cutoff stress of the original material (A). The figure illustrates an example of $5 \times 10^5$ in./cycle as the important crack-growth rate for material comparison.

The residual strength (or fracture toughness, $K_c$) cutoff at ultimate design load for a new material is obtained from fracture stress versus flaw size data as shown in Figure C-4.

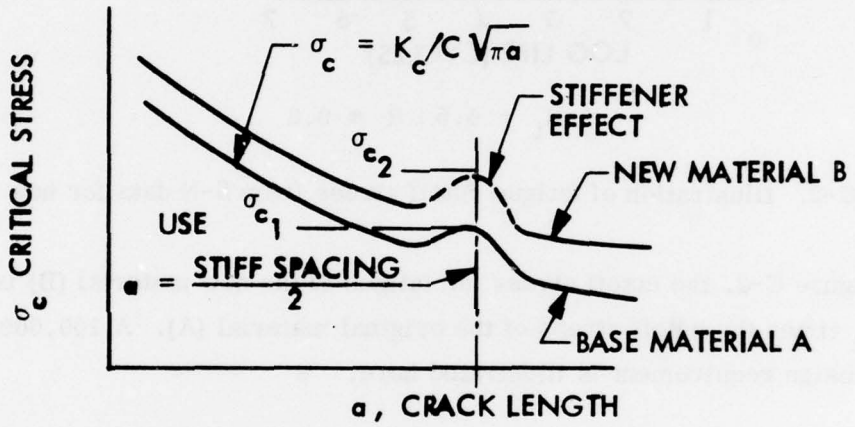


Figure C-4. Illustration of residual strength cutoff terms from critical stress versus crack length data.

From Figure C-4, the residual strength cutoff stress for the new material (B) is the ratio of $\sigma_{c_2}/\sigma_{c_1}$ times the residual cutoff stress for the original material (A).

The stress corrosion tensile stress cutoff at ultimate design load for a new material is obtained from sustained loading stress corrosion versus time-to-failure data as shown in Figure C-5.

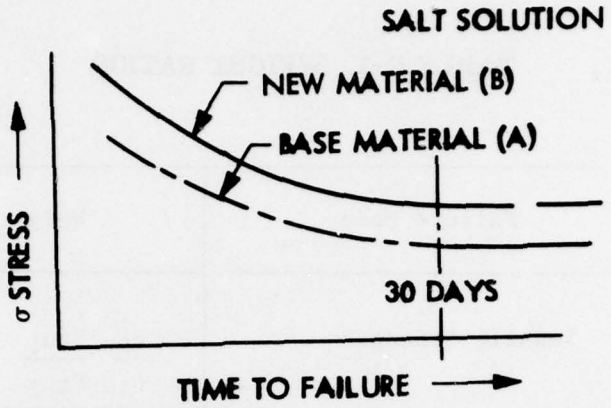


Figure C-5. Illustration of stress corrosion cutoff terms from sustained stress versus time-to-failure in sea water data.

From Figure C-5, the stress corrosion cutoff stress for the new material (B) is the ratio of $\sigma_2/\sigma_1$ times the cutoff stress of the original material (A). The example shown in this figure is for an infinite time-to-failure (threshold) criterion.

For the S-3A Viking Airplane, the DADTA ultimate stress cutoff is the lowest cutoff stress of the following:

- Fatigue life, based on $10^5$ cycles, $K_t = 4.5$ and $R = -0.3$
- Crack propagation, based on $5 \times 10^5$ in./cycle crack growth rate
- Residual strength (fracture toughness) based on 1.5× critical fracture stress of crack length equal to spacing of stiffeners or crack-arrest splices
- Stress corrosion, based on 5.25 g ultimate load factor × stress corrosion threshold stress in salt water

C.2.2 STEP 2 – Compute Equivalent Weight Ratios

Seven failure criteria (critical failure modes) are considered for sizing the structure and for computing the weight ratios. These criteria and the equations for computation of the weight ratios are presented in Table C-1. These weight ratios are based upon certain material properties which govern the specified critical conditions for failure.

## TABLE C-1. WEIGHT RATIOS

| Criteria No. | Failure Mode | Weight Ratio $\frac{W_2}{W_1}$ |
|---|---|---|
| 1 | Tensile Strength | $\frac{\delta_2}{\delta_1} \frac{Ftu_1}{Ftu_2}$ |
| 2 | Compressive Strength | $\frac{\delta_2}{\delta_1} \frac{Fcy_1}{Fcy_2}$ |
| 3 | Crippling | $\frac{\delta_2}{\delta_1} \left[\frac{E_{s_1}}{E_{s_2}}\right]^{.25} \left[\frac{Fcy_1}{Fcy_2}\right]^{.25}$ |
| 4 | Compression Surface Column & Crippling | $\frac{\delta_2}{\delta_1} \left[\frac{E_1}{E_2}\right]^{.4} \left[\frac{F_{cy_1}}{F_{cy_2}}\right]^{.2}$ |
| 5 | Buckling Compression or Shear | $\frac{\delta_2}{\delta_1} \left[\frac{E_1}{E_2}\right]^{.33}$ |
| 6 | Aeroelastic Stiffness | $\frac{\delta_2}{\delta_1} \frac{E_1}{E_2}$ |
| 7 | Durability and Damage Tolerance Assessment Cutoff (DADTA) | $\frac{\delta_2}{\delta_1} \frac{F_1}{F_2}$ |

Derivation of the weight ratio equation for each failure mode category is presented below.

Failure Mode Category No. 1 – Tensile Strength

$$\frac{W_2}{W_1} = \frac{\delta_1}{\delta_2} \frac{F_{tu_1}}{F_{tu_2}} \qquad \text{(C.1)}$$

EXAMPLE

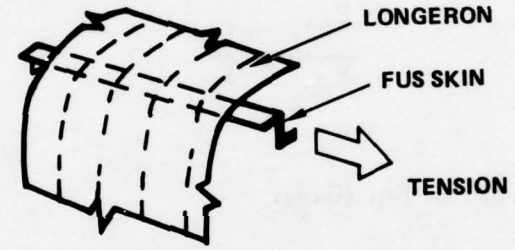


Failure Mode Category No. 2 – Compressive Strength

$$\frac{W_2}{W_1} = \frac{\delta_1}{\delta_2} \frac{F_{cy_1}}{F_{cy_2}} \qquad \text{(C.2)}$$

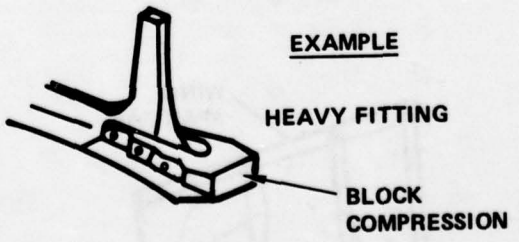

Failure Mode Category No. 3 – Crippling

$$F_{cr} = K\left(E_S F_{cy}\right)^{0.5}\left(\frac{t}{b}\right) \tag{C.3}$$

$$\frac{F_{cr_1}}{F_{cr_2}} = \left(\frac{E_{S_1}}{E_{S_2}}\frac{F_{cy_1}}{F_{cy_2}}\right)^{0.5}\left(\frac{t_1}{t_2}\right)\left(\frac{b_2}{b_1}\right) \tag{C.4}$$

also,

$$\frac{F_{cr_1}}{F_{cr_2}} = \frac{t_2}{t_1} \tag{C.5}$$

Substituting Eq. (C.5) into Eq. (C.4),

$$\frac{t_2}{t_1} = \left(\frac{E_{S_1}}{E_{S_2}}\frac{F_{cy_1}}{F_{cy_2}}\right)^{0.25} \tag{C.6}$$

then,

$$\frac{W_2}{W_1} = \frac{\delta_2}{\delta_1}\left(\frac{E_{S_1}}{E_{S_2}}\frac{F_{cy_1}}{F_{cy_2}}\right)^{0.25} \tag{C.7}$$

Example

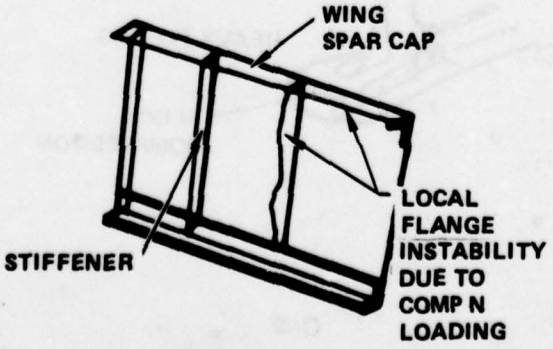

## Failure Mode Category No. 4 – Compression Surface

$$F_c = \frac{N}{t_e} \qquad \text{(C.8)}$$

Example

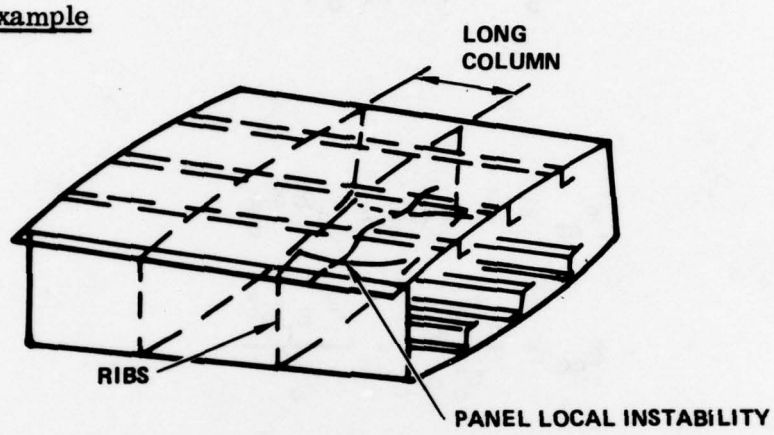


The section shape factor is assumed constant:

$$K_s = \frac{\rho}{t_e}\frac{t}{b} \qquad \text{(C.9)}$$

Examples


CRIPPLING ALLOWABLE STRESS

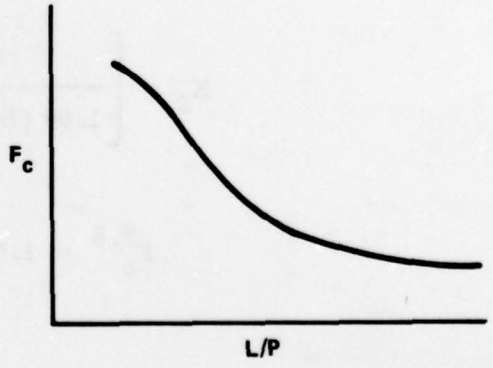


LONG COLUMN ALLOWABLE STRESS

For an optimum design structure, the crippling and column allowable stresses are equated.

$$\frac{K_S N}{L_o} = \frac{F_c}{(b/t)(L_o/\rho)} \qquad \text{(C.10)}$$

and,

$$F_{cr} = 1.60 (E_S F_{cy})^{0.5} \frac{t}{b} \qquad \text{(C.11)}$$

$$F_{cc} = \frac{\pi^2 E_t I}{L_o^2 A} = \frac{\pi^2 E_t \rho^2}{L_o^2} \qquad \text{(C.12}$$

For constant rib spacing,

$$\frac{K_S N}{L_o} \quad \text{is a constant, } K_2 \qquad \text{(C.13)}$$

Combining the above equations,

$$K_2 = \left[\frac{F_c^2}{1.60 (E_S F_{cy})^{0.5}}\right]\left(\frac{F_c}{E_t}\right)^{0.5} \qquad \text{(C.14)}$$

$$F_c^{2.5} = 1.60 \pi K_2 (E_t) F_{cy}^{0.5} \qquad \text{(C.15)}$$

Assuming $E_t = E_S = E$ and allowable stress $< F_{cy}$,

$$F_c = K_3 (E)^{0.4} (F_{cy})^{0.2} \quad , \tag{C.16}$$

where $K_3$ is a constant.

Then

$$\frac{F_{c_1}}{F_{c_2}} = \frac{t_2}{t_1} = \left(\frac{E_1}{E_2}\right)^{0.4} \left(\frac{F_{cy_1}}{F_{cy_2}}\right)^{0.2} \tag{C.17}$$

Finally,

$$\frac{W_2}{W_1} = \frac{\delta_2}{\delta_1} \left(\frac{E_1}{E_2}\right)^{0.4} \left(\frac{F_{cy_1}}{F_{cy_2}}\right)^{0.2} \tag{C.18}$$

Failure Mode Category No. 5 – Buckling

$$F_{c_{cr}} = KE \left(\frac{t}{b}\right)^2 \tag{C.19}$$

$$\frac{F_{c_{cr_1}}}{F_{c_{cr_2}}} = \left(\frac{E_1}{E_2}\right)\left(\frac{t_1}{t_2}\,\frac{b_2}{b_1}\right)^2 \tag{C.20}$$

If spacing is constant, $b_1 = b_2$, then

$$\frac{F_{c_{cr_1}}}{F_{c_{cr_2}}} = \frac{E_1}{E_2}\left(\frac{t_1}{t_2}\right)^2 \qquad \text{(C.21)}$$

Also,

$$\frac{t_2}{t_1} = \frac{F_{c_{cr_1}}}{F_{c_{cr_2}}} \qquad \text{(C.22)}$$

Combining Eqs. (C.22) and C.21),

$$\frac{t_2}{t_1} = \left(\frac{E_1}{E_2}\right)^{0.33} \qquad \text{(C.23)}$$

Finally,

$$\frac{W_2}{W_1} = \left(\frac{E_1}{E_2}\right)^{0.33} \frac{\delta_2}{\delta_1} \qquad \text{(C.24)}$$

Examples:

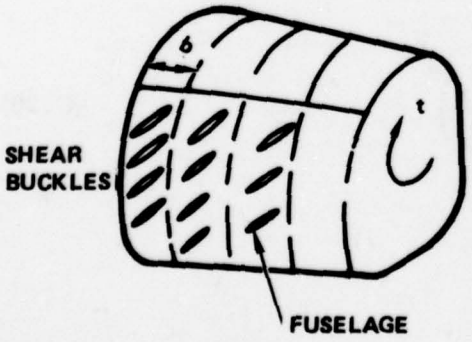


SHEAR BUCKLING

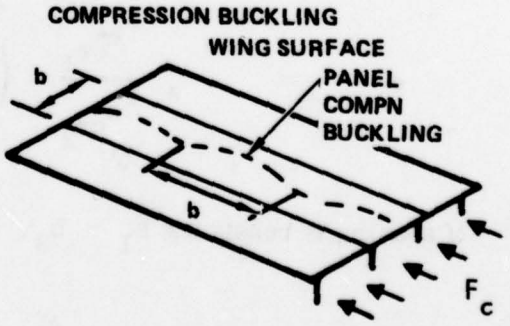

Failure Mode Category No. 6 – Aeroelastic Stiffness

The torsional stiffness is proportional to the skin thickness and shear modulus.

$$G = \frac{E}{2(1+\mu)} \tag{C.25}$$

$$\frac{t_2}{t_1} = \frac{E_1}{E_2} \quad \text{for a constant box area} \tag{C.26}$$

Finally,

$$\frac{W_2}{W_1} = \frac{E_1}{E_2}\frac{\delta_2}{\delta_1} \tag{C.27}$$

Failure Mode Category No. 7 – Durability and Damage Tolerance Assessment (DADTA)

$$\frac{W_2}{W_1} = \frac{\delta_1}{\delta_2}\frac{F_1}{F_2} \tag{C.28}$$

Example:

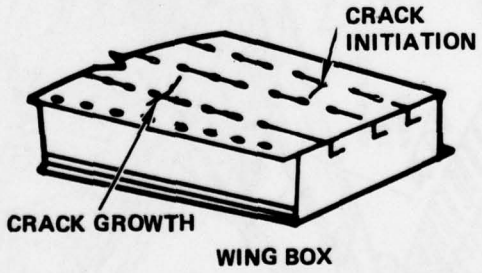


Examples of different aluminum alloy structural components in the S-3A Viking and pertinent Failure Modes are shown in Figure C-6.

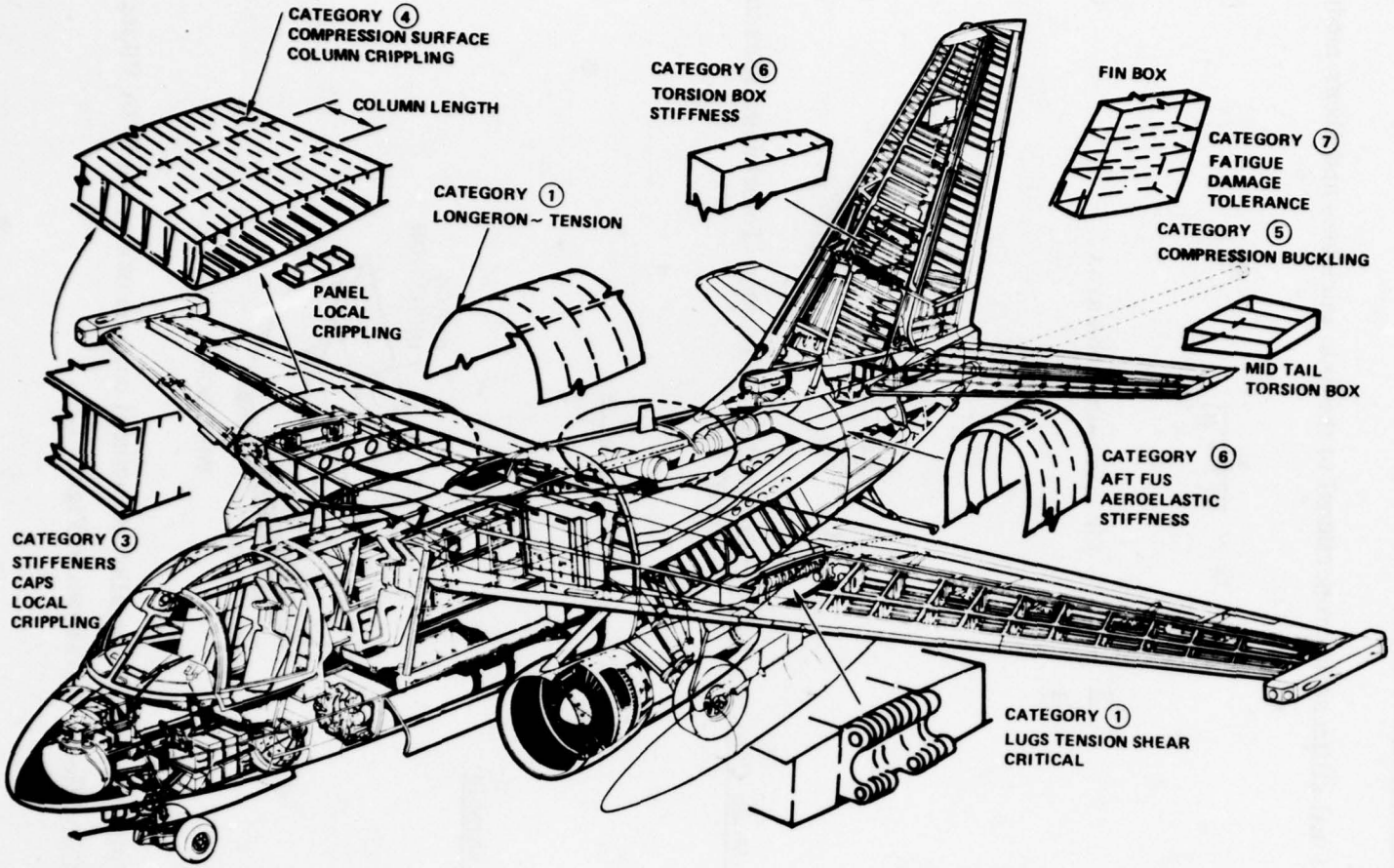


Figure C-6. Typical criteria category areas.

C.2.3 STEP 3 – Determine Weight Breakdown by Failure Mode Category

The structural weight fraction which is critical for each failure mode category is unique for each aircraft or other aerospace structure.

For the S-3A Viking airplane, the aluminum structural weight in the airframe is distributed by failure mode category and structural group according to Table C-2. The weight breakdown by failure mode category for each major component is presented in Table C-3. This allocation of weight was obtained from a detailed review of stress analyses of the structural components and identifying their critical failure modes.

TABLE C-2. S-3A VIKING AIRPLANE PRIMARY STRUCTURAL WEIGHT BREAKDOWN (LB)

| Criteria Category | Criteria Description | Wing | Fuselage | Empennage | Control Surfaces | Total |
|---|---|---|---|---|---|---|
| 1 | Tensile Strength | 562 | 1873 | 75 | 178 | 2688 |
| 2 | Compressive Strength | | | | | |
| 3 | Crippling | 581 | | 247 | 452 | 1280 |
| 4 | Compressive Surface | 583 | | 138 | | 721 |
| 5 | Buckling | 642 | 740 | 54 | 321 | 1757 |
| 6 | Aeroelastic Stiffness | 495 | 299 | 100 | 365 | 1259 |
| 7 | Damage Tolerance or Fatigue Cutoff | 552 | 476 | 115 | 77 | 1220 |
| Total | | 3415 | 3388 | 729 | 1393 | 8925 |

## TABLE C-3. COMPONENT WEIGHT BREAKDOWN BY FAILURE MODE CATEGORY

| Component \ Category | 1 | 2 | 3 | 4 | 5 | 6 | 7 |
|---|---|---|---|---|---|---|---|
| **Wing** | | | | | | | |
| Upper Surface | | | | | | | |
| Inner Wing (500 lbs) | | | | 380 | | 120 | |
| Outer Wing (240 lbs) | | | | 125 | 65 | 100 | |
| Lower Surface | | | | | | | |
| Inner Wing (550 lbs) | 130 | | | | | 200 | 220 |
| Outer Wing (240 lbs) | | | | | 115 | 75 | 50 |
| Spars | | | | | | | |
| Inner (291 lbs) | 145 | | 65 | | | | 81 |
| Outer (181 lbs) | | | | 78 | 43 | | 60 |
| Ribs | | | | | | | |
| Inner Wing (383 lbs) | 143 | | 120 | | 120 | | |
| Inner Fold Jt (251 lbs) | 76 | | 100 | | | | 75 |
| Outer Wing (84 lbs) | | | 34 | | 150 | | |
| Outer Fold Jt (222 lbs) | 68 | | 88 | | | | 66 |
| Leading Edge | | | | | | | |
| Inner and Outer Wing (93 lbs) | | | 39 | | 54 | | |
| Trailing Edge | | | | | | | |
| Inner (170 lbs) | | | 70 | | 100 | | |
| Outer (160 lbs) | | | 65 | | 95 | | |
| Total | 562 | | 581 | 583 | 642 | 495 | 552 |
| **Fuselage** | | | | | | | |
| Longerons | | | | | | | |
| Fwd. Fus. (280 lbs) | | | | | 140 | | 140 |
| Mid Fus. (150 lbs) | | | | | 70 | | 81 |
| Aft Fus. (15 lbs) | | | | | 15 | | |

| Component \ Category | 1 | 2 | 3 | 4 | 5 | 6 | 7 |
|---|---|---|---|---|---|---|---|
| **Fuselage** (Continued) | | | | | | | |
| Skins | | | | | | | |
| Fwd & Mid Fus. (353 lbs) | 173 | | | | 180 | | |
| Aft. Fus. | | | | | | 64 | |
| Bulkheads & Frames | | | | | | | |
| Fwd Fus. (655 lbs) | 400 | | | | | | 255 |
| Mid Fus. (778 lbs) | 600 | | | | | 178 | 178 |
| Aft Fus. (177 lbs) | 120 | | | | | 57 | 57 |
| Flooring & Decks (494 lbs) | 300 | | | | 194 | | |
| Keelson (421 lbs) | 280 | | | | 141 | | |
| Total | 1873 | | | | 740 | 299 | 476 |
| **Empennage** | | | | | | | |
| Vert. & Horiz. | | | | | | | |
| Surfaces (238 lbs) | | | | 138 | | 100 | |
| Spars (166 lbs) | 60 | | 82 | | 24 | | |
| Ribs & Fittings (105 lbs) | 15 | | 90 | | | | |
| Leading Edge & Trailing Edge (220 lbs) | | | 75 | | 30 | | 115 |
| Total | 75 | | 247 | 138 | 54 | 100 | 115 |
| **Control Surfaces** | | | | | | | |
| Elevator (295 lbs) | | | 100 | | | 185 | |
| Rudder (157 lbs) | | | 57 | | | 100 | |
| Aileron (96 lbs) | | | 26 | | | 70 | |
| Flap T.E. (452 lbs) | 178 | | 122 | | 75 | | 77 |
| Flap L.E. (247 lbs) | | | 47 | | 200 | | |
| Spoilers (146 lbs) | | | 100 | | 46 | | |
| Total | 178 | | 452 | | 321 | 365 | 77 |

### C.2.4 STEP 4 — Determine Weight Savings

The weight savings resulting from a material substitution in a specific aerospace structure are obtained by summing the calculated weight savings for the components in each failure mode category. To illustrate this procedure, the weight savings are calculated for the S-3A Viking for substitution of each of three hypothetical alloys — A, B, and C — for a baseline aluminum alloy 7075-T76.

1. Definition of Primary and Secondary Structural Properties Which Size the Airframe

The properties given in Table C-4 are assumed in this example.

TABLE C-4. ASSUMED ALLOY PROPERTIES AND PARAMETERS

ALLOY PROPERTIES

| Material | $F_{tu}$ | $F_{cy}$ | E | $\delta$ | F (DADTA Cutoff) |
|---|---|---|---|---|---|
| 7075T76 | 73 | 73 | 10.4 | 0.101 | 55 |
| A | 80 | 80 | 11.6 | 0.087 | 50 |
| B | 95 | 95 | 14.4 | 0.108 | 50 |
| C | 75 | 75 | 10.4 | 0.101 | 65 |

PARAMETERS

| Material | $\frac{F_{tu_1}}{F_{tu_2}}$ | $\frac{F_{ty_1}}{F_{ty_2}}$ | $\left[\frac{F_{cy_1}}{F_{cy_2}}\right]^{0.2}$ | $\left[\frac{F_{cy_1}}{F_{cy_2}}\right]^{0.25}$ | $\frac{E_1}{E_2}$ | $\left(\frac{E_1}{E_2}\right)^{0.25}$ | $\left(\frac{E_1}{E_2}\right)^{0.33}$ | $\left(\frac{E_1}{E_2}\right)^{0.4}$ | $\frac{F_1}{F_2}$ |
|---|---|---|---|---|---|---|---|---|---|
| 7075-T76 | 1.00 | 1.00 | 1.00 | 1.00 | 1.00 | 1.00 | 1.00 | 1.00 | 1.00 |
| A | .91 | .92 | .98 | .98 | .90 | .97 | .97 | .96 | 1.10 |
| B | .77 | .77 | .95 | .94 | .72 | .92 | .90 | .88 | 1.10 |
| C | .97 | .97 | .99 | .99 | 1.00 | 1.00 | 1.00 | 1.00 | .85 |

2. Computation of Equivalent Weight Ratios for Each Failure Mode Criterion

Using equations from Table C-1 and appropriate parameters from Table C-4, calculate the weight ratios, $W_2/W_1$ for each failure mode category. Table C-5 summarizes these data.

TABLE C-5. CALCULATED WEIGHT RATIOS, $(W_2/W_1)$

| Alloy \ Category | 1 | 2 | 3 | 4 | 5 | 6 | 7 |
|---|---|---|---|---|---|---|---|
| 7076-T76 | 1.00 | 1.00 | 1.00 | 1.00 | 1.00 | 1.00 | 1.00 |
| A | .78 | .79 | .82 | .81 | .83 | .77 | .95 |
| B | .83 | .82 | .93 | .89 | .97 | .77 | 1.18 |
| C | .97 | .97 | .99 | .99 | 1.00 | 1.00 | .85 |

3. Determination of Aircraft Structural Weight Fraction Sized by Each Failure Mode Criterion

For the S-3A airplane, the weight fraction sized by each failure mode category is presented above in Table C-2. As an example, for category No. 1 failure mode criterion, the weight fraction in the wing is 562 lb, and for all structural components the total weight fraction is 2688 lb.

4. Determine Weight Reduction Payoff

For each failure mode category and structural component, the new weight is obtained by multiplying the pertinent weight fraction (Table C-2) by the calculated weight ratio related to the new alloy (Table C-5). For example, the original weight of tensile strength critical (failure mode category No. 1) components in the wing is 562 lb. By substitution of Alloy A, the new weight for these components would be $562 \times 0.78 = 438$ lb. As shown in Table C-6, substitution of Alloy A for all seven failure mode categories would result in a new total of 2823 lb for wing components originally weighing 3415 lb. This represents a weight savings of 3415 - 2823 = 592 lb, a 17.3-percent weight savings.

In the entire airframe, the total payoff for a new alloy in terms of weight savings is the sum of weight saved in all of the structural components. For

TABLE C-6. WEIGHT SAVINGS – HYPOTHETICAL ALLOYS A, B & C

| Component / Category | Wing | | | | Fuselage | | | | Empennage | | | | Control Surfaces | | | |
|---|---|---|---|---|---|---|---|---|---|---|---|---|---|---|---|---|
| | Alloy | | | | Alloy | | | | Alloy | | | | Alloy | | | |
| | 7075-T76 | A | B | C | 7075-T76 | A | B | C | 7070-T76 | A | B | C | 7075-T76 | A | B | C |
| 1 | 562 | 438 | 466 | 545 | 1873 | 1460 | 1554 | 1817 | 75 | 59 | 62 | 73 | 178 | 139 | 107 | 173 |
| 2 | | | | | | | | | | | | | | | | |
| 3 | 581 | 476 | 540 | 577 | | | | | 247 | 202 | 229 | 244 | 452 | 370 | 420 | 447 |
| 4 | 583 | 472 | 519 | 577 | | | | | 138 | 111 | 123 | 136 | | | | |
| 5 | 642 | 532 | 522 | 642 | 740 | 514 | 718 | 740 | 54 | 45 | 52 | 54 | 321 | 266 | 311 | 321 |
| 6 | 495 | 381 | 381 | 495 | 299 | 230 | 230 | 299 | 100 | 77 | 77 | 100 | 365 | 281 | 281 | 365 |
| 7 | 552 | 524 | 651 | 469 | 476 | 452 | 561 | 404 | 115 | 109 | 136 | 98 | 77 | 73 | 91 | 65 |
| Total | 3415 | 2823 | 3079 | 3305 | 3388 | 2655 | 3063 | 3260 | 729 | 530 | 579 | 705 | 1393 | 1129 | 1210 | 1371 |
| Weight Saving Lbs | | 592 | 336 | 110 | | 733 | 325 | 128 | | 199 | 150 | 24 | | 264 | 183 | 22 |
| Weight Saving % | | 17.3 | 9.8 | 3.2 | | 21.6 | 9.5 | 3.8 | | 27.2 | 20.6 | 3.3 | | 18.9 | 13.1 | 1.5 |

Alloy A, the total weight savings is 592 (wing) + 733 (fuselage) + 199 (empennage) + 264 (control surfaces) = 1788 lb, or 20 percent of the total aluminum structure considered. Using the data in Table C-6, the summary of weight saved by substitution of each alloy is given below.

| Alloy | Weight Saved (lb) | Percent Change |
|---|---|---|
| A | 1788 | -20 |
| B | 994 | -11 |
| C | 284 | -3 |

Alloy A was assumed to have 14 percent lower density, 10-percent higher modulus of elasticity, and 10-percent lower DADTA ultimate design stress cutoff, with respect to Al 7075-T76.

Alloy B was assumed to have 30-percent increased strength, 38-percent increased modulus of elasticity, 6 percent increased density, and 10-percent lower DADTA ultimate design stress cutoff.

Alloy C was assumed to have an 18-percent increase in DADTA ultimate design stress cutoff.

The effect of density decrease on weight savings is illustrated by comparing the above results for alloys A and B. Both alloys were assumed to have the same specific modulus increase, 29.5 percent, and almost the same specific strength increase, 27.2 and 21.7 percent, respectively. But alloy A saves almost twice as much weight than alloy B in this particular airframe. The reason is that a change in density affects weight change to the first power in all seven failure mode categories, but modulus or strength changes affect weight to less than the first power in six of the seven categories, aeroelastic stiffness excepted.

If only DADTA ultimate design stress cutoff is higher in a new alloy than 7075-T76, for example, the payoff in terms of weight savings is likely to be small, because DADTA is a critical failure criterion in only a small percent of the structure. In the case of the S-3A airplane, DADTA is critical for only 14 percent of the structure.